SYNTHESIS OF ZIRCONIUM TUNGSTATE AND ITS USE IN COMPOSITES
WITH TUNABLE THERMAL EXPANSION COEFFICIENT

A THESIS SUBMITTED TO
THE GRADUATE SCHOOL OF NATURAL AND APPLIED SCIENCES
OF
MIDDLE EAST TECHNICAL UNIVERSITY

BY

İREM VURAL

IN PARTIAL FULFILLMENT OF THE REQUIREMENTS
FOR
THE DEGREE OF MASTER OF SCIENCE
IN
CHEMICAL ENGINEERING

JANUARY 2011

Approval of the thesis:

SYNTHESIS OF ZIRCONIUM TUNGSTATE AND ITS USE IN COMPOSITES WITH TUNABLE THERMAL EXPANSION COEFFICIENT

submitted by **İREM VURAL** in partial fulfillment of the requirements for the degree of **Master of Science in Chemical Engineering Department, Middle East Technical University** by,

Prof. Dr. Canan Özgen   _____
Dean, Graduate School of **Natural and Applied Sciences**

Prof. Dr. Deniz Üner   _____
Head of Department, **Chemical Engineering Dept.**

Prof. Dr. Güngör Gündüz   _____
Supervisor, **Chemical Engineering Dept., METU**

Assist. Prof. Dr. Bora Maviş   _____
Co-supervisor, **Mechanical Engineering Dept., HU**

Examining Committee Members:

Prof. Dr. Işık Önal   _____
Chemical Engineering Dept., METU

Prof. Dr. Güngör Gündüz   _____
Chemical Engineering Dept., METU

Prof. Dr. Hayrettin Yücel   _____
Chemical Engineering Dept., METU

Prof. Dr. Abdullah Öztürk   _____
Metallurgical and Materials Engineering Dept., METU

Assist. Prof. Dr. Emrah Ünalan   _____
Metallurgical and Materials Engineering Dept., METU

Date: **31.01.2011**

I hereby declare that all information in this document has been obtained and presented in accordance with academic rules and ethical conduct. I also declare that, as required by these rules and conduct, I have fully cited and referenced all material and results that are not original to this work.

Name, Last name   : İREM VURAL

Signature   :

ABSTRACT

**SYNTHESIS OF ZIRCONIUM TUNGSTATE AND ITS USE IN
COMPOSITES WITH TUNABLE THERMAL EXPANSION COEFFICIENT**

Vural, İrem

M.Sc., Department of Chemical Engineering

Supervisor   : Prof. Dr. Güngör Gündüz

Co-Supervisor : Assist. Prof. Dr. Bora Maviş

January 2011, 149 pages

Thermal mismatch between different components of a system could be sources of problems like residual stress induced cracking, thermal fatigue or even optical misalignment in certain high technology applications. Use of materials with tailored thermal expansion coefficient is a counter-measure to overcome such problems. With its negative thermal expansion coefficient zirconium tungstate (ZrW_2O_8) is a candidate component to be used in synthesis of composites with controlled thermal expansion coefficient (CTE).

ZrW_2O_8 is typically produced by solid-state reaction between zirconium oxide and tungsten oxide at 1200^oC. However, it has been demonstrated that ZrW_2O_8 can also be synthesized using wet chemical techniques, which provide a superior chemical homogeneity that often extents down to the atomic scale, and the convenient means of controlling nucleation and growth

of the primary crystallites. With the commonly adopted wet chemical approaches, it is possible to crystallize particles with sizes in the submicrometer range at temperatures as low as 600 ^{o}C or even lower. In these studies, precursors are aged either below 100 ^{o}C (7 days – 3 weeks), or at 160-180 ^{o}C under hydrothermal conditions (1–2 days). Besides the obvious disadvantage in the ageing steps, use of tungsten sources with high cost in all approaches, constitutes the other disadvantage.

Production of composites with tunable controlled thermal expansion (CTE) has been achieved by blending negatively and positively expanding materials in different proportions. In majority of these studies composites have been produced by conventional sintering methods. Spark Plasma Sintering (SPS) is a recent technique; in which sintering can be achieved at relatively low temperatures in short durations. There is only one study made by Kanamori and coworkers on the use of SPS in sintering of a composite, in which ZrW_2O_8 is one of the constituents [1].

This study aims the synthesis of ZrW_2O_8 particles and composites that possess tunable or zero CTE. A novel precursor recipe for ZrW_2O_8 synthesis was developed. In preparation of the precursor a total of 2 days of ageing and a temperature less than 100 ^{o}C was used. It was developed using a cost-effective tungsten source, namely tungstic acid and its final pH was lower than 1. The particles obtained from 'unwashed' procedure had sizes in micrometer range, while those obtained from 'washed' case had sizes in the range of 400-600 nm. These precursors could readily be crystallized at 600 ^{o}C, which in turn provided the desired particle sizes for composite applications. Experimental details on the precursor development are hereby presented with a discussion on the effects of solution parameters (i.e. solubility of tungstic acid, adjustment of the stoichiometry, ageing time) on the phase purity of the fired product. Zirconium oxide (ZrO_2) has positive

thermal expansion, therefore ZrW_2O_8/ZrO_2 was selected as the composite system, and for their synthesis both conventional and spark plasma sintering methods were experimented. Composition ranges that provide composites with almost zero CTE's were determined. The composite having a composition of containing 35% ZrW_2O_8, 65% ZrO_2, and 35 w/o Al_2O_3 and sintered at 1200 ^oC for 24 hours had an expansion coefficient of 0.20×10^{-6}/K for conventional method, while the one having a composition of 55% ZrW_2O_8, 45% ZrO_2 and sintered at 1000 ^oC for 5 minutes had an expansion coefficient of 0.94×10^{-6}/K for spark plasma sintering method. For characterization of the products X-ray diffraction (XRD), scanning electron microscopy (SEM), photon correlation spectroscopy (PCS), and thermal and dilatometer analyses (DTA/TGA/DMA) were used.

Key words: zirconium tungstate, tungstic acid, negative thermal expansion, ageing time, precipitation, composite, zirconia, spark plasma sintering.

ÖZ

ZİRKONYUM TUNGSTAT ÜRETİMİ VE ISIL GENLEŞME KATSAYISI AYARLANABİLEN KOMPOZİTLERDE KULLANIMI

Vural, İrem

Yüksek Lisans, Kimya Mühendisliği Bölümü

Tez Yöneticisi : Prof. Dr. Güngör Gündüz

Ortak Tez Yöneticisi : Yrd. Doç. Dr. Bora Maviş

Ocak 2011, 149 sayfa

Bir sistemi oluşturan bileşenlerde meydana gelen ısıl genleşme katsayısındaki uyumsuzluklar, çatlama, ısıl yorulma sorunlarına yol açan artık gerilimlerin ve hatta hassas optik sistemlerde odaklama sorunlarının oluşmasına neden olabilir. Bu sorunların çözümü, eşdeğer miktarda ısıl büzüşme gösteren malzemelerin kompozit halinde kullanılmaları durumunda olasıdır. Zirkonyum tungstatın (ZrW_2O_8) birçok ileri teknoloji seramiğinin ısıl genleşme sabitlerine eşdeğer bir negatif genleşme göstermesi onu yakın gelecekte sıfır ya da ayarlanabilir ısıl genleşme sabitine sahip seramik-seramik kompozitlerinin yapımında vazgeçilmez bir malzeme kılacaktır.

ZrW_2O_8 genellikle tungsten oksit ve zirkonyum oksidin 1200 $^{\circ}$C'de gerçekleştirilen katı hal tepkimeleriyle üretilmektedir. Fakat atomik düzeyde tek düzeliğin sağlandığı ve asıltı parçacıkların oluşumunun ve büyümesinin

daha iyi denetlenebildiği çözelti kimyasına dayalı yöntemlerle de üretilebildiği görülmüştür. Kaynaklarda, 100 ^{o}C'nin altında 1 ile 3 hafta arasında veya hidrotermal ortamda, 160-180°C'de 1 ile 2 gün arasında yaşlandırma süreleri kullanılarak, 600 ^{o}C ve altında kristallenebilen mikron-altı ZrW_2O_8 parçacıklarının üretilebileceği belirtilmektedir. Yaşlandırma süreçlerinde kullanılan yöntemlerin uzun süreli olması veya yüksek basınç gerektiriyor olması ve ayrıca öncül hazırlamada maliyeti yüksek tungsten kaynaklarının kullanılması endüstriyel uygulama açısından sakınca oluşturmaktadır.

Negatif ve pozitif ısıl genleşme katsayılarına sahip parçacıkların karıştırılmasıyla ayarlanabilir katsayıya sahip kompozitler üretilebilmektedir. Geleneksel sinterleme yöntemleriyle neredeyse sıfır genleşme katsayısına sahip kompozitler üretilmiştir. Son dönemde, Spark Plazma Sinterleme (SPS) yöntemi kullanılarak geleneksel sinterleme yöntemlerinde gereken sıcaklık ve sürelerin önemli oranda düşürülebileceği görülmüştür. ZrW_2O_8'ın bir kompozit bileşeni olarak kullanıldığı çalışmalar arasında, Kanamori ve arkadaşlarının SPS yöntemini kullanıldığı bir çalışmaya rastlanmıştır [1].

Bu araştırmanın amacı ZrW_2O_8 parçacıklarının sentezi ve ısıl genleşmesi ayarlanabilir kompozit yapıların üretilmesidir. Bu amaçla tungstik asit gibi maliyeti görece daha düşük bir tungsten kaynağı kullanılarak, sentezin düşük pH bölgelerinde gerçekleştirildiği bir yöntem geliştirilmiştir. Bu yeni yöntemle, 100 ^{o}C altında toplamda en çok 2 günlük yaşlandırma süresi kullanılarak, 600 ^{o}C'de kristallenebilen ZrW_2O_8 öncülleri üretilmiştir. Yıkama yönteminin uygulanmadığı parçacıklar mikron boyutlarda iken yıkamadan sonra elde edilen parçacıkların boyları 400-600 nm arasındadır. Geliştirilen öncüllerle üretilen tozlar kompozit uygulamaları için gerekli parçacık boylarının elde edilmesini sağlamıştır. Ürünün saflığına etki eden deneysel değişkenler (tungstik asitin çözünürlüğü, kimyasal oran ayarlaması ve yaşlandırma etkileri gibi) ayrıntılarıyla incelenmiştir. Kompozit olarak ZrW_2O_8/ZrO_2 sistemi seçilmiş

ve üretiminde geleneksel ve SPS yöntemleri uygulanmıştır. Her iki yöntemde de sıfır genleşme katsayısına sahip kompozit üretimi için gerekli karışım aralıklarını saptamak üzere sistemli deneyler yürütülmüştür. %35 ZrW_2O_8, %65 ZrO_2 ve %35 Al_2O_3 içeren ve 1200 ^oC'de 24 saat geleneksel yöntem ile sinterlenen kompozitin ısıl genleşme katsayısı 0.20×10^{-6}/K olurken, %55 ZrW_2O_8 ve %45 ZrO_2 içeren ve 1000 ^oC'de 5 dakika SPS'de sinterlenen kompozitin ısıl genleşme katsayısı 0.94×10^{-6}/K olmuştur. Çalışmalar sırasında X-ışını kırınımı (XRD), taramalı elektron mikroskopisi (SEM), parçacık analizi, ve ısıl ve dilatometre analiz (DTA/TGA/DMA) yöntemleri kullanılmıştır.

Anahtar Sözcükler: zirkonyum tungstat, tungstik asit, negatif ısıl genleşme, yaşlandırma süresi, çökeltme, kompozit, zirkonya, spark plazma sinterleme.

To My Parents and Korhan

ACKNOWLEDGEMENTS

TABLE OF CONTENTS

LIST OF TABLES

TABLES

LIST OF FIGURES

FIGURES

xvii

xx

xxi

xxii

LIST OF SYMBOLS AND ABBREVIATIONS

CTE	Thermal Expansion Coefficient
PTE	Positive Thermal Expansion
NTE	Negative Thermal Expansion
w/o	Weight Percent
Al_2O_3	Aluminum Oxide (alumina)
ATA	Ammoniacal Tungstic Acid Solution
AMT	Ammonium Metatungstate
EtOH	Ethanol
γ_o	Orthorhombic γ
γ_t	Trigonal γ
H_2O_2	Hydrogen Peroxide
HCl	Hydrochloric Acid
IPA	Isopropyl Alcohol
METU-CL	Middle East Technical University Central Laboratory
METU-METE	Middle East Technical University Materials and Metallurgical Engineering Dept.
NaT	Sodium Tungstate
PCS	Photon Correlation Spectroscopy

PVP	Polyvinylpyroldinone
SA	Sintering Agent
SEM	Scanning Electron Microscopy
SPS	Spark Plasma Sintering
TA	Tungstic Acid
TGA/DTA	Thermal Gravimetric and Differential Thermal Analysis
UNAM	Bilkent University National Nanotechnology Research Center
USM or US mixing	Ultra Sonic Mixing
W	Tungsten
WC	Tungsten Carbide
XRD	X-Ray Diffraction
Zr	Zirconium
ZrO_2	Zirconium Oxide (zirconia)
ZrOc	Zirconium Oxychloride ($ZrOCl_2$)
ZrOn	Zirconium Oxynitrate ($ZrO(NO_3)_2$)
ZrW_2O_8	Zirconium Tungstate
YSZ	Yttrium Stabilized Zirconia

CHAPTER 1

INTRODUCTION

In today's world there is an extensive research on high performance advanced materials owing to their excellent physical, chemical and mechanical properties. Although there are a large number of properties to be considered one of the most important of all is the thermal expansion coefficient (CTE), which is described as the change of the dimensions of the materials with temperature. It is important to have materials that would resist extreme thermal fluctuations.

Most materials have positive thermal expansion (PTE) coefficient, which means that they expand on heating. On the other hand, there is limited number of materials which shrink on heating. These materials possess negative thermal expansion (NTE) coefficient. Thermal mismatch between components of composites can cause failures at interfaces due to cracking, thermal fatigue, and residual stresses. Alignment of optical devices in advanced applications can be another area, in which excessive thermal expansion and/or mismatch pose important challenges to engineers. Such problems can potentially be solved by making composites with tunable CTE. This could be realized by the use of PTE and NTE materials together.

CTE of selected materials are given in Table 1.1. The highest CTE values are found in polymers, especially among linear polymers, in which weak secondary intermolecular forces are present. Thermal expansion values

generally decrease from polymeric materials to ceramics. While the expansion values are in between 50×10^{-6} and 400×10^{-6} $^{o}C^{-1}$ for polymeric materials, these values decrease to 5×10^{-6} and 25×10^{-6} $^{o}C^{-1}$ for metals.

Table 1.1 CTE of selected materials [2-5].

MATERIALS	α (x 10^{-6} $^{o}C^{-1}$)
Polymers	
Polyethylene	106-198
Polypropylene	145-180
Polystyrene	90-150
Teflon	126-216
Nylon 6,6	144
Metals	
Al	23.6
Cu	17.0
Au	14.2
Fe	11.8
Ni	13.3
W	4.5
Invar	1.6
Ceramics	
Al_2O_3	7.6
Fused SiO_2	0.4
α-ZrW_2O_8	-8.7
MgO	13.5

Stronger atomic bonds in ceramic materials make the expansion values smaller than that of metals and polymers. CTE values for ceramics can be divided into four categories [3]:

(i)   Negative thermal expansion $\alpha < 0 \times 10^{-6}$ °C

(ii) Very low expansion $0 < \alpha < 2 \times 10^{-6}$ °C

(iii) Low expansion $2 < \alpha < 8 \times 10^{-6}$ °C

(iv) High expansion $\alpha > 8 \times 10^{-6}$ °C

AX_2O_8 (A = Zr, Hf; X= W, Mo) family of materials shows isotropic negative thermal expansion up to elevated temperatures. Among them, ZrW_2O_8 is the most famous one and it shows large isotropic negative thermal expansion in a wide range of temperatures from 0.3 to 1050 K [6-9]. ZrW_2O_8 is produced mainly in two ways; solid state reaction methods (direct synthesis from oxides and salts) [10-15] and wet chemical techniques (combustion, sol-gel, precipitation, and hydrothermal) [12, 16-31]. In the solid state reaction methods, the disadvantages are; (i) inhomogenity in mixing, (ii) necessity of multiple grinding and re-heating steps, and (iii) need for crystallization at high temperatures for long times. On the other hand, chemical homogeneity at the atomic and/or nano scale, and nucleation/growth of the primary colloidal particles can be controlled better in wet chemical techniques. ZrW_2O_8 can be synthesized either at high temperature or low temperature after the production of its precursor by one of the wet chemical techniques. In the high temperature approach, ZrW_2O_8 can be crystallized at temperatures like 1130-1180 °C, but then it has to be quenched in order to prevent its decomposition. From Figure 1.1, it can be seen that ZrW_2O_8 is stable only from 1105 to 1257 °C. Because of this reason, it is necessary to apply a quenching step from elevated temperatures rather than slow cooling in a furnace. If this is not applied, ZrW_2O_8 will decompose into ZrO_2 and WO_3 below 1105 °C. Additionally, WO_3 volatilizes easily over 1105 °C. Since there is no solubility limit for ZrW_2O_8, any shift from stoichiometry (W:Zr = 2:1)

would decrease the phase purity. Furthermore, due to partial sintering of precursor particles at these high crystallization temperatures, the resulting particles are almost always several micrometers in size. Therefore, wet chemical precursor synthesis methods need to be modified such that the products can be crystallized at relatively low temperatures.
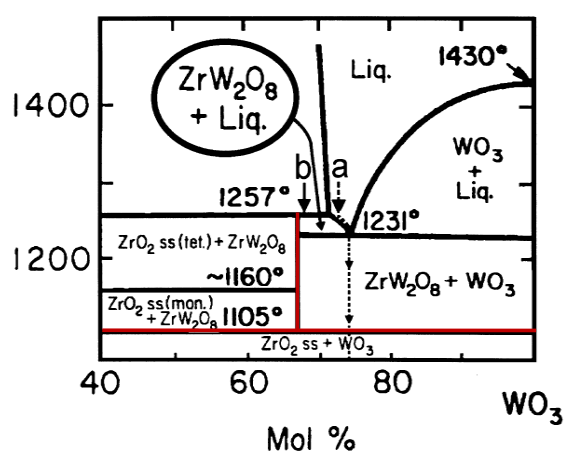
Figure 1.1 ZrO_2-WO_3 binary phase diagram [13].

ZrW_2O_8 particles with sizes in the submicrometer range can only be produced by low-temperature crystallization of precursors produced by precipitation or hydrothermal ageing. With their conditioned chemistries, crystallization temperature can be kept below 800 $^{\circ}$C for these precursors. In order to produce ZrW_2O_8 at 600 $^{\circ}$C or lower temperatures, 7 days to 3 weeks of ageing times [12, 16] below 100°C for sol-gel, and 1-2 days of ageing times [17, 29] at 160-180 $^{\circ}$C for hydrothermal methods have been reported. Without exception, the commonly used tungsten sources (ammonium meta/para tungstate and tungsten chloride) in wet chemical methods have been the costly alternatives.

4

Isotropic negative thermal expansion material ZrW_2O_8 is expected to have several application areas. It can be used in prospective ZrW_2O_8-ceramic, ZrW_2O_8-metal, and ZrW_2O_8-polymer composites. Such composites can potentially be used in satellite optics/mirrors (focal point alignment), sensor shields, electronic devices, dental prostheses, seals (fuel cell), shock absorbers, and thermal barrier coatings [2]. By adjusting the volume fractions of the respective components, feasibility of production of composites with tunable and even zero CTE have been demonstrated.

In this study, a novel precipitation technique was developed to synthesize ZrW_2O_8 precursors. The technique was based on use of a low cost tungsten source (tungstic acid – TA), and a total of two days of ageing below 100 ^{o}C was adequate for crystallization of the precursors at low temperatures. Calcination at 600 ^{o}C for crystallization of cubic ZrW_2O_8 submicrometer particles from the obtained precursors was followed by its use in ceramic-ceramic composite production. As a PTE ceramic material, granulated particles of a commercial zirconium oxide (zirconia-ZrO_2) was used. Conventional sintering and spark plasma sintering (SPS) methods were used for the production of tunable thermal expansion composites. Use of SPS method in sintering of ZrW_2O_8-ZrO_2 composites for the first time was another novelty investigated within the framework of this study.

CHAPTER 2

LITERATURE REVIEW

In this chapter, crystal structure of ZrW_2O_8 and cause of negative thermal expansion behavior are briefly described. Available particle synthesis and composite production methods are summarized. Phase changes induced by temperature and pressure are also discussed due to their importance in understanding challenges of the use of ZrW_2O_8 in composite applications.

2.1 ZrW_2O_8: Crystal Structure and Origin of Negative Thermal Expansion (NTE)

Thermal expansion is described as the change of geometrical parameters, length and volume, of the materials with temperature. It can be positive as well as negative depending on the structure and strength of the type of bonds in a material. As indicated in Table 1.1, ceramics have lower expansion coefficients than those of metals and polymers. Ceramics with low CTE also have relatively stronger interatomic forces. Since ceramics are brittle and may undergo fracture, they should have isotropic low thermal expansion to resist the thermal shocks.

CTE of a solid material is closely related to interatomic potentials. If the bonds are strong, interatomic potentials have smaller values, and narrow and symmetrical potential energy curve are obtained as given in Figure 2.1.a [5].

Therefore, vibration shows more harmonic behavior and so affects the interatomic distance less. As the harmonic vibrations are obtained, average distance between two atoms does not change much with the increase of temperature. However, interatomic potential functions are not harmonical in real cases. Therefore, average distances between two atoms increase with temperature, which results in PTE (Figure 2.1.b) [5].
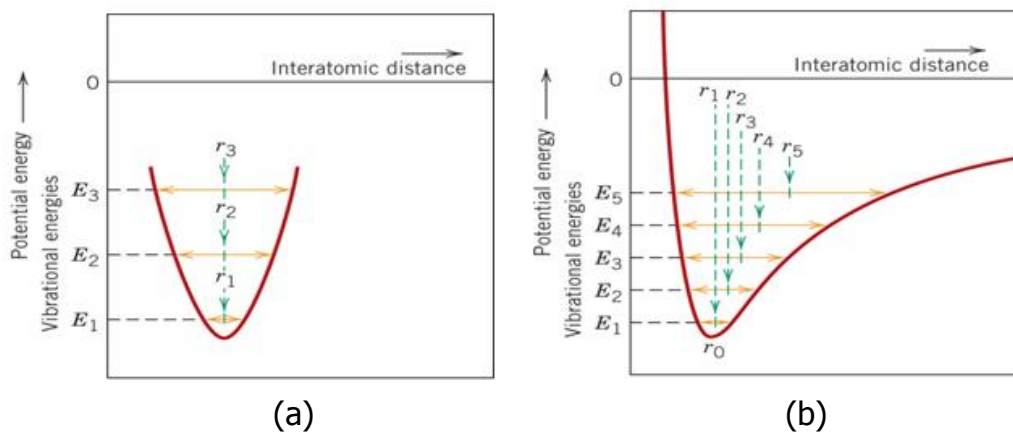
Figure 2.1 Plot of potential energy versus interatomic distance (a) harmonic oscillator and (b) non-harmonic oscillator [5].

If the materials have stronger atomic interactions, therefore stronger bonds, in their crystal structures, they have generally low or NTE coefficients.

Although stronger bonds affect the expansion coefficient of the materials, there are some additional mechanisms that play an important role on NTE mechanism for certain families of materials. Atomic vibrations of the materials occur mainly in two directions, longitudinal and transversal. These two mechanisms are presented in Figure 2.2. If the materials show longitudinal vibration with temperature increase, the vertical distance between the two atoms increase, therefore PTE is observed in the material.

On the other hand, transversal vibration of the atoms may causes a decrease in distance between two atoms, so NTE can be observed [33].
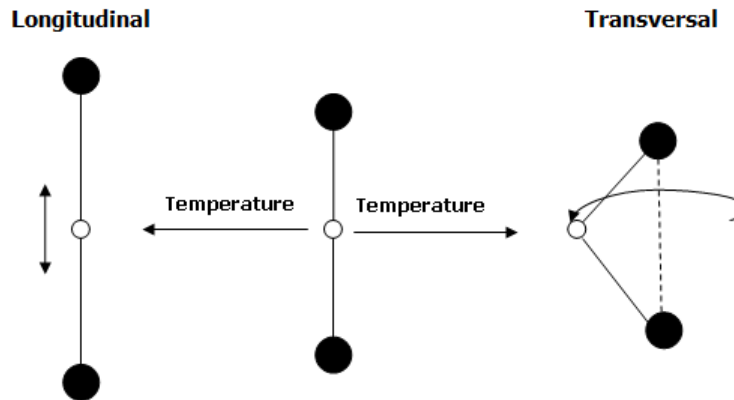
Figure 2.2 Longitudinal and transversal vibration modes [33].

ZrW_2O_8, a NTE material over a wide range of temperature, belongs to AX_2O_8 (A = Zr, Hf; X= W, Mo) family of materials. This family shows negative thermal expansion because of transversal vibration of oxygen atom in M-O-M (M: metal and O: oxygen) linkages, W-O-Zr in this case [33]. Vibration of the oxygen atom is perpendicular to the strongly bonded W-O-Zr linkage, therefore the distance between W and Zr decreases. In Figure 2.3, global lattice shrinkage is illustrated. As the temperature increases (from Figure 2.3.a to 2.3.b) vibration of the oxygen atom and the angle θ will increase. Therefore crystal lattice will deform such that this results in an effective bond shortening in the unit cell [34-35]. If this shortening is greater than the thermal expansion of individual polyhedral units, a net negative thermal expansion will be observed in the overall structure.
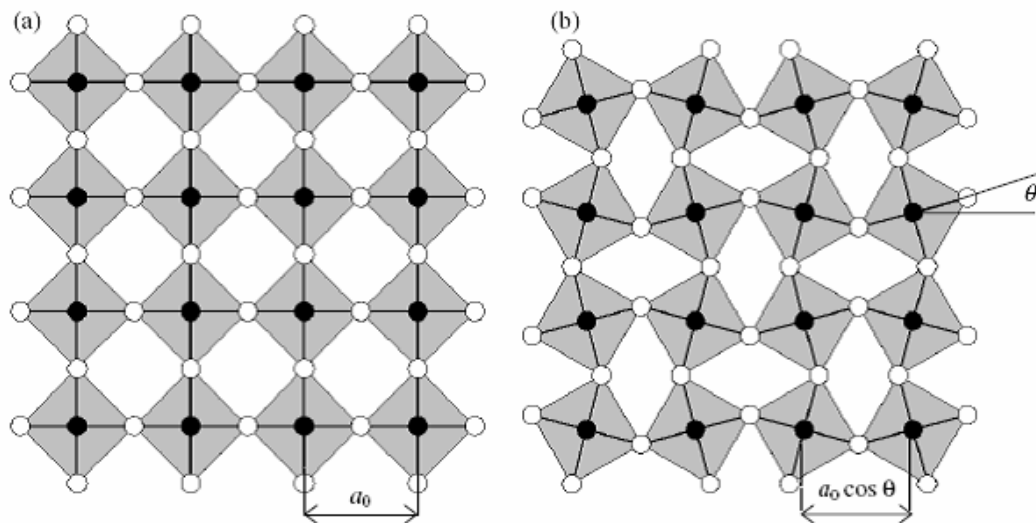
Figure 2.3 Schematic representation of global lattice shrinkage with temperature increase [34, 36].

There are some conditions to have this type of negative thermal expansion mechanism [33];

1. There should be a high M-O covalency (M = W^{6+}, V^{5+}, Si^{4+}) because of the necessity of strong M-O bonds.
2. Coordinate oxygens should vibrate transversally.
3. There should be an open framework structure to support these transverse vibrational modes with low-energy.
4. All metal ions should be coordinated with oxygen atoms. Therefore, there should be no interstitial cations.
5. For lower symmetry and lower volume structures, displacive phase transitions are needed.

AX_2O_8 family of materials, and so ZrW_2O_8, meet these requirements and they show isotropic NTE.

9

ZrW_2O_8 was first synthesized by J. Graham et al. in 1959 by heating a mixture of ZrO_2 and WO_3 together at 1200^oC followed by quenching [11]. Cage structure of ZrW_2O_8 consists of ZrO_6 octahedra and WO_4 tetrahedra. In the structure ZrO_6 octahedrons share all corners with six WO_4 tetrahedrons, whereas WO_4's share only 3 of its 4 oxygens with adjacent ZrO_6. Therefore, one oxygen atom remains unshared [37]. The crystal structure at room temperature is illustrated in Figure 2.4.
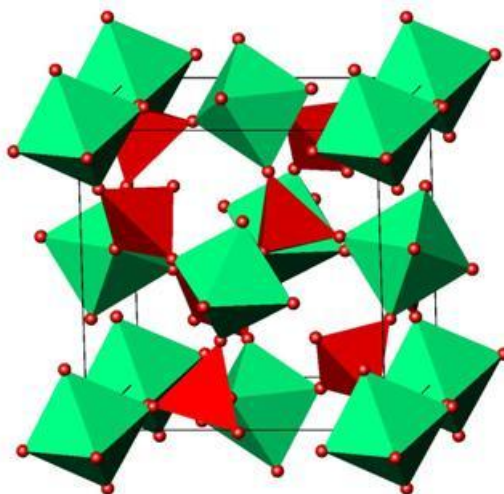
Figure 2.4 Crystal structure of ZrW_2O_8. WO_4 tetrahedrons and ZrO_6 octahedrons are shown in red and green, respectively. Oxygen atoms at the corners are shown as red spheres [36].

In the WO_4 tetrahedron, one oxygen atom is terminal and the arrangement of the WO_4 groups is such that pairs of tetrahedra are positioned along the main three-fold axis of the cubic unit cell with an asymmetric W$\cdots$O–W bridge. Because of this geometry, the distance between W and terminal O is 1.7 Å, whereas the distance between this terminal O and adjacent W is 2.4 Å. Therefore, vibrations of the bridging oxygen atoms in the rigid open framework structure of the ZrW_2O_8 result in NTE [38]. Additionally, a

transversal vibration of O atoms in W-O-Zr linkages promotes NTE behavior. It was found that unit cell parameter is reduced from 9.3 Å to 8.8 Å without any deformation of the polyhedra [36] (Figure 2.5).

(a) 9.3 Å Cell Edge   (b) 8.8 Å Cell Edge
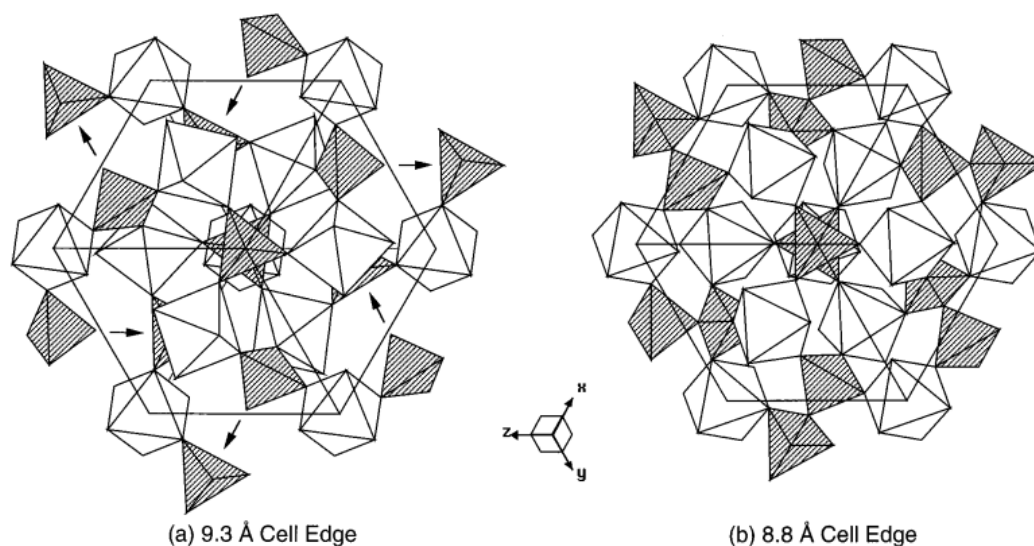
Figure 2.5 Idealized structures down the [111] axis. The arrows in (a) show motion of the WO_4 tetrahedra (shaded) after, (b) tilting of ZrO_6 octahedra (unshaded) [36].

Refined structural parameters, space group and lattice parameters of ZrW_2O_8 are given in Appendix A.

2.2 ZrW_2O_8 Synthesis Methods

In the literature, several methods have been reported on the synthesis of ZrW_2O_8 particles. These methods can be divided into two main parts; solid state reaction methods, and wet chemical techniques. In these two main topics, there are different production techniques which can be listed as;

11

Solid state reaction methods

    (i)   Direct synthesis from oxides [10-15]

    (ii) Direct synthesis from salts [10-15]

Wet chemical techniques

    (i)   Combustion [12, 30, 39]

    (ii) Sol-gel [18-22, 24, 27]

    (iii) Precipitation [12, 16, 25-26]

    (iv) Precipitation followed by hydrothermal ageing [12, 16-17, 23, 28-29, 31]

Precursors produced by direct synthesis from oxides, direct synthesis from salts, combustion, and several sol-gel methods necessitates a heat treatment for crystallization at temperatures higher than 1100 ^{o}C. Being close to its melting point, even minutes spent at this temperature can be expected to yield large particle sizes in the final ZrW_2O_8 products. Indeed, a sub-micrometer particle size have never been reported in the cases these methods were used. On the contrary precipitation, hydrothermal ageing and some modified sol-gel methods permit the crystallization of precursors at temperatures as low as 600 ^{o}C. Preservation of precursor particle sizes and their distributions has been the key for production of particles with submicrometer sizes and homogeneous distributions.

2.2.1 Solid state reaction methods

Solid state reaction can also be called as dry media reaction and/or solventless reaction which means that the reactants are chemically reacting with each other in the absence of a solvent.

In order to produce ZrW_2O_8, tungsten and zirconium sources are required with the right stoichiometry (i.e. tungsten to zirconium ratio should be 2/1). Two main variations have been reported; synthesis from oxides [10-15], and synthesis from salts [12].

(i) Synthesis from oxides

In this method, WO_3 and ZrO_2 are used as tungsten and zirconium sources, respectively. All studies show that ZrW_2O_8 can be produced from a stoichiometric mixture of ZrO_2 and WO_3. Typically, mechanically or manually ground oxide particles are placed in a platinum crucible and then, different heat treatment procedures are applied (Figure 2.6). Graham et al. synthesized cubic ZrW_2O_8 for the first time in 1959 by applying the procedure at 1200 ^{o}C followed by a quenching step [11]. While Kameswari and coworkers applied the same method, but for 18 hours with intermittent quenching and regrinding steps [12], Kowach et al. used a different method, in which powders were calcined at 1300 ^{o}C for 2 hours. This was followed by a temperature decrease to 1230 ^{o}C at a rate of 0.5 ^{o}C/h and a quenching step from that temperature [13]. Chen et al. [10] and Nishiyama et al. [15] chose to use a dry pressing step to prepare the mixture of WO_3 and ZrO_2. Calcination of pellets was carried out at around 1200 ^{o}C for several hours.

(ii) Synthesis from salts

In the literature, there is only one study for direct synthesis from salts. Solid state reaction methods are usually applied by using the oxides. Kameswari et al. used ammonium metatungstate (AMT) and zirconium oxynitrate (ZrOn) as tungsten and zirconium sources, respectively. Like in the case of direct

synthesis from oxides, after a grinding step heat treatment was applied for 6 hours at 1200 $^{\circ}$C (Figure 2.6) [12].
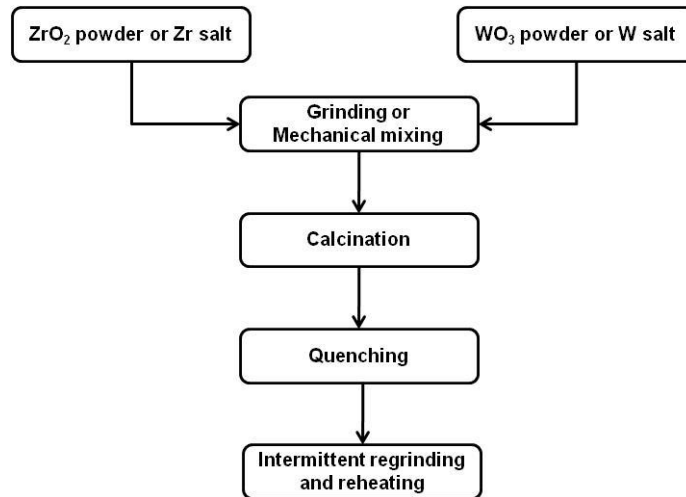
Figure 2.6 Flow chart of solid state reaction methods.

Even though, solid state reaction methods are widely used in the synthesis of ZrW_2O_8, there are some drawbacks;

- Since W and Zr are mixed in solid state, mixing in atomic level cannot be achieved and this increases the diffusion paths.

- High heat treatment temperatures and long processing times are needed to start a chemical reaction between W and Zr.

- Since diffusion distances are long, additional grinding and reheating steps are usually needed.

- Use of high calcination temperatures in the production step increases the risk of W volatilization. Since W:Zr stoichiometry cannot be preserved, phase purity of the product is generally affected negatively. In order to solve this problem, use of excess W source [13] or closed platinum crucibles have been offered [10].

- Particle sizes of the resulting products are several micrometers in size because of high calcination temperatures.

14

2.2.2 Wet chemical techniques

In order to overcome the disadvantages of solid state reactions, wet chemical techniques, which are combustion [12, 30, 39], sol-gel [18-22, 24, 27], precipitation [12, 16, 25-26] and hydrothermal methods [12, 16-17, 23, 28-29, 31] are used. In these techniques, reactants are dissolved in a solvent before any mixing step. Although an atomic level mixing homogeneity can be achieved in solution, there are certain disadvantages, which will be described in the following sections.

(i) Combustion

Kamaswari et al. and Yang et al. used the same combustion procedure except the starting chemicals and applied temperatures in some steps. AMT and ZrOn or zirconium oxychloride (ZrOc) were used as W and Zr sources, respectively. First, stoichiometric amounts of tungsten and zirconium salts were dissolved in separate 3 N nitric acid solutions and then these solutions were mixed quickly to prevent any precipitation. Upon the addition of urea and boric acid, mixture was stirred in a Pyrex container which was placed in a furnace preheated to 773-775 K. After evolution of gases, temperature rose to 1325-1475 K in a very short time and then rapidly decreased down to 773 K. Combustion synthesis is relatively faster than any other method; however XRD patterns showed that it was not possible to produce a single phase product. Therefore, an additional 30 to 60 minutes heating at 1473 K was applied to obtain single phase ZrW_2O_8. Nevertheless this high temperature treatment caused an expected growth in the sizes of the particles [12, 30].

(ii) Sol-gel

Sol-gel method can be described as synthesis of inorganic materials from colloidal solutions produced by hydrolysis of metal alkoxides. Starting solution acts as a precursor for the network structure (gel), which contains both liquid phase and solid phase. Therefore, starting chemicals determine the properties of the final product.

In the literature, used sol-gel methods can be divided into two main classes; hydrolitic sol-gel [18-20, 22], and non-hydrolitic sol-gel [21, 24, 27]. Detailed summary of the methods reported in the literature can be followed from Table 2.1. Some of the drawbacks of solid state methods can be overcome by using the sol-gel technique. These advantages can be listed as;

- Mixing homogeneity achieved at the atomic level,
- Ease of control over the growth and nucleation of primary particles,
- Elimination of the multiple grinding and reheating steps.

Particle sizes observed were generally in the micrometer ranges among the products derived from sol-gel solutions those had a precursor pH that is higher than 2 in the literature. This points to the fact that pH would be an important parameter in intervening the chemistry of the solutions that are to be used in wet chemical methods. Smallest reported ZrW_2O_8 particles were obtained by Kanamori and coworkers at 450 ^{o}C [21]. However, it is important to note that they had used a non-hydrolitic sol-gel method, in which the starting chemicals were toxic and inert gas use was indispensible in solution preparation steps.

Table 2.1   Studies on sol-gel method in the literature.

Author	Title	Method	Chemicals	Experimental	Results
Wilkinson et al. [27]	A New Polymorph of ZrW_2O_8 Prepared Using Nonhydrolytic Sol−Gel Chemistry	Non-hydrolytic Sol−Gel	WCl_6 (tungsten chloride) $Zr(OiPr)_4.iPrOH$ (zirconium isopropoxide)	➢ WCl_6 and $Zr(OiPr)_4.iPrOH$ was dissolved in $CHCl_3$ and THF-diisopropyl ether, respectively. ➢ Zr soln. was added to W soln. and stirred for 1 hour. ➢ Mixture was cooled in liq. nitrogen and sealed. Then, was heated at 110 ^{o}C for 7 days. ➢ ZrW_2O_8 raw gel was heated at 500, 600, 740 and 1200 °C.	➢ No crystallization was obtained at 600 ^{o}C. ➢ Crystallization started at 740 ^{o}C (trigonal ZrW_2O_8) ➢ Cubic ZrW_2O_8 was obtained at 1200 ^{o}C with impurity as well as at 700 ^{o}C with the use of suitable seeds.
Lind et al. [24]	Seeding and the Non-Hydrolytic Sol-Gel Synthesis of ZrW_2O_8 and $ZrMo_2O_8$				
Kanamori et al. [21]	Preparation and Formation Mechanism of ZrW_2O_8 by SolGel Process		WCl_6 $ZrOCl_2$ (ZrOc-zirconium oxychloride)	➢ WCl_6 and ZrOc was dissolved in buthanol and buthanol-ethanol, respectively ➢ W and Zr sources was mixed under nitrogen atmosphere to prevent hydrolysis of W. ➢ pH was lower than 1 ➢ Mixture was aged for 3 days at room temperature. ➢ Precursor was calcined at 450 ^{o}C for 12 h	➢ Crystallization of amorphous precursor depended on the heat treatment. ➢ 50-300 nm ZrW_2O_8 was obtained.

Table 2.1   Studies on sol-gel method in the literature (continued).

Author	Title	Method	Chemicals	Experimental	Results
De Buyyser et al. [18]	Aqueous sol-gel processing of precursor oxides for ZrW_2O_8 synthesis	Hydrolytic Sol−Gel	$(NH_4)_6H_2W_{12}O_4$ (AMT-Ammonium metatungstate)	➢ Aqueous W and Zr sources were mixed. ➢ Citric acid (CA) to avoid precipitation of Zr^{4+} and NH_4OH was added. ➢ pH was greater than 7. ➢ Mixture was aged 1 day at 60 ^{o}C ➢ Precursor was calcined at 700-800 ^{o}C for 12 hours and sintered at 1180 ^{o}C for 5-12 hours.	➢ In the high CA/Zr, no precipitation was observed at pH<1 or pH>7. ➢ Particle sizes of ZrW_2O_8 were 11-30 μm.
De Buyyser et al. [19]	EDTA assisted sol-gel synthesis of ZrW_2O_8		$ZrOCl_2$	➢ Zr-EDTA and W-EDTA solutions were and mixed. ➢ pH of the precursor was 4 ➢ Gelation was done at 60 ^{o}C for 12 h ➢ Precursor powders were sintered at 1180 ^{o}C for 2 hours	➢ Homogeneous precursor gel was obtained. ➢ Direct transform from precursor gel to pure ZrW_2O_8 was achieved
Khazeni et al. [22]	A Precursor for Synthesis of Zirconium Tungstate		H_2WO_4 (TA-tungstic acid) $Zr(CH_3COO)_4$ (ZrAc-zirconium acetate)	➢ Ammonia was used to dissolve TA in water. Then, aqueous Zr soln. was added. ➢ Soln. was aged for different times (0.5-16 hours) ➢ 2 step heat treatment was applied. Powders were calcined at 600 ^{o}C for 3 hours. Then pressed and calcined again at 1200 ^{o}C for 4 hours.	➢ Phase pure cubic ZrW_2O_8 was synthesized by using max. 7 hours ageing. ➢ As the ammonia conc. increased, product became relatively pure. ➢ Particle sizes were 8-10 μm.

(iii) Precipitation

Chemicals used in precipitation method have been AMT and ZrOc as tungsten and zirconium sources, respectively. pH values are kept relatively low (lower than 1) in this method compared to sol-gel methods described above. Studies based on precipitation method are summarized in Table 2.2. Besides the advantages similar to that of sol-gel method, there are some additional advantages which could be given as follows;

- Heat treatment temperatures and durations for crystallization are relatively low.
- Particle sizes, size distributions and morphologies can be controlled with better precision.

It can be argued that, due to the low pH values attainable in the precursors, the diffusion distances between W in Zr ions in the precipitates decrease such that it becomes possible to crystallize ZrW_2O_8 at low temperatures like 600 ^{o}C. Although precipitation method is easier to conduct compared to non-hydrolytic sol-gel method, long ageing times (1-3 weeks) and the use of high cost chemicals are the most important drawbacks. In the literature, ageing under hydrothermal conditions have been offered to decrease the ageing durations needed in the precipitation method [12, 16].

Table 2.2 Studies on precipitation method in the literature.

Author	Title	Method	Chemicals	Experimental	Results
Closmann et al. [16]	Low-Temperature Synthesis of ZrW_2O_8 and Mo-Substituted ZrW_2O_8	Precipitation	AMT	➢ Aqueous W and Zr sources were mixed for 10 hours. ➢ 6M HCl was added for final [HCl]=3M and the solution was refluxed for 2 days.	➢ ZrW_2O_8 crystallization was achieved at 600 ^{o}C. ➢ Average particle sizes were 10 μm.
Kamaswari et al. [12]	Rapid synthesis of ZrW_2O_8 and related phases, and structure refinement of $ZrWMoO_8$		ZrOc	➢ pH of precursor was lower than 0. ➢ After refluxing, 7 days to 3 weeks ageing was applied at room temperature. ➢ After filtering the precursor, powder was calcined at 600 ^{o}C for 10 hours.	➢ **In order to decrease the ageing time, hydrothermal method was used.**

(iv) Precipitation followed by hydrothermal ageing

Hydrothermal conditions that can be created in pressurized vessels have been widely used in the synthesis of single crystal particles of ceramics from high-temperature aqueous solutions. With the aid of high temperature and pressure conditions, crystallization can be initiated while the solid precursor phases still remain in their mother liquor which can be prepared under ambient conditions before hydrothermal conditioning. Recently, many studies, in which production of submicrometer-sized ZrW_2O_8 is achieved by use of a hydrothermal ageing method with lower ageing times, have appeared in literature [12, 16-17, 23, 28-29, 31]. In these methods, applied procedure is almost same as in the precipitation method except that the prepared solution is fed into a hydrothermal vessel instead of refluxing it at temperatures lower than 100 ^{o}C for long durations. Resulting particles are reported to take on generally a nanorod-like morphology. A flowchart of the modified ageing process can be seen in Figure 2.7. Starting chemicals have been selected from ZrOc or ZrOn, and AMT or sodium tungstate (NaT). After combining aqueous solutions of Zr and W sources the mixtures were generally stirred for some time before different acids were added at different concentrations. Hydrothermal ageing of the prepared solutions were continued for 1 to 72 hours between 160 and 200 ^{o}C's. XRD patterns of the filtered products showed a crystalline precursor powder which is identified as $ZrW_2O_7(OH)_2(H_2O)_2$ can be obtained under the described conditions. On the other hand, calcination at 300-650 ^{o}C was still needed for isomorphic phase transition to cubic ZrW_2O_8. Without exception, in all these studies, it was shown that crystallinity of the final products strongly depends on the acid concentration used in the precursor. As the acid concentrations were decreased, precursors remained amorphous and ZrW_2O_8 crystals could not be obtained even after heat treatment. Conversely, too high acid concentrations restricted the crystallization of the precursors [17, 23, 28-29].

21

In addition to these, it was recently found that the type of acid can affect the morphology of the final particles [23]. However, crystallization was observed to be much faster in the case of HCl additions [17].
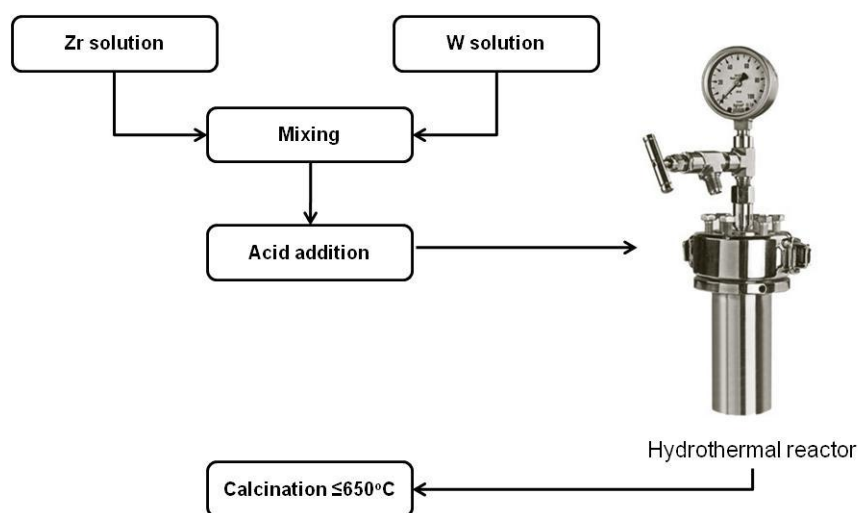
Figure 2.7 Flow chart of hydrothermal method.

Although ageing under hydrothermal conditions is a promising alternative to produce ZrW_2O_8 nano particles in relatively short times, it has some disadvantages. The use of starting chemicals with relatively high cost is the common disadvantage that was also noted for other methods. In addition, hydrothermal methods are generally avoided if possible, due to the potential problems that arise in the scale-up of these processes. The extremely acidic conditions that need to be maintained in ZrW_2O_8 production pose an additional problem. Use of Teflon lined vessels is one solution for protection of metallic vessels against high pressure, temperature, and acidic corrosion. Nevertheless this does not alleviate, but in fact aggravate the foreseen problems in scale-up.

The chemistry of ZrW_2O_8 precursors is complicated due to complex structures of especially tungsten ions in aqueous medium. If the long ageing durations that had been needed in precipitation methods could be lowered to values similar to those used in the hydrothermally aged precursors, scale-up of precipitation methods would take on a faster pace. If this could be achieved also with low cost starting chemicals, it would become easier to envision and work on the many applications areas, in which ZrW_2O_8 could be used.

2.3 Use of ZrW_2O_8 in Composites

ZrW_2O_8 composites are produced mainly by the conventional dry-pressing and sintering method [30, 40-52]. Kanamori and coworkers were first to try spark plasma sintering (SPS) of ZrW_2O_8 and ZrW_2O_8-SiO_2 composites, in which ZrW_2O_8 was the main phase [1, 53]. In the next sections, the studies on ZrW_2O_8-ceramic composites will be summarized, and a brief background on SPS method will be given.

2.3.1 Conventional sintering

In conventional methods, besides simple mixing techniques, also in-situ reactive sintering with excess ZrO_2 has been used. The composite systems that have been studied are; ZrW_2O_8-cement [40], ZrW_2O_8-copper [41-43], ZrW_2O_8-magnesium [44], ZrW_2O_8-polymer [45-46], ZrW_2O_8-$Zr_2WP_2O_{12}$ [52], and ZrW_2O_8-ZrO_2 [30, 47-51]. In Table 2.3, the studies on ZrW_2O_8-ZrO_2 system are given with the SEM micrographs taken from the composite surfaces. The table also includes the two studies in which SPS method was used. Alumina (Al_2O_3) was used as a sintering agent in some of these

systems. With the aid of liquid phase forming, densities were increased to 90% of the theoretically calculated values [30, 49-50]. The reason for using alumina as a sintering agent is the reaction between alumina and WO_3. The phase diagram is given in Figure 2.8 [54]. It was later proved that this reaction can actually occur at a different chemical ratio of alumina and WO_3 from what is given in the phase diagram [55]. Since the amount of alumina used in the composites was below the detection limits, whether the liquid phase forming was $2Al_2O_3 \cdot 5WO_3$ or $Al_2(WO_4)_3$ could not be determined from XRD patterns. The minimum temperature for liquefaction is 1190 $^{\circ}$C according to the phase diagram given in Figure 2.8. However, this temperature was detected as 1135 $^{\circ}$C in one of the studies [55]. Because of this reason, a sintering performed at 1190 $^{\circ}$C would certainly has the potential to provide the desired liquid phase that would help in sintering and increasing the density of the composites.

Studies also showed that the optimum amount of sintering agent is in the range of 0.07-0.35 w/o. Cases in which higher amounts of Al_2O_3 were used, $Al_2(WO_4)_3$ phase was started to be observed in the XRD patterns [30, 49].

Table 2.3   Studies on ZrW_2O_8-ZrO_2 composites, and ZrW_2O_8, ZrW_2O_8-SiO_2 composites sintered with SPS method.
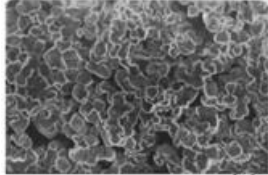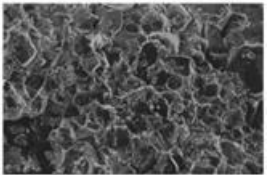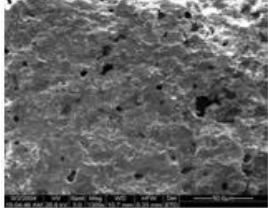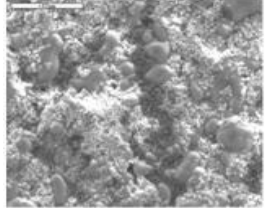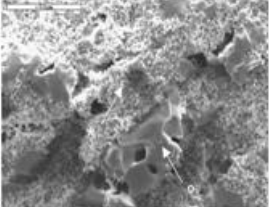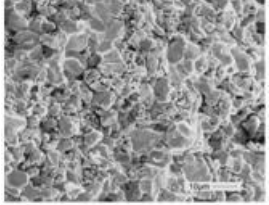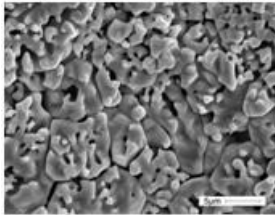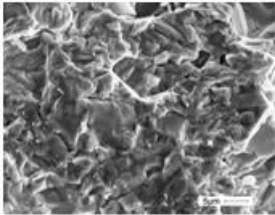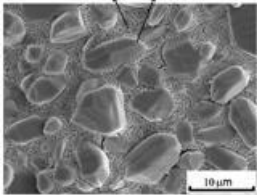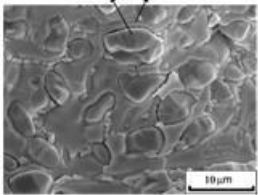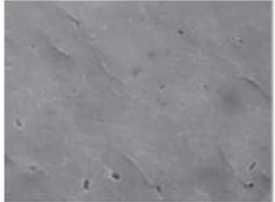
Author	Title	Method	Product	SEM Micrographs
Niwa et al. [49]	Preparation of Dense ZrW_2O_8/ZrO_2 Cosintered Ceramics with Controlled Thermal Expansion Coefficients	Mixing-sintering	ZrO_2-ZrW_2O_8 composite (*Al$_2$O$_3$ as sintering agent*)	without sintering agent with sintering agent
De Buyyser et al. [47]	ZrO_2-ZrW_2O_8 Composites with Tailor-made Thermal Expansion	In-situ reaction and mixing-sintering	ZrO_2-ZrW_2O_8 composite	conventional method in-situ reaction
Lommens et al. [48]	Synthesis and Thermal Expansion of ZrO_2/ZrW_2O_8 Composites	Mixing-sintering	ZrO_2-ZrW_2O_8 composite	
Yang et al. [51]	In Situ Synthesis of ZrO_2/ZrW_2O_8 Composites with Near-Zero Thermal Expansion	In-situ reaction	ZrO_2-ZrW_2O_8 composite	

Table 2.3 Studies on ZrW_2O_8-ZrO_2 composites, and ZrW_2O_8, ZrW_2O_8-SiO_2 composites sintered with SPS method (continued).

Author	Title	Method	Product	SEM Micrographs
Yang et al. [30]	Synthesis of ZrO_2/ZrW_2O_8 Composites with Low Thermal Expansion	Mixing-sintering	ZrO_2-ZrW_2O_8 composite (*Al_2O_3 as sintering agent*)	 without sintering agent with sintering agent
Sun et al. [50]	ZrW_2O_8/ZrO_2 Composites by In Situ Synthesis of ZrO_2+WO_3: Processing, Coefficient of Thermal Expansion, and Theoretical Model Prediction	In-situ reaction	ZrO_2-ZrW_2O_8 composite (*Al_2O_3 as sintering agent*)	 without sintering agent with sintering agent
Kanamori et al. [53]	Spark Plasma Sintering of Sol–Gel Derived Amorphous ZrW_2O_8 Nanopowder	SPS	ZrW_2O_8 alone	
Kanamori et al. [1]	Low-Temperature Sintering of ZrW_2O_8–SiO_2 by Spark Plasma Sintering	SPS	SiO_2-ZrW_2O_8 composite	No SEM
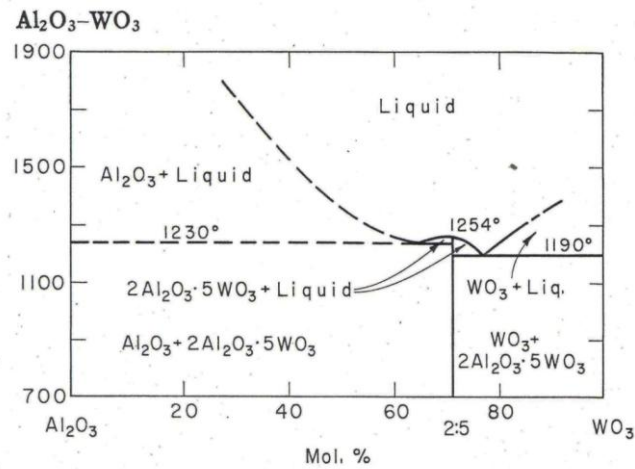
Figure 2.8 Phase relation between Al_2O_3 and WO_3 [54].

SEM micrographs in Table 2.3 show that entirely dense structures cannot be obtained in many of the studies, reasons of which can be explained by the;

- Difference in particle sizes of the oxides in composite bodies,
- Inefficiency of the mixing methods in providing a homogeneous particle mixture.

Both of these factors seem to induce formation of ZrO_2 rich regions in the to-be-sintered bodies. However, since used temperatures (below 1200 ^{o}C) can never be enough for sintering of zirconia particles among themselves, and liquid phase formation is expected to be initiated only from WO_3-rich regions at these temperatures, the limitations on densification in ZrW_2O_8-ZrO_2 system even in the presence of Al_2O_3 can be understood. Since ZrW_2O_8 decomposes to its oxides under 1100 ^{o}C, the quenching step applied in some of the particle synthesis methods should also be applied after sintering around 1200 ^{o}C. This naturally causes thermal stresses in a sintered composite body.

The alternative of simple mixing method is the use of an in-situ reaction between ZrO_2 and WO_3. In this method, ZrW_2O_8 should first form and then sintering shall commence between the remaining ZrO_2 and formed ZrW_2O_8. The main disadvantage of this method is the long sintering duration needed.

Another point that needs to be discussed is the CTE's that have been measured in these studies. By changing the quantity of positively and negatively expanding components, it was possible to produce composites with variable CTE's. The theoretically calculated CTE values according to rule of mixtures were different from those measured from the composites actually produced [30, 47-51]. This is an expected result considering the requirements of obedience to rule of mixtures [48];

- Samples should not contain any voids.
- Composite body should not have residual thermal stresses.
- Different phases of a sample should have the same elastic modulus.

Since ZrW_2O_8 and ZrO_2 particles used in these studies generally had different particle sizes, and the produced composite bodies are quenched from high temperature, it is expected to have a difference between the calculated and measured CTE values.

2.3.2 Spark plasma sintering (SPS)

SPS was another recent method that was adapted for the production of $ZrW_2O_8 - SiO_2$ composite. SPS is also called field assisted sintering technique and/or pulsed electric current sintering. SPS setups couple a direct current (DC) pulse generator that can provide high amperage with single axis compaction and vacuum capabilities. Direct current that is passed through the graphite dies enclosing the particles supplies a high heating rate, which

is on the order of minutes. During the process, a predefined pressure can be applied to the graphite die. By generating spark at the particle contacts during compaction, heat is concentrated uniformly throughout the material [56]. The fast and homogeneous nature of heating up minimizes grain growth problems and provides rapid and uniform sintering. Fully dense sintered bodies can be produced at relatively lower temperatures within shorter times compared to conventional sintering methods [1, 53, 56]. A typical SPS setup is given in Figure 2.9.
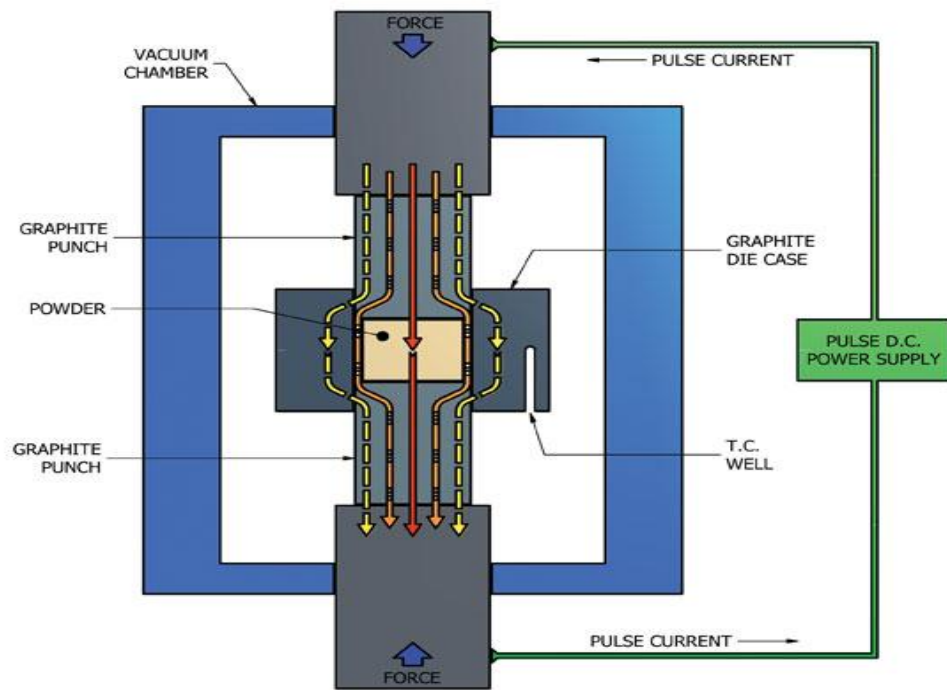
Figure 2.9   Basic components of an SPS setup [57].

There are only two studies on the use of SPS method in sintering of ZrW_2O_8 and both studies were performed by Kanamori and coworkers in 2009. While first study was on sintering of bodies that consists of only ZrW_2O_8 [53], second one was on the ZrW_2O_8-SiO_2 system [1]. ZrW_2O_8 particles used in

both studies were produced from non-hydrolytic sol-gel technique and they had the smallest sizes (50-300 nm) reported until now [21]. .

Dense (98.6%) ZrW_2O_8 bodies were obtained after 10 minutes at 600 ^{o}C in the first study [53]. Hot isostatic pressing was applied to the same particles for comparison. However, there was no sintering after 1 hour at 600 ^{o}C. For the ZrW_2O_8 – SiO_2 system, 10 minutes at 650 ^{o}C was adequate for sintering [1]. The particle size of SiO_2 was lower than 63 μm. The amounts of SiO_2 used were 15 w/o and 30 w/o and it was reported that as the SiO_2 amount increased, the density of the composite body decreased. Since the produced composites had high amounts of ZrW_2O_8, the CTE's of the composites were negative. In addition, measured CTE values were close to the calculated values from rule of mixing. This is not unexpected because composites had less porosity and since the sintering temperatures were low, there was no need for a quenching step. Therefore thermal stresses in the composites could be minimized.

To our knowledge, there is no report on the use of SPS technique in sintering of ZrW_2O_8-ZrO_2 composites.

2.3.3 Phase transition and composites

For the composite applications, it is important to take into account phase transitions that can be induced in ZrW_2O_8 with temperature and pressure. ZrW_2O_8 has mainly three different phases and their CTE values are given in Table 2.4 [58-61].

Table 2.4 CTE values of different phases of ZrW_2O_8 [58-61].

Phases	CTE value (x $10^{-6}K^{-1}$)	Temperature Range (^{o}C)
γ-ZrW$_2$O$_8$	-1.0	-253-27
α-ZrW$_2$O$_8$	-8.9	-253-157
β-ZrW$_2$O$_8$	-4.7	157-677

α-ZrW$_2$O$_8$ [20, 24, 47-48, 58, 62-63] and β-ZrW$_2$O$_8$ [47-48] are cubic compounds whereas γ-ZrW$_2$O$_8$ has been reported to have both orthorhombic (γ_o) [47-48, 58, 62] and trigonal (γ_t) symmetries [20, 24, 58, 62-63]. Because of the shifts in atomic positions in the crystal structure, all phases of ZrW$_2$O$_8$ have different CTE values. XRD pattern of α phase is given in Figure 2.10 [19]. At around 150 ^{o}C, α to β phase transition occurs with an increase in volume of the unit cell. This transition can be seen in Figure 2.11 [47].
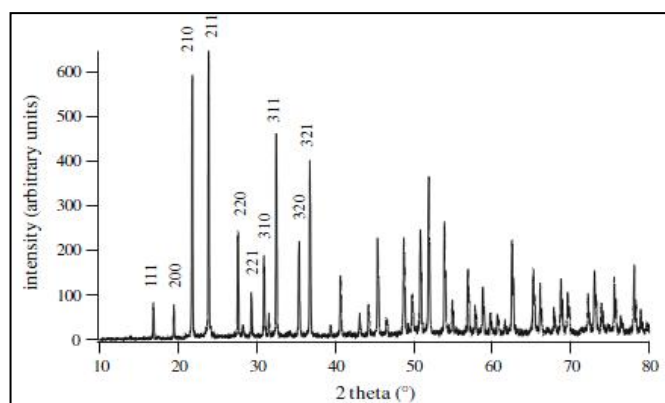
Figure 2.10 XRD pattern of α-ZrW$_2$O$_8$ [19].
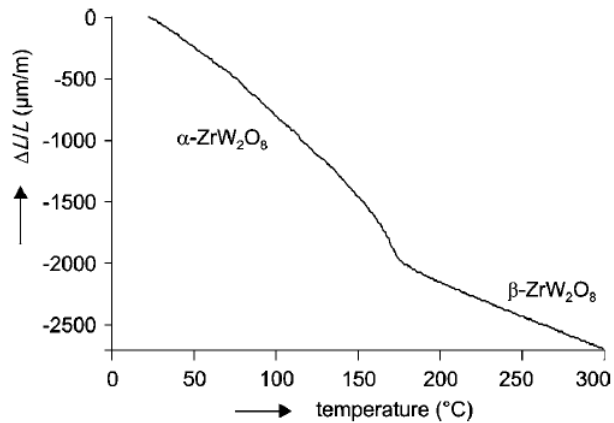
Figure 2.11 Thermal contraction of ZrW_2O_8 during a phase transition from α to β phase [47].

Another phase transition was detected to occur from α to γ_o phase at the interfaces of particles especially during the pressing of the powders in preparation of sintering the composites [47-48, 58, 62]. At room temperature, the cubic α phase is known to be stable below 0.21 GPa. However, above this pressure there is a first-order transition to γ_o phase. At low temperature, γ_o phase has a thermal expansion that is also negative, but an order of magnitude smaller than for the α phase. Lommens and coworkers showed in their study that 20% of the particles can turn into γ_o phase after pressing pure α-ZrW_2O_8 particles under 750 MPa (Figure 2.12) [48]. Figure 2.13 shows the thermal expansion curves of both $\alpha+\gamma$-ZrW_2O_8 mixture and pure α-ZrW_2O_8 [48]. Large volume expansion can be seen at 100-150 ^{o}C because of γ to α transition. Applied pressures less than 1 GPa in any processing step can be expected to cause this type of a phase transition. This should be taken into account in explaining deviations from predictions of CTE's of composites according to rule of mixtures.
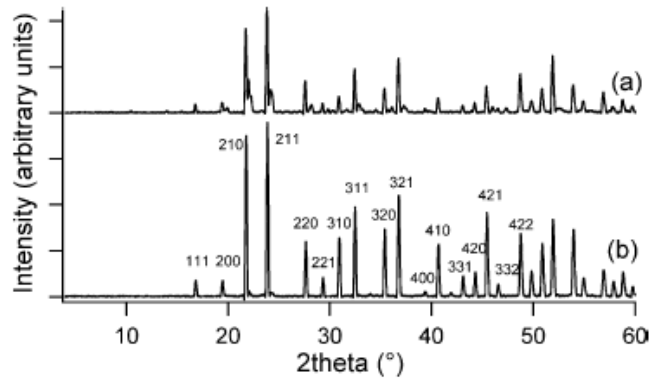
Figure 2.12 XRD patterns from (a) $\alpha+\gamma_o$-ZrW$_2$O$_8$ mixture after pressing (20% of the particles turn into γ_o), and (b) a pure α-ZrW$_2$O$_8$ phase [48]
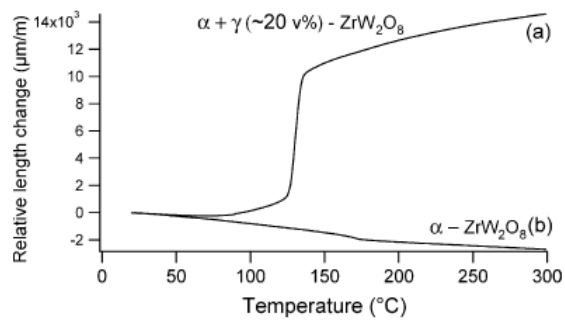
Figure 2.13 Thermal expansion curve of (a) a pressed bar containing the $\alpha+\gamma$-ZrW$_2$O$_8$ mixture and (b) a bar containing pure α-ZrW$_2$O$_8$ [48].

ZrW$_2$O$_8$ becomes amorphous under the pressures between 1.5 GPa and 3.5 GPa. Above 4.5 GPa and 800 °C , a new polymorph can be observed and it is called trigonal ZrW$_2$O$_8$ (γ_t) (Figure 2.14) [62]. γ_t can also be synthesized from aerogels. Noailles and coworkers analyzed the ZrW$_2$O$_8$ particles produced from aerogels by Thermal Gravimetric and Differential Thermal Analysis (TGA/DTA). The two exothermic peaks indicated that there can be two

33

crystal structures at 700 ^{o}C and 900 ^{o}C. Respective XRD patterns showed that γ_t was the phase at 700 ^{o}C, whereas it transformed to α at 900 ^{o}C (Figure 2.15) [63].
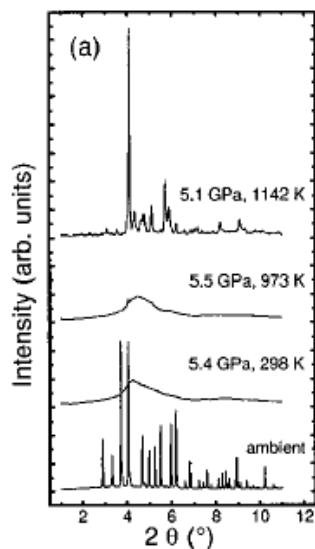
Figure 2.14 XRD patterns of α-ZrW$_2$O$_8$ at low and high temperatures under high pressure [62].
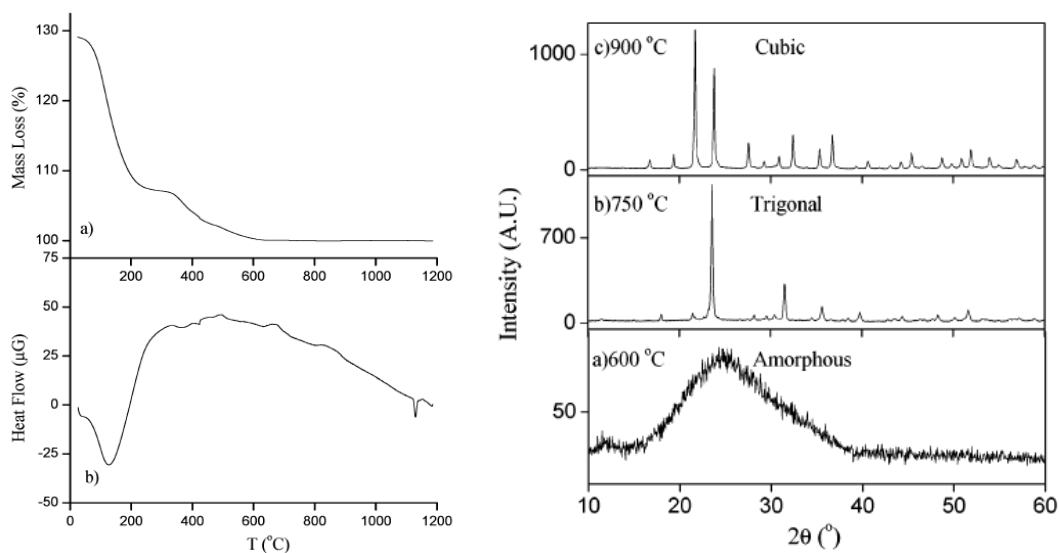
Figure 2.15 TGA/DTA (left) and XRD patterns (right) of ZrW$_2$O$_8$ aerogels [63].

α and γ phases also have different densities. Density of α is 5.08 g/cm^3, and that of γ is 5.36 g/cm^3. When pressure is released γ_o remains stable, but can transform back into α by heating at 120 °C (Figure 2.16) [48], and γ_t can be recrystallized into α at 600 °C [27]. The volume change associated with this γ to α transition is about 5% (Figure 2.17) [48, 58].
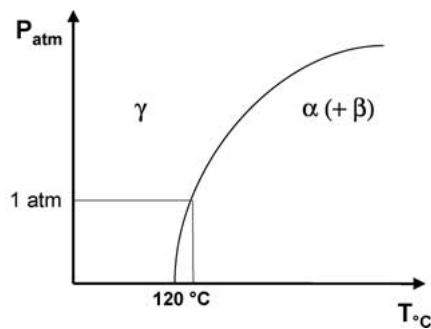
Figure 2.16 Schematic representation of the phase diagram predicted for γ_o to α transition [48].
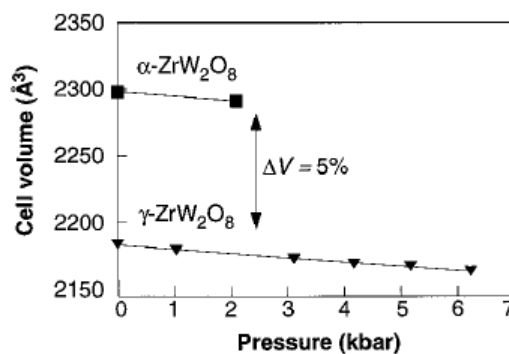
Figure 2.17 Relative volume change in the γ to α transition [58].

Phase transitions in ZrW$_2$O$_8$ are important for composite applications because each phase has a different CTE value. Even the dry pressing can potentially

35

be enough to induce an α to γ_o phase transition. During the sintering or quenching steps, one can expect higher pressures at the interfaces of composite components. This can cause amorphization or even the appearance of γ_t phase as an interphase depending on the severity of pressure. Such transitions could be reversed by proper post-treatments. Furthermore, although the phase diagram of $ZrO_2 - WO_3$ system indicates a decomposition above 800 ^{o}C as explained in previous sections, under certain conditions, there is a possibility for having different phases of ZrW_2O_8 at temperatures between 750-1105 ^{o}C. This possibility will be used in overcoming certain difficulties related to composites that are to be synthesized by SPS method in this study.

CHAPTER 3

EXPERIMENTAL

In this chapter, the materials used in this work are explained. Also given are detailed information on the novel ZrW_2O_8 precursor preparation, heat treatment procedure, and composite preparation methods. Characterization methods used in each step are also described.

3.1   Materials

Tungstic acid (TA), hydrogen peroxide (H_2O_2), zirconium oxychloride (ZrOc), and hydrochloric acid (HCl) are the materials used for the ZrW_2O_8 precursor preparation. Zirconium oxide (zirconia-ZrO_2), isopropyl alcohol (IPA), polyvinylpyrrolidone (PVP), and aluminum oxide (alumina-Al_2O_3) are used for composite preparation.

3.1.1 Tungstic acid (TA) and hydrogen peroxide (H_2O_2)

In all wet chemical techniques, ammonium meta/para tungstate and/or tungsten chloride have been used as tungsten sources. These sources are generally used after dissolving them in water. TA is the first leach product of traditional tungsten mining. All the other tungsten sources mentioned above are produced from TA [64] and since they are secondary products, their costs are almost always more than TA. In this study TA (Sigma Aldrich) was

selected as the tungsten source. Properties of TA and structural formula of TA are given in Table 3.1 and Figure 3.1, respectively.

Table 3.1   Properties of TA and H_2O_2 used in this study.

	TA	H_2O_2 solution
Chemical formula	H_2WO_4	H_2O_2
Molecular weight (g/mol)	249.86	34.01
Density (g/ml) (at 25°C)	5.5	1.1
Weight percent	-	30
Appearance	Yellow solid	Liquid
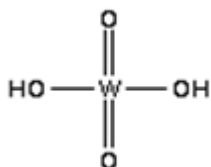
Figure 3.1   Structural formula of TA [65].

The most important disadvantage of TA is its low solubility in water. Ammonia (NH_3) is added to the aqueous solutions of TA to increase the solubility of TA. Because of the ammonia addition, the pH of the solution increases and this solution is called 'Ammoniacal Tungstic Acid (ATA)' solution [66]. To our best knowledge, there are only two studies in which ATA is used to produce ZrW_2O_8 [22, 60]. Due to the high temperatures needed for the crystallization of the 100% single phase product, particle size of the products were several μm [22].

Precursors prepared at low pH values are promising in that; their products can be crystallized at temperatures as low as 600 $^{\circ}$C which is advantageous in preserving the primary particle sizes obtained in the precursor phase. Literature on electrochromic devices based on WO_3 films provides methods of preparing clear TA solutions at low pH values. In order to dissolve TA at low pH hydrogen peroxide (H_2O_2) was used in the majority of these studies [67-71]. It is known that, at low pH, tungsten exists as polyanionic species in an aqueous solution. H_2O_2 is claimed to break down these polyanionic species of tungsten and form peroxo complexes which are simpler in structure [67]. Properties of H_2O_2 (Merck) used in this study are given in Table 3.1.

3.1.2 Zirconium oxychloride (ZrOc)

Zirconium salts or alkoxides (like zirconium oxychloride/oxynitrate, zirconium isopropoxide, and zirconium acetate) have been used as zirconium sources. In this study, ZrOc (Merck) was selected as the zirconium source. Properties and structural formula of ZrOc are given in Table 3.2 and Figure 3.2, respectively.

Table 3.2 Properties of ZrOc used in this study.

Chemical formula	$ZrOCl_2.8H_2O$
Molecular weight (g/mol)	322.28
Density (g/ml)	1.91
Appearance	White solid
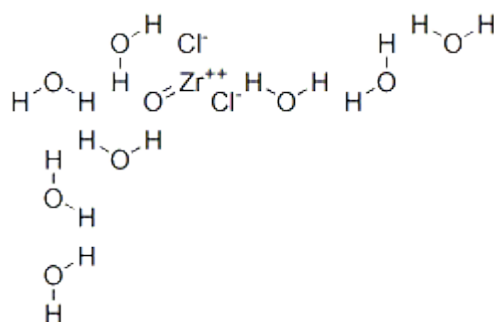
Figure 3.2 Structural formula of ZrOc [65].

3.1.3 Hydrochloric acid (HCl)

Reason of acid addition in high concentrations had been put forward as the acceleration of the formation of crystalline phase under hydrothermal conditions [17]. The effect of HCl concentration on the phase purity of the products obtained from precursors aged at temperatures lower than 100 $^\circ$C has been studied. Properties of HCl (Merck) used in this study are given in Table 3.3.

Table 3.3 Properties of HCl used in this study.

Chemical formula	HCl
Molecular weight (g/mol)	36.46
Density (g/ml)	1.19
Weight percent	37
Appearance	Liquid

3.1.4 Zirconium oxide (zirconia-ZrO_2)

For the composite studies, commercial yttrium stabilized ZrO_2 granules (Tosoh) were used (Table 3.4).

Table 3.4   Properties of ZrO_2 used in this study.

Chemical formula	ZrO_2
Molecular weight (g/mol)	123.22
Density (kg/lt)	5.83
Yttria (mol percent)	3
Appearance	White solid

3.1.5 Isopropyl alcohol (IPA) and polyvinylpyrrolidone (PVP)

IPA was selected as the mixing medium to prepare particle blends of ZrW_2O_8 and ZrO_2 that were used in composite production. PVP (2 weight percentage -2 w/o) was used in the above mixture to give plasticity to the dry pressed pellets which was needed in the flawless ejection of the pellets from the die.

3.1.6 Aluminum oxide (alumina-Al_2O_3)

Al_2O_3 (Sigma-Aldrich) was used as the sintering agent in composite production. It can react with W and form a liquid phase. It had a particle size less than 10 μm on the average.

3.2   Synthesis of ZrW$_2$O$_8$ Particles

3.2.1 Precipitation method reported in literature

The precipitation method reported in literature was repeated as a preliminary experiment. The flow chart of the method is given in Figure 3.3. AMT (Figure 3.4) is used as tungsten source and ZrOc is used as zirconium source. After preparing 1 M AMT and 0.5 M ZrOc solutions (W:Zr=2 stoichiometric ratio), they were mixed simultaneously in a third beaker that contains water, volume of which was half ml of the individual syringes. This mixture with white precipitates was stirred for 10 h, after which 6 M HCl was added such that, final HCl concentration in the solution was 3M. Mixture was then refluxed for 2 days at 80 ^{o}C with stirring, and then aged for 7 days on the filter paper after filtering. Due to the ambiguity in the two reported methods about this 7 days ageing step, in another experiment, mixture was aged for 7 days without filtering and after which the regular filtering and drying steps were carried out. Finally, the obtained powders were calcined at 600 ^{o}C for 10 h [16, 72]. Experiments were repeated 3 times.
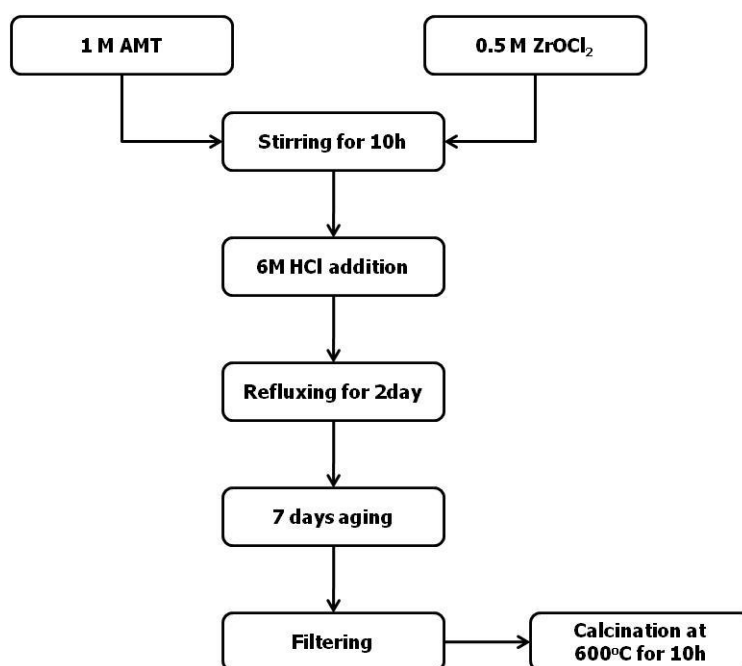
Figure 3.3 Precipitation method reported in literature [72].
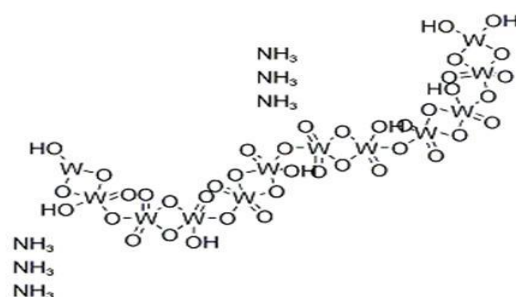
Figure 3.4 Structural formula of AMT [65].

3.2.2 ZrW$_2$O$_8$ precursor preparation and heat treatment procedure

TA and ZrOc were used for tungsten and zirconium sources, respectively. In order to dissolve TA in water, H$_2$O$_2$ was used and the novel low-pH ZrW$_2$O$_8$ precursor was prepared. It allowed use of shorter ageing times and lower ageing temperatures. Flow chart of the precursor preparation is given in

Figure 3.5. TA solution is mixed with H_2O_2 at 60 $^{\circ}$C for about an hour. The clear TA solution was mixed simultaneously with separately prepared ZrOc solution of equal volume in a third beaker that contains water, volume of which was half ml of the individual syringes, in it by using two syringes. Then, the mixture was stirred at 80 $^{\circ}$C for 1 day and different molarities and volumes of HCl were added, followed by 1 day ageing at 90 $^{\circ}$C. While no special treatment concerning atmosphere control was needed, solutions were kept in media bottles with screw caps during any ageing step to prevent evaporation. After a total of 2 days of ageing, the solutions were filtered and/or washed and the powders were left aside for drying at 60 $^{\circ}$C [25-26]. The effects of use of excess zirconium source, the concentrations of HCl and metal ions, and washing procedures on phase purities of the products were examined systematically.
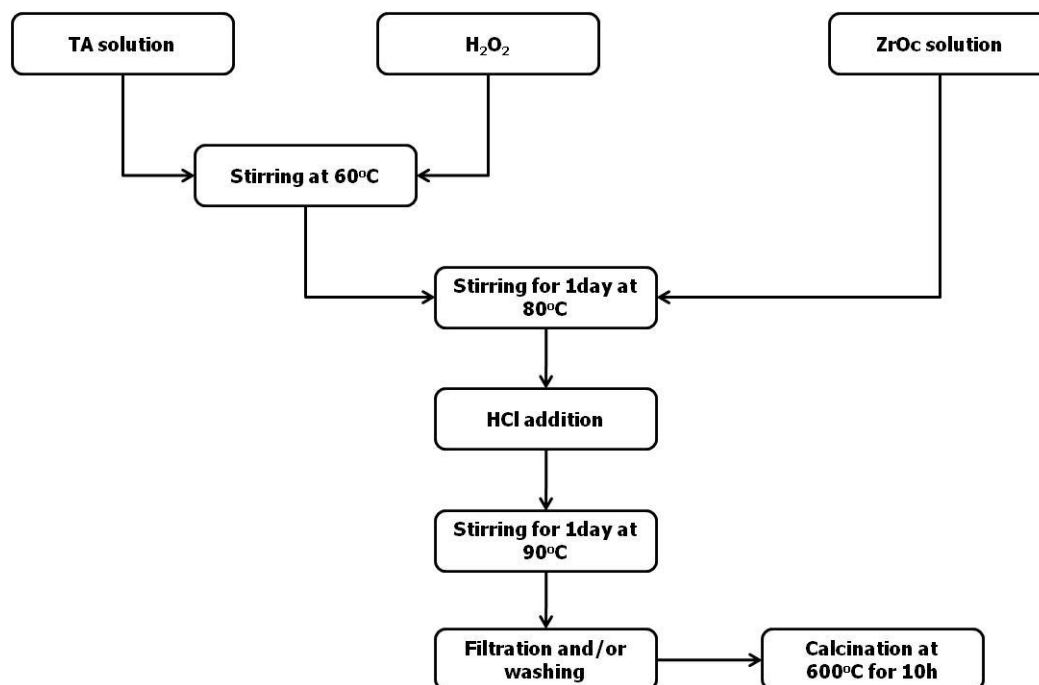
Figure 3.5 Preparation of the low-pH ZrW_2O_8 precursor using TA.

All precursor powders were calcined at 600 °C for 10 hours in a Protherm box furnace (Figure 3.6) by using alumina crucibles. Temperature profile applied to precursor powders are given in Figure 3.7.

Figure 3.6 Box furnace used in heat treatment of precursors.
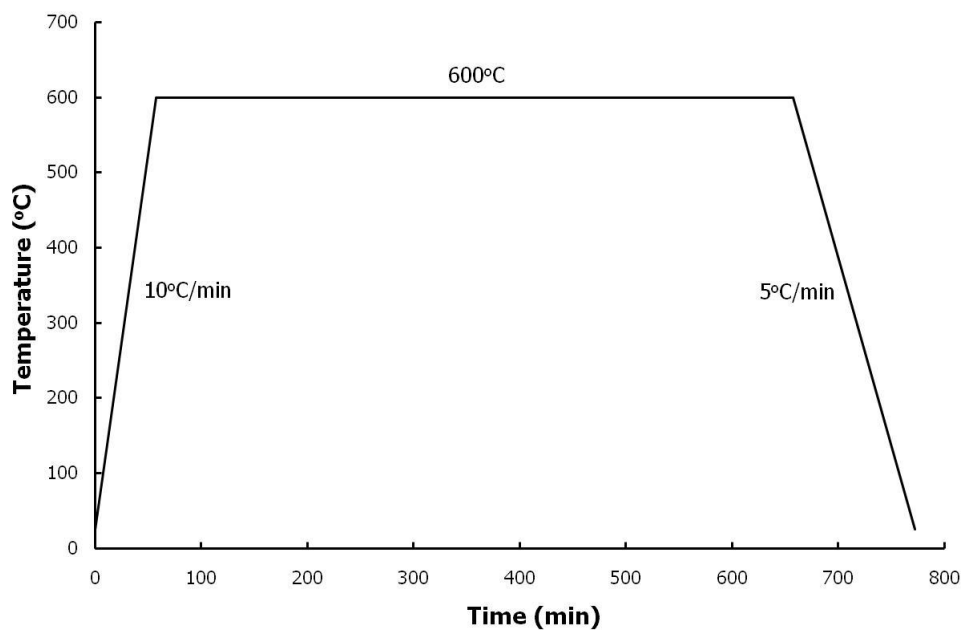
Figure 3.7 Temperature profile applied to ZrW_2O_8 precursor powders.

3.3 ZrW$_2$O$_8$-ZrO$_2$ Composites

ZrW$_2$O$_8$ particles produced from the low pH precipitation approach described above were used together with the commercial ZrO$_2$ particles in production of composites. In some experiments, Al$_2$O$_3$ was used as a sintering agent. Composite studies were performed by using conventional and SPS methods.

3.3.1 Conventional sintering

As described in Chapter 2, manual mixing and sintering of constituents of a ceramic-ceramic composite has been a convenient method to produce ZrW$_2$O$_8$-ZrO$_2$ composites. Although powder mixtures can be prepared by mixing ZrW$_2$O$_8$ and ZrO$_2$ in a mortar, in this study mixing of oxide powders is conducted in liquid medium, namely IPA. As a sintering agent, different amounts of Al$_2$O$_3$ were added to the powder dispersions in IPA. To improve the green strength and plasticity of the pressed pellets 2 w/o PVP was added to the mixing solutions.

In Figure 3.8 the flowchart showing the steps in the conventional composite preparation method is given. Briefly, first the required amount of PVP was dissolved in IPA, and then calculated amount of ZrW$_2$O$_8$ was added under ultra sonic mixing (USM). Separately sonicated Al$_2$O$_3$-IPA and ZrO$_2$-IPA mixtures were added to the initial ZrW$_2$O$_8$-IPA-PVP mixture under USM one after the other, respectively. The final mixture was continued to be magnetically stirred while IPA was evaporated at 150-200 $^{\circ}$C. After almost complete evaporation of IPA, the remaining small amount of IPA was dried while the powder mixture was ground manually for the last time. The mixture was uniaxially cold pressed under a pressure of 250 MPa for 10 minutes. Pellets were then sintered for different times and at different

46

temperatures in a box furnace (Figure 3.6) by using a platinum crucible. A platinum crucible was used instead of alumina to prevent any reaction of W with the alumina crucible. At the end of planned sintering durations, pellets were quenched in water to prevent ZrW_2O_8 decomposition.

Effects of volume ratio of ZrW_2O_8 to ZrO_2, amount of alumina, sintering time and temperature on different properties of composite bodies were examined.
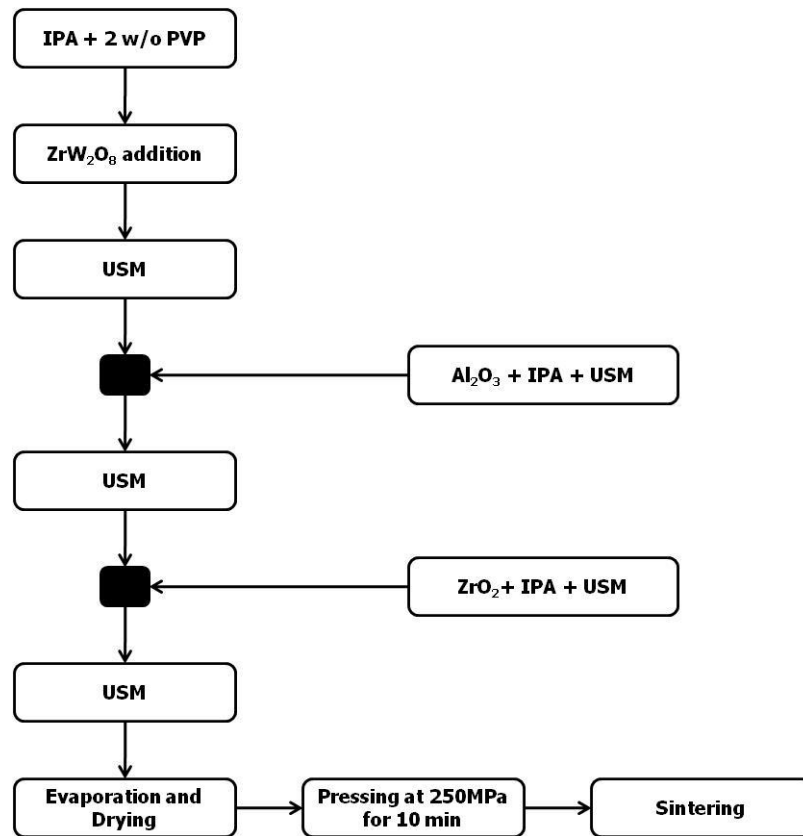
Figure 3.8 Composite preparation by conventional method.

3.3.2 Spark plasma sintering (SPS)

Powder mixtures for SPS were prepared as in the conventional method. Flow chart showing the steps in the composite preparation by the SPS method is given in Figure 3.9. Alumina addition (shown as red box in Figure 3.9) was used only in some trials. Since sintering and pressing are applied simultaneously in SPS method, powders were not pressed after preparation.

SPS runs were carried out in Spark plasma sintering furnace (FCT GmBH) located in Material Science and Engineering Department of Anadolu University and the picture of the instrument used is given in Figure 3.10.
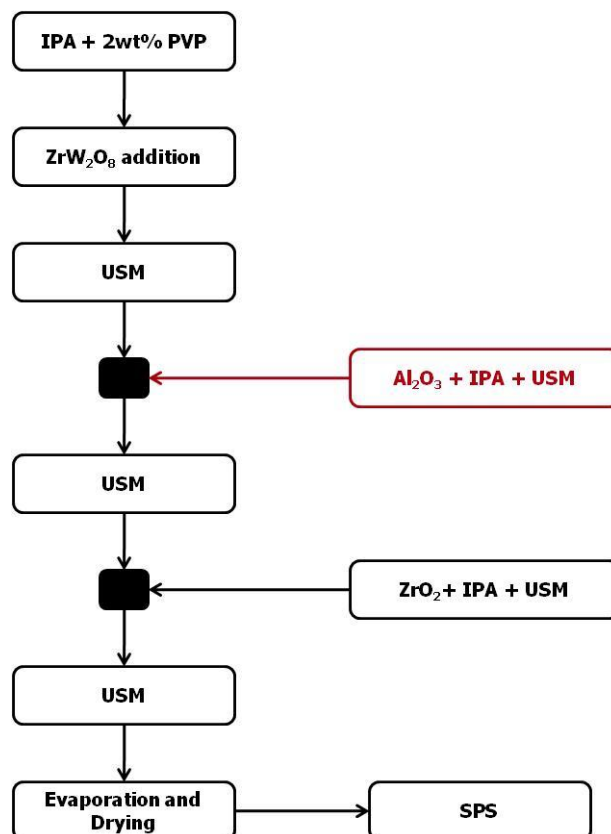
Figure 3.9 Flow chart of composite preparation for SPS method.

Figure 3.10 SPS instrument at Anadolu University.

A constant pressure of 50 MPa was applied between the two graphite dies having inner diameter of 20 mm during the sintering period. Composites were prepared with different volume ratios of ZrW_2O_8 and ZrO_2. Different sintering durations and temperatures were used to find optimum sintering conditions. Effect of sintering agent was examined by adding 0.25 w/o alumina to the powder mixtures. It was used a sequence of twelve pulses followed by two periods of zero current for all experiments.

CTE and theoretical density of the composites were calculated by using rule of mixture from equations (1) and (2) [50,1], respectively.

$$\alpha_{comp} = \alpha_1 V_1 + \alpha_2 V_2 \tag{1}$$

$$\rho_{comp} = \rho_1 V_1 + \rho_2 V_2 \tag{2}$$

where; α = thermal expansion coefficient (CTE)

ρ = density

V = volume fraction

3.4 Characterization Methods

Different characterization methods were used for ZrW_2O_8 and composites. These were XRD (X-ray Diffraction), PCS (Photon Correlation Spectroscopy), SEM (Scanning Electron Microscopy), and dilatometry. Details of instruments and methods used are described in this section.

3.4.1 XRD analysis

Structural characterization of the produced particles and composites were carried out by using X-ray Diffractometer (Model No: RIGAKU – D/Max-2200/PC) and $CuK\alpha$ (λ = 0.154 nm) radiation at 40 kV and 40 mA in a 2θ ranging from 10° to 80°. The instrument is located at Middle East Technical University Materials and Metallurgical Engineering Department. Phase purity or assembly of samples was assessed by comparing the area underneath the highest intensity peaks of WO_3, ZrO_2, and ZrW_2O_8 (Peak Fit v. 4.11). Standard peaks are given in Appendix B. X-ray line broadening values were used in Scherrer equation, which is given in equation (3), for crystallite size calculations;

$$t = \frac{k \times \lambda}{B \times \cos(\theta)} \tag{3}$$

where; t = thickness of crystallite (nm)

k = constant dependent on crystallite shape

λ = X-ray wavelength (nm)

B = FWHM (full width at half max) or integral breadth (radians)

θ = Bragg angle (^{o})

Instrumental broadening of the peaks was accounted for by correcting the full width at half maximum (FWHM) values with those of the (210) and (211) peaks of the highly crystalline ZrW_2O_8 produced in our previous studies.

3.4.2 PCS

The particle size and zeta potential values can give detailed information on the stability and dispersion mechanism in a colloidal solution. The sizes of the produced particles were measured by laser diffraction technique using Malvern Zetasizer Nano Instrument (Model No: ZEN3500, Malvern Instruments Ltd.) located in Nuclear Application Laboratory of Chemical Engineering Department (METU), and Malvern Mastersizer 2000 located in Central laboratory (METU). The primary crystallite sizes calculated from XRD patterns were small. As a consequence, these were found to agglomerate to form secondary particles, sizes of which could be measured effectively by this method. Measurement range of Malvern Zetasizer is from 1 nm to 5 μm whereas that for Malvern Mastersizer is from 0.02 μm to 2000 μm. For Zetasizer measurements, samples were prepared either in water or in IPA, and 2-5 minutes USM was applied to have better dispersion. Measurements were carried out by using zeta cells provided by the instrument manufacturer.

3.4.3 SEM analysis

Morphologies and sizes of the produced ZrW_2O_8 particles and sintered composite bodies were characterized by Scanning Electron Microscopy located either in Middle East Technical University Central laboratory (Model No: Quanta 400F Field Emission SEM - FEI) or in Bilkent University National

Nanotechnology Research Center (Ulusal Nanoteknoloji Araştırma Merkezi – UNAM) (Model No: FEI SEM Quanta 200 FEG). The specimens were sputtered with gold before analysis.

3.4.4 Dilatometry (Thermomechanical analysis – TMA)

CTE's of the sintered composite bodies were measured with a TMA unit (Model no: Setaram Labsys TMA) that is located in Middle East Technical University Central Laboratory. Probe was spherical-ended (with 5mm diameter). Measurement was carried out at a rate of 5 ^{o}C/min under nitrogen atmosphere.

CHAPTER 4

SYNTHESIS of ZrW$_2$O$_8$

ZrW$_2$O$_8$ was initially produced using high pH approach. Used chemicals were TA and ZrAc in our group. In order to dissolve TA in water, ammonia, which resulted in precursors with high pH values, was used. Only ZrO$_2$ and WO$_3$ were obtained after 600 ^{o}C heat treatment. To produce ZrW$_2$O$_8$, particles were calcined at 600 ^{o}C, and this was followed by crystallization at 1200 ^{o}C for 2 hours. Due to the sintering effect of this high temperature heat treatment procedure, produced particles were approximately 8 μm in size [22, 73]. At high pH values the dominant aqueous species of tungsten is WO$_4^{2-}$ [74]. This simpler and smaller form was presumed to come in more close contact with Zr^{4+} ions in the solution and therefore should have resulted in crystallization at lower temperature. However, it is a fact that Zr^{4+} ions hydrolyzes rapidly over pH values of 3, causing the precipitation of Zr(OH)$_4$ as a separate entity. This probably prevented the 'atomic' scale mixing which is an important assertion of wet chemical methods.

Smaller ZrW$_2$O$_8$ particles could be produced using precursors prepared at low pH values. In this chapter, preliminary studies on the production of ZrW$_2$O$_8$ are given initially. Then, problems associated with solubility of Zr^{4+} ions at low pH values, general effects of HCl concentration and washing procedure on phase purity are presented and discussed. In the second part of this chapter; results of parametric studies, which were on the HCl concentration

and ageing time, and conducted on the best conditions obtained from preliminary studies, are discussed.

4.1 Preliminary Studies

4.1.1 Precipitation method reported in literature

The method developed by Closmann et. al. and Zhang et. al. [16, 72] was applied as explained in Chapter 3.2.1. When aqueous solutions of AMT and ZrOc were mixed in a third beaker an immediate precipitation resulted in a heterogeneous gel-like solution which became homogeneous only after 10 hours of stirring. Then, HCl was added to have 3M HCl in the final solution and the mixture was refluxed at 80 ^{o}C for 2 days. After cooling this mixture to room temperature, it was aged for 7 days before calcination. Finally, 10 hours calcination was carried out at 600 ^{o}C in air. It was reported that there was no crystallization after calcination when reflux was continued for 1 day or ageing was continued for 5 days and the values given set the lower limits of ageing conditions for obtaining crystallization at 600 ^{o}C [16].

XRD patterns obtained from particles before and after calcination and characteristic peaks of all possible crystal structures are given in Figure 4.1 and Appendix B, respectively. As seen from patterns, produced particles remained amorphous at room temperature, contrary to literature in which precursor was claimed to be crystallized to $ZrW_2O_7(OH)_2(H_2O)_2$. Particles were crystallized to ZrW_2O_8 after calcination at 600 ^{o}C as expected; however, single phase product could not be obtained. Overall process takes approximately 11 days with calcination.

The drawbacks and confusing points about the procedure reported in literature were identified as follows;

- When Zr and W sources are mixed, immediate gel-like formation that takes place was not mentioned and it takes time to homogenize. The initial 10 hours spent in mixing before HCl addition also seems indispensible, besides the 2 days reflux, and 7 days of room temperature ageing.

- Overall processing time (11 days) is unacceptably long for all practical purposes.

- Precursor does not crystallize to $ZrW_2O_7(OH)_2(H_2O)_2$ during 7 days room temperature ageing despite what is reported in the literature.

- Single phase product could not be obtained.

- Exact separation and washing procedures were not described.

- To decrease ageing times, hydrothermal ageing at $T>180^{o}C$ was used.

- High concentration of acid in the precursor can corrode almost any hydrothermal reactor, so Teflon-lined reactors have been needed in all similar studies. Applicability in large-scale is at scale.
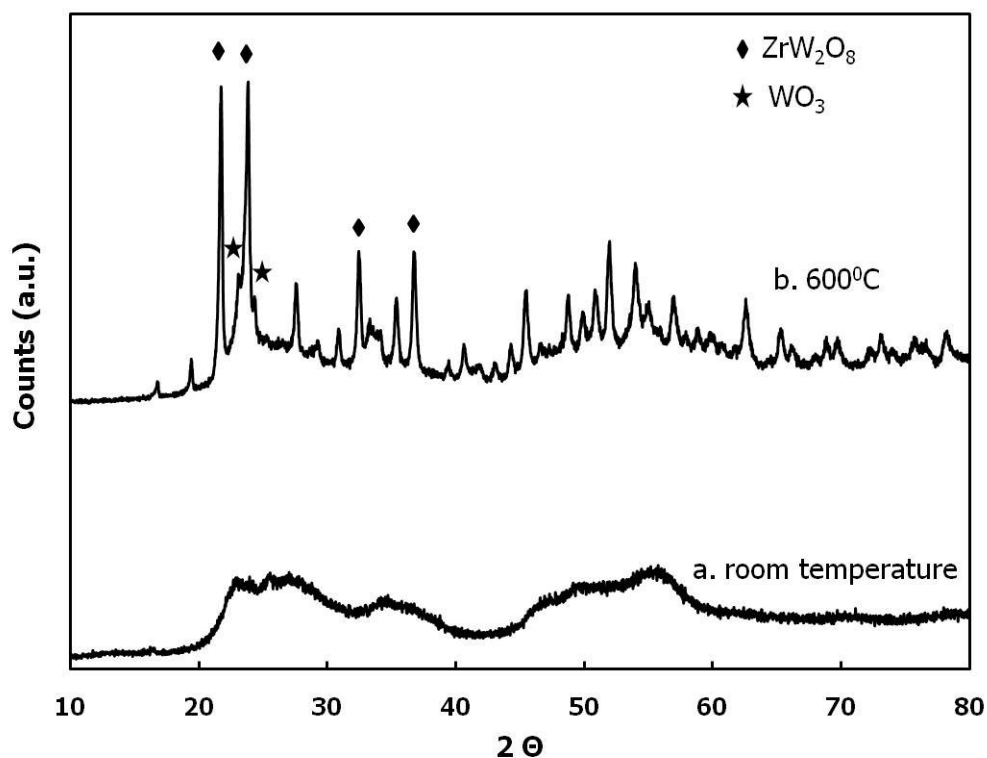
Figure 4.1 XRD patterns of ZrW_2O_8 particles, which were produced using the precipitation procedure reported in literature, (a) at room temperature, and (b) after calcination.

4.1.2 Low pH approach developed using TA

After repeating the precipitation experiment reported in the literature, it was evaluated to shorten the long ageing durations. Whether, if this could be achieved by using TA or not was the other quest. By dissolving TA in aqueous H_2O_2 solution and using this as the tungsten source, and by only modifying the ageing procedure described in the previous section, experiments were carried out again.

a. Solubility of Zr^{4+} ions

Phase purity could not be obtained when W and Zr sources were mixed in a stoichiometric ratio (W:Zr = 2:1). As presented in Figure 4.2, similar results were obtained in the modified method with TA. The reason of this was thought to be the higher solubility of Zr ions compared to that of W ions at low pH values in reference to the similar observations made by Kozy and coworkers [23]. Therefore, soluble Zr ions remaining in the solution could have been washed out in the filtering step, which would eventually cause the product to lose its purity. Such a problem can be solved by putting excess amount of Zr source in the precursor solution. The approximate excess amount that would be needed was determined by gravimetric analysis. In order to do that, ammonia was added to filtrate, which was obtained after filtering the precursor solution. pH of the filtrate was raised and Zr ions that remained in the filtrate precipitated. These particles were then filtered and calcined at 500 ^{o}C to crystallize them as zirconium oxide, from which Zr^{4+} that remains in the precursor solution can be determined indirectly. This experiment was repeated three times and the amount of Zr ions passed through the filter was found to vary between 10 and 15 w/o.

Experimental details, in which stoichiometric and excess amounts of Zr sources were used, are given in Table 4.1. It should be noted that in this set of experiments, the starting molarities of both W and Zr sources were kept lower than what is generally used in the literature. W and Zr sources were mixed in a stoichiometric ratio in experiment A1, whereas 15% excess zirconium amount was used in A2. W and Zr sources were mixed and then aged for 1 day at 80 ^{o}C. Afterwards, HCl addition was followed with 1 more day ageing at 90 ^{o}C.

Table 4.1 Experimental conditions to determine the excess amount of zirconium source needed in the precursors.

Exp. Name	Initial Molarities		Final Molarities				Ratios in the Final Solution			Excess Zr (%)
	TA	ZrOc	TA	ZrOc	HCl	H_2O_2	ZrOc/ TA	H_2O_2/ TA	HCl/ TA	
A1	0.2	0.100	0.03	0.015	3	0.18	0.50	6	100	0
A2	0.2	0.115	0.03	0.017	3	0.18	0.58	6	100	15

XRD patterns of the particles obtained from experiments A1 and A2 are given in Figure 4.2 with the standard peaks of ZrW_2O_8 (ICDD-JCPDS-PDF No 50-1868). All standard peaks can also be seen from Table B.2 in Appendix B. 100% single phase ZrW_2O_8 was obtained from A2, in which excess amount of Zr source was used. In Table 4.2, the approximate phase purities calculated from these patterns are presented. In view of these results, the excess amount of zirconium source to be used in the experiments was decided to 15%.
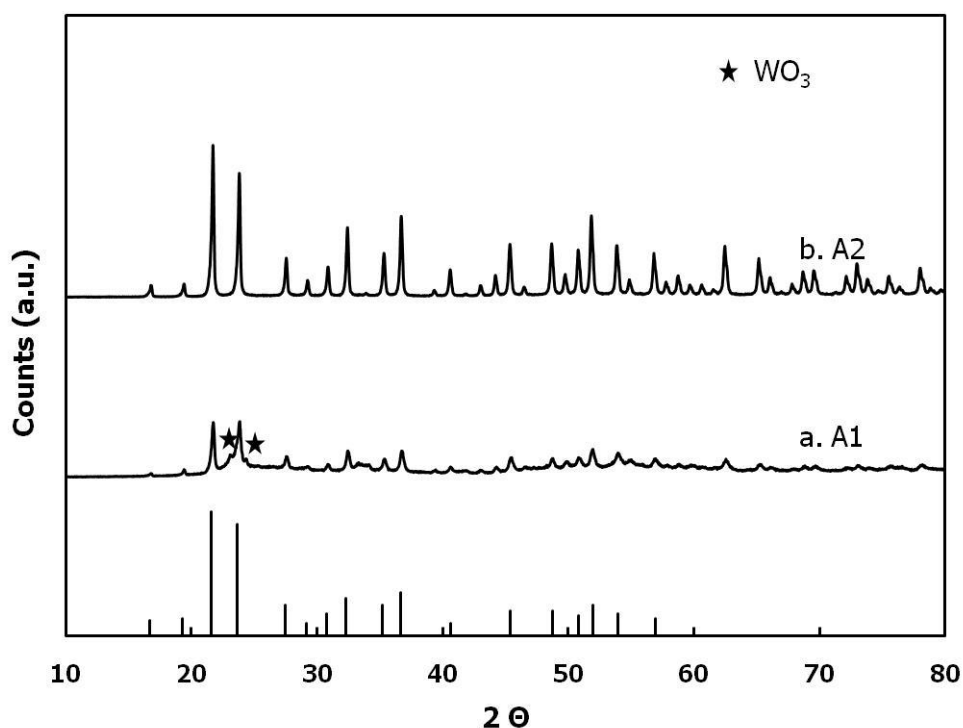
Figure 4.2 XRD patterns of experiments (a) A1 and (b) A2, bottom pattern: standart peaks of ZrW_2O_8 (ICDD-JCPDS-PDF No 50-1868).

Table 4.2 Phase purities obtained in experiments A1 and A2.

Exp. Name	Phase Purity (%)
A1	92.5
A2	100.0

b. Effect of HCl concentration on phase purity

In order to understand the effect of HCl concentration on phase purity, in a set of experiments HCl concentrations were varied. 6 M HCl solution was added to the reaction medium in different volumes by keeping all other

parameters constant. Conditions of the three experiments can be followed from Table 4.3. In these experiments, the initial molarities of prepared W and Zr solutions were again kept lower than what is usually used, but with the 15% excess amount of Zr^{4+} ions in the Zr source.

Table 4.3 Experimental conditions used in experiments towards understanding the effect of HCl concentration on phase purity.

Exp. Name	Initial Molarities		Final Molarities				Ratios in the Final Solution			Excess Zr (%)
	TA	ZrOc	TA	ZrOc	HCl	H_2O_2	ZrOc/ TA	H_2O_2/ TA	HCl/ TA	
A3	0.2	0.115	0.07	0.04	1.00	0.40	0.58	6	15	15
A4	0.2	0.115	0.06	0.03	1.71	0.34	0.58	6	30	15
A5	0.2	0.115	0.03	0.017	3.00	0.18	0.58	6	100	15

XRD patterns of the results are given in Figure 4.3. Results showed that ZrW_2O_8 crystallization was only observed in the case when HCl concentration was 3 M in the final reaction mixture (A5). In other words, only WO_3 crystallization (ICDD-JCPDS-PDF No 72-0677) can be observed if HCl concentration was kept lower than 3 M in the final solution, i.e. HCl/TA concentration ratios were 15 and 30 (A3 and A4, respectively).
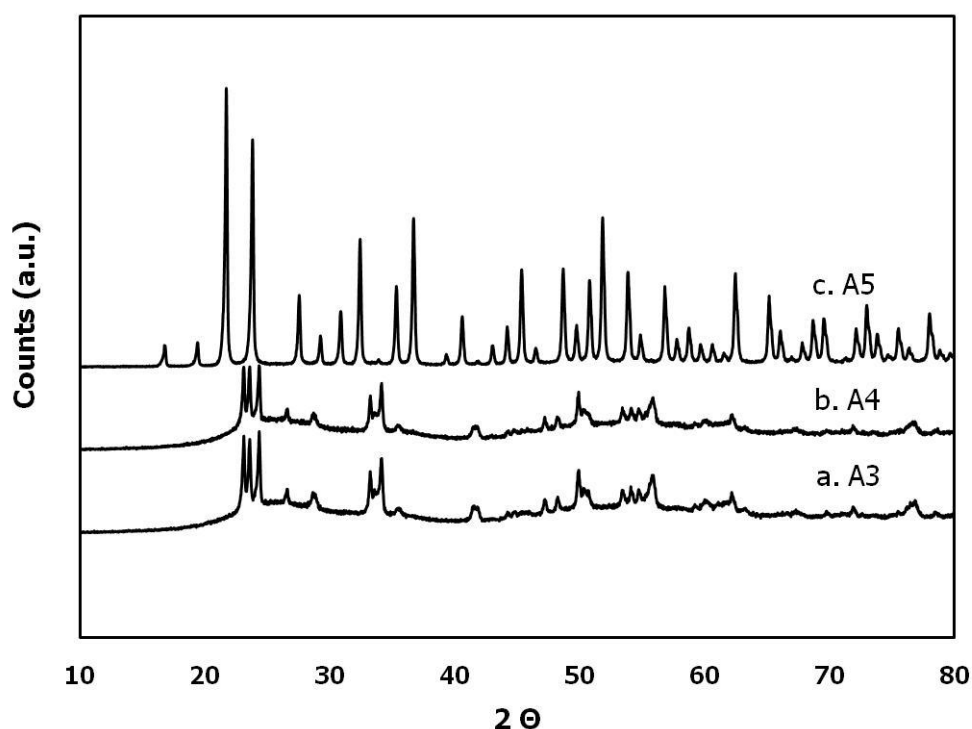
Figure 4.3 XRD patterns of experiments (a) A3, (b) A4, and (c) A5.

The mechanism with which higher HCl concentrations provide the conditions for ZrW_2O_8 crystallization at 600 °C and why such a long ageing time was a stringent necessity have not been widely discussed in the literature. It was shown that higher amounts of acid additions accelerate formation of the crystalline phase $ZrW_2O_7(OH)_2(H_2O)_2$ under hydrothermal conditions [17]. Although a crystalline phase was expected to form in the three precipitation experiments conducted according to the reported method, this was not the case. $ZrW_2O_7(OH)_2(H_2O)_2$ did not crystallize also in the cases TA was used instead of AMT. Bearing this in mind, one can resort to the fundamental information on aqueous chemistry of early transition metals to initiate a discussion on different possibilities [74].

61

Tungstate ions (WO_4^{2-} - tetraoxo ion) that are stable in alkaline aqueous medium, polymerize in acid solutions and polyanionic species of tungsten ions (isopolytungstates) form. It can further be followed from Figure 4.4 that the metatungstate anion ($H_2W_{12}O_{40}^{6-}$) becomes the dominant species at low pH values. Structure of metatungstate anion is given in Figure 4.5 and it consists of twelve WO_6 octahedra arranged around tetrahedrally coordinated heteroatom, which is presumed to be the two protons in the metatungstate case. The octahedra are divided into four tritungstate groups by the edge sharing of octahedra. The tetrahedrally coordinated atom is linked to these four tritungstate groups, which also share corners with each other [74].
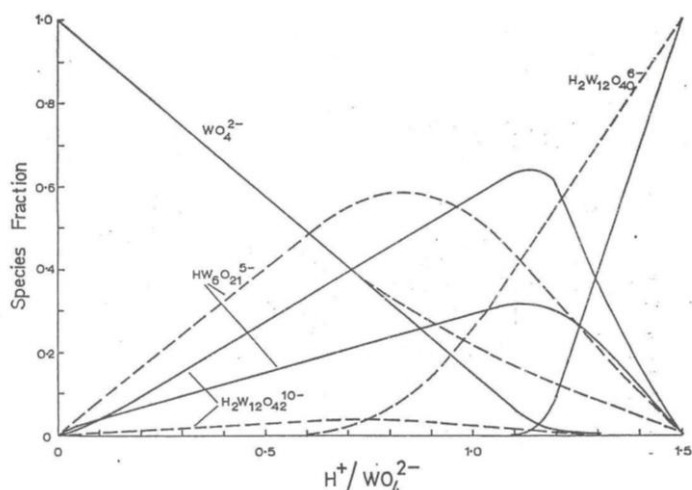
Figure 4.4 Effect of increasing proton concentration on the fractional distribution of tungsten species in an aqueous solution (3 M LiCl, 0.2 M W^{6+}: solid lines, 0.002 M W^{6+}: broken lines) [74]. Note how metatungstate ($H_2W_{12}O_{40}^{6-}$) become the dominant species at H^+/WO_4^{2-} ratio over 1.5.
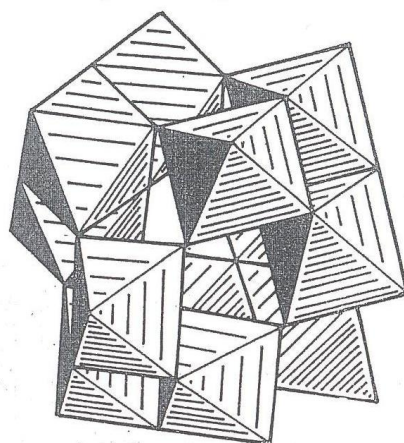
Figure 4.5 Structure of metatungstate anion ($H_2W_{12}O_{40}^{6-}$) which forms at low pH values. Heteroatom site at the center of metatungstate cage is presumed to be occupied by the 2 protons in the absence of any other cation in the solution [74].

Isopolyanions can react with almost any cation that is present in the medium to form hetereopolyanionic species. Over 30 elements were shown to function as a heteroatom by replacing the two protons and taking over the site occupancy in the metatungstate cage. These hetereopolyanions have different structures with different groups of elements. Structurally characterized hetereopolyanions can be divided into three groups, depending upon whether the heteroatom is tetrahedrally, octahedrally, or icosahedrally coordinated. If molybdenum isopolyanions are adjoined with zirconium, cerium, and thorium, the structure will be an icosahedra similar to that is shown in Figure 4.6. In the structure given, a cerium atom is surrounded by six Mo_2O_9 units which share corners with each other; and each Mo_2O_9 unit is formed by two MoO_6 octahedra sharing a common face. The chemistries of molybdenum and tungsten are similar such that they are generally considered interchangeably by Kepert in his discussions [74].
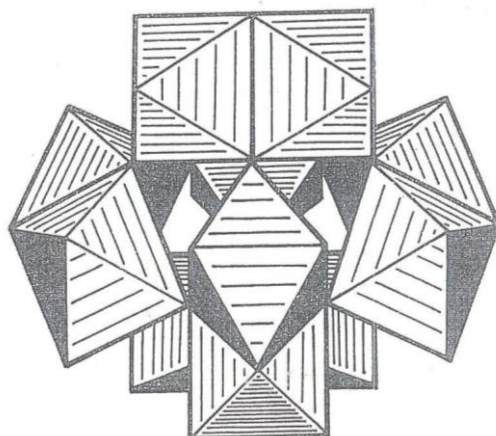
Figure 4.6 Icosahedral structure of cerium heteromolybdate anion (it could be considered as zirconium heterotungstate) [74].

Although not listed literally, Zr cations could also be strong candidates for the heterotungstate formation reactions, in which case one Zr would be associated with twelve W. Such a W:Zr ratio (12:1) would not be enough for the 2:1 ratio needed for ZrW_2O_8. Nevertheless, it is also stated that surplus metal hydroxyls would remain hydrogen bonded to the anion cages, if there are any in the solution. With them around, it can be possible to bring down the ratio to desired stoichiometric values, while keeping the metal ions and W in close proximity. For example, such a ratio can be lowered to 3:1 for $Te(OH)_6$ system [74].

It is probable that for all these intimacy building mechanisms to initiate and proceed, the exchange of two protons in the heteroatom sites with Zr ions can be a priority, for which a certain level of proton activity might be needed in solution, besides high temperatures and long durations. In the pH regime, at which the initial mixing takes place, the precipitating entities are probably formed of only metatungstate cages which are randomly coordinated by the surplus Zr ions that are hydrogen-bonded to the W cages. The added protons would penetrate into the entities to break them down with time,

which can be critical in the reorganization of W ions; as they would be in possible zirconium heterotungstates, or into tetrahedral coordination rather than the octahedral coordination seen in the cage structures. The latter should especially be important to initiate the crystallization of $ZrW_2O_7(OH)_2(H_2O)_2$ since W is tetrahedrally coordinated in this structure. Determining whether the TA-based precursor developed in this study would provide an easier path for this reorganization or not, or whether it would aid this reorganization through a different mechanism, but with a similar rate is out of the scope of this study. However, in the next section, whether or not the overall ageing times can be taken below 2 days will be pursued.

Previous experiments were conducted by using low molarity starting solutions (i.e. 0.2 M TA and 0.115 M $ZrOCl_2$ with 15% excess). However, in the literature 5 times more concentrated solutions were used [16, 72]. Therefore, two experiments were done using high molarity starting solutions (Table 4.4). Applied experimental procedure was the same. Washing was not applied and excess Zr source was used in both experiments. By considering the fact that minimum amount of HCl should be 3M in the final solution to produce ZrW_2O_8 at 600 °C, experiments were performed in such a way that final HCl concentrations were 3 M (A6) and 5 M (A7).

Table 4.4   Conditions used in experiments conducted with higher TA and ZrOc concentrations.

Exp. Name	Initial Molarities		Final Molarities				Ratios in the Final Solution			Excess Zr (%)
	TA	ZrOc	TA	ZrOc	HCl	H_2O_2	ZrOc/ TA	H_2O_2/ TA	HCl/ TA	
A6	1	0.575	0.2	0.12	3	1.2	0.58	6	15	15
A7	1	0.575	0.2	0.12	5	1.2	0.58	6	25	15

In Figure 4.7 XRD patterns of products are given. The results of A6 and A7 were same with that of A5 (i.e. 100% single phase products were obtained from both A6 and A7). Only difference was the crystallite sizes. Higher concentration of HCl concentration gave ZrW_2O_8 particles with smaller crystallite sizes as seen in Table 4.5.
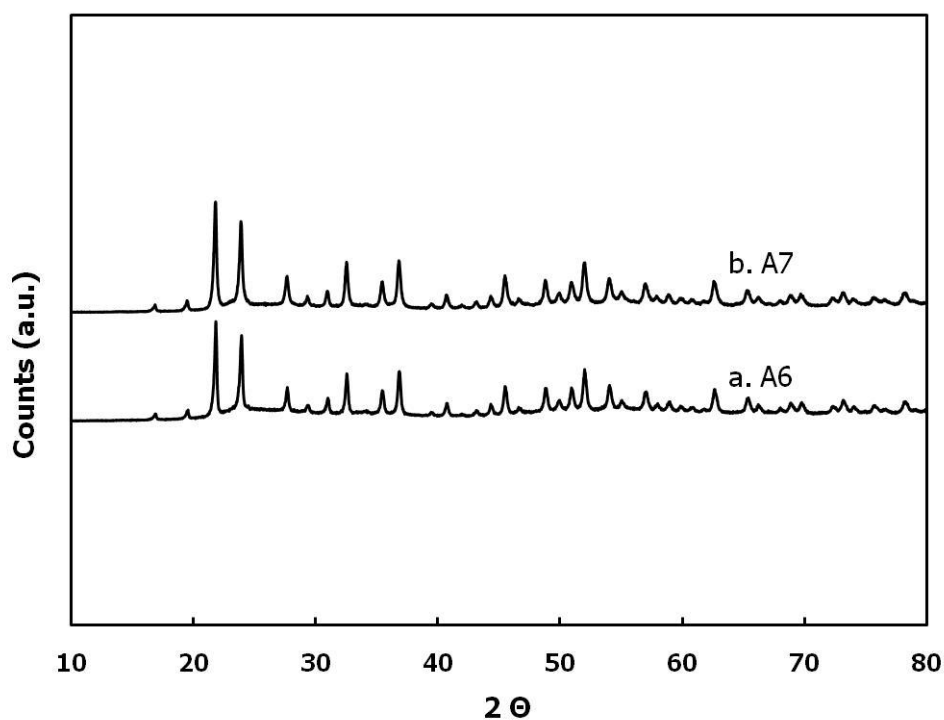
Figure 4.7   XRD patterns of experiments (a) A6 and (b) A7.

Table 4.5   Phase purities obtained in experiments A6 and A7.

Exp. Name	Phase Purity (%)	Crystallite size (nm)
A6	100	83.0
A7	100	55.8

SEM micrographs of produced particles are shown in Figure 4.8. Although calculated crystallite sizes were less than 100 nm, the visually measured sizes were much bigger. Since a washing procedure was not applied after filtering the precursor, the remaining water between the particles caused strong agglomeration of primary crystallites. The secondary (large) particle sizes seen in SEM micrographs of A6 and A7 were nearly same because of agglomerations.
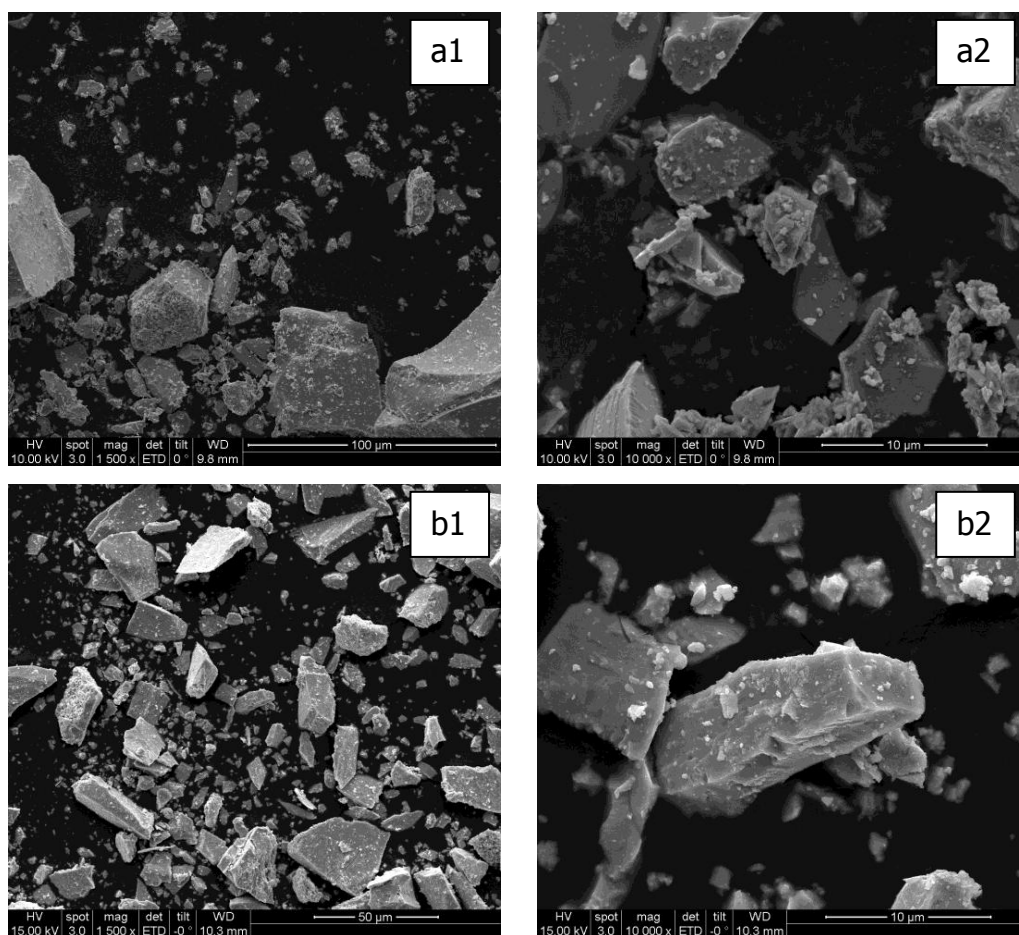
Figure 4.8 SEM micrographs of products (a) A6 and (b) A7. Magnification in a1 and b1 is ×1500 while that in a2 and b2 is ×10000.

In order to prevent agglomeration among the crystallites, it was decided to wash the particles after filtering and effect of different washing procedures are explained in the next section. There is no information about washing procedures in the literature except in one PhD thesis [75].

c. Effect of washing on phase purity

Particles produced from experiment A6 (Table 4.4) were only filtered in the previous section. However they were also washed after filtering and both powders were calcined at 600 ^{o}C for 10 hours. XRD patterns are given in Figure 4.9. Precursor particles were washed with IPA in the first trial. It can be seen that washed particles did not give 100% ZrW_2O_8 crystallization. Particles produced from A7 were also washed, but this time not only with IPA, but also with ethanol (EtOH) and acetone. XRD patterns (Figure 4.10) showed that proper ZrW_2O_8 crystallization was observed only in acetone case; although, formed ZrW_2O_8 was not completely phase pure. In other cases WO_3 was the dominant oxide.
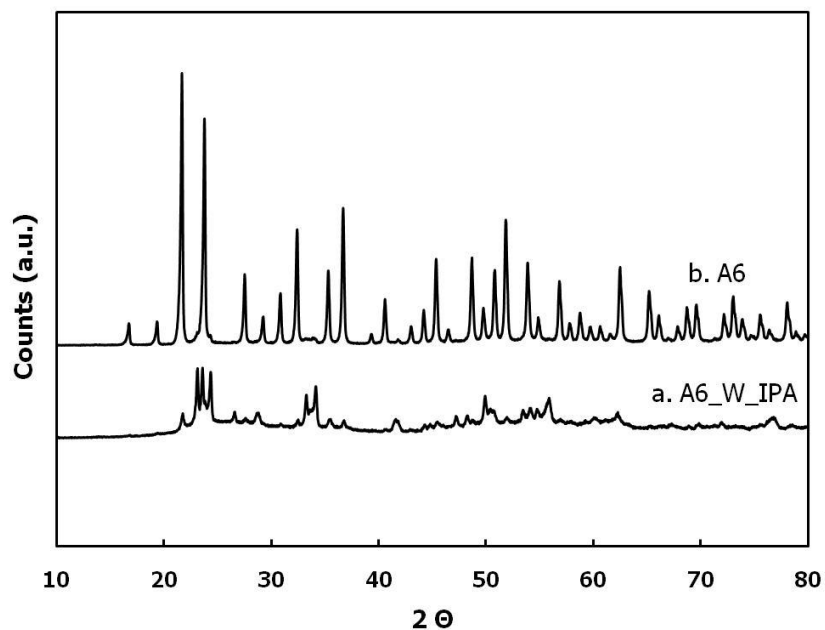
Figure 4.9 XRD patterns of calcined A6 after (a) washing with IPA and (b) only filtering. W stands for 'washing'.
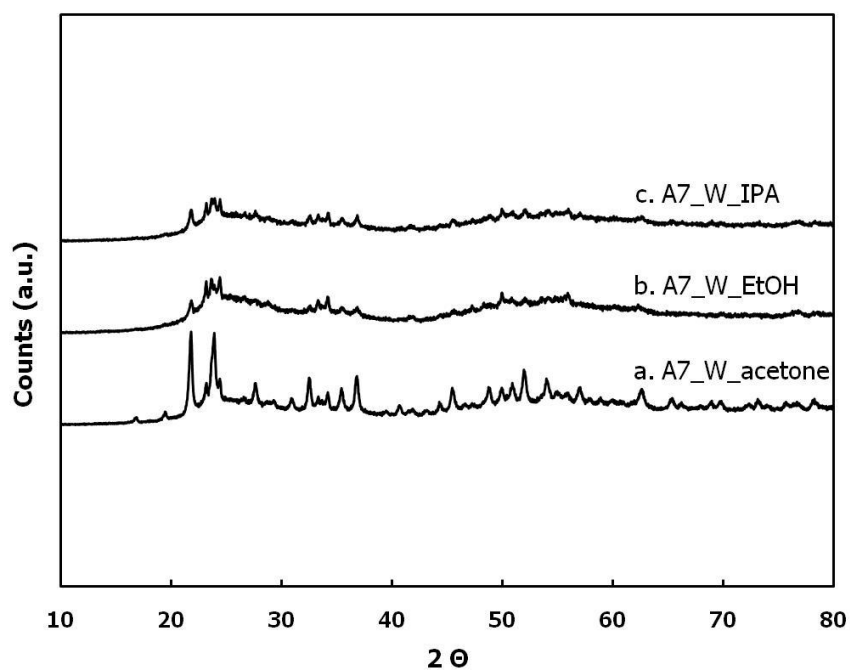
Figure 4.10 XRD patterns of precursor particles produced from A7 after washing with (a) acetone, (b) EtOH, and (c) IPA.

69

In order to understand the reason of not having crystallizations after washing steps, washed particles were burned at different temperatures and times. It can be identified whether the unsuccessful washing procedures change the stoichiometry or not with these experiments. Since ZrW_2O_8 should definitely form at temperatures above 1130 ^{o}C according to the phase diagram, precursor particles produced from A6 were burned at 1130 ^{o}C and 1180 ^{o}C for very short durations. XRD patterns are given in Figure 4.11. Results revealed that washing do not cause any change in the overall stoichiometric balance, because all three samples gave ZrW_2O_8 crystallization. The particles burned at 1130 ^{o}C for 20 seconds contained both α-ZrW_2O_8 (ICDD-JCPDS-PDF No 50-1868) and γ_o-ZrW_2O_8 (ICDD-JCPDS-PDF No 56-566). On the other hand 3 minutes burning (both at 1130 ^{o}C and 1180 ^{o}C) yielded α-ZrW_2O_8 with 100% purity. Therefore, it was concluded that diffusion distance between the W and Zr ions becomes larger in the case of washing procedures with IPA and EtOH. It is probable that during the exchange of alcohols and water in the washing steps, at the same time a mass transport phenomenon also takes place. This probably takes place from points with high chemical potentials (like sharp points) to points with lower chemical potentials (the particle contact points). This can also occur in such a way that, one of the components (Zr or W) could be carried to the contact with relatively higher flux, which would in turn spheroidize the particles, but render the diffusion distances large for 600 ^{o}C activation, and still cause strong agglomerations.
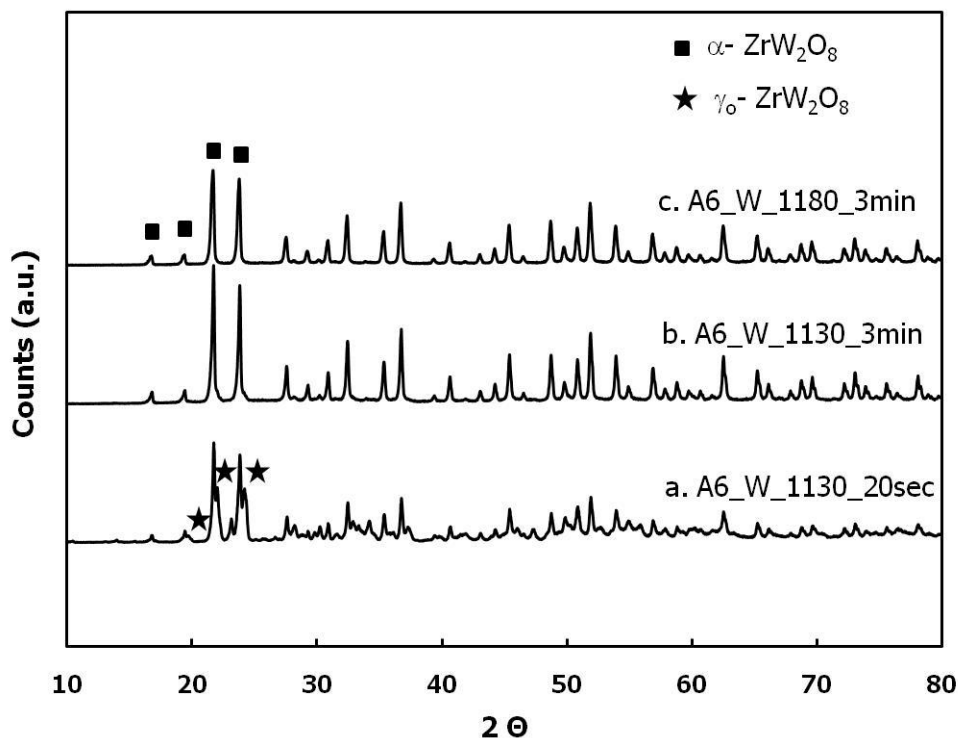
Figure 4.11 XRD patterns of A6_W_IPA burned at (a) 1130 $^{\circ}$C for 20 seconds, (b) 1130 $^{\circ}$C for 3 minutes, and (c) 1180 $^{\circ}$C for 3 minutes.

In Figure 4.12 SEM micrographs of washed particles produced from A6 (A6_W_IPA) are given. It can be concluded that washing decreases the agglomeration (comparing Figure 4.12(b) with 4.8). There were still some agglomerated particles, but they could be broken with USM. Figure 4.12(a) and 4.12(b) showed that there was no change in the particle sizes of precursor particles before and after heat treatment at 600 $^{\circ}$C. On the contrary, particles treated at 1130 $^{\circ}$C and 1180 $^{\circ}$C started to sinter at the contact points and became larger even after seconds. Although high temperature provided the formation of ZrW_2O_8, it caused an enormous increase in particle sizes.
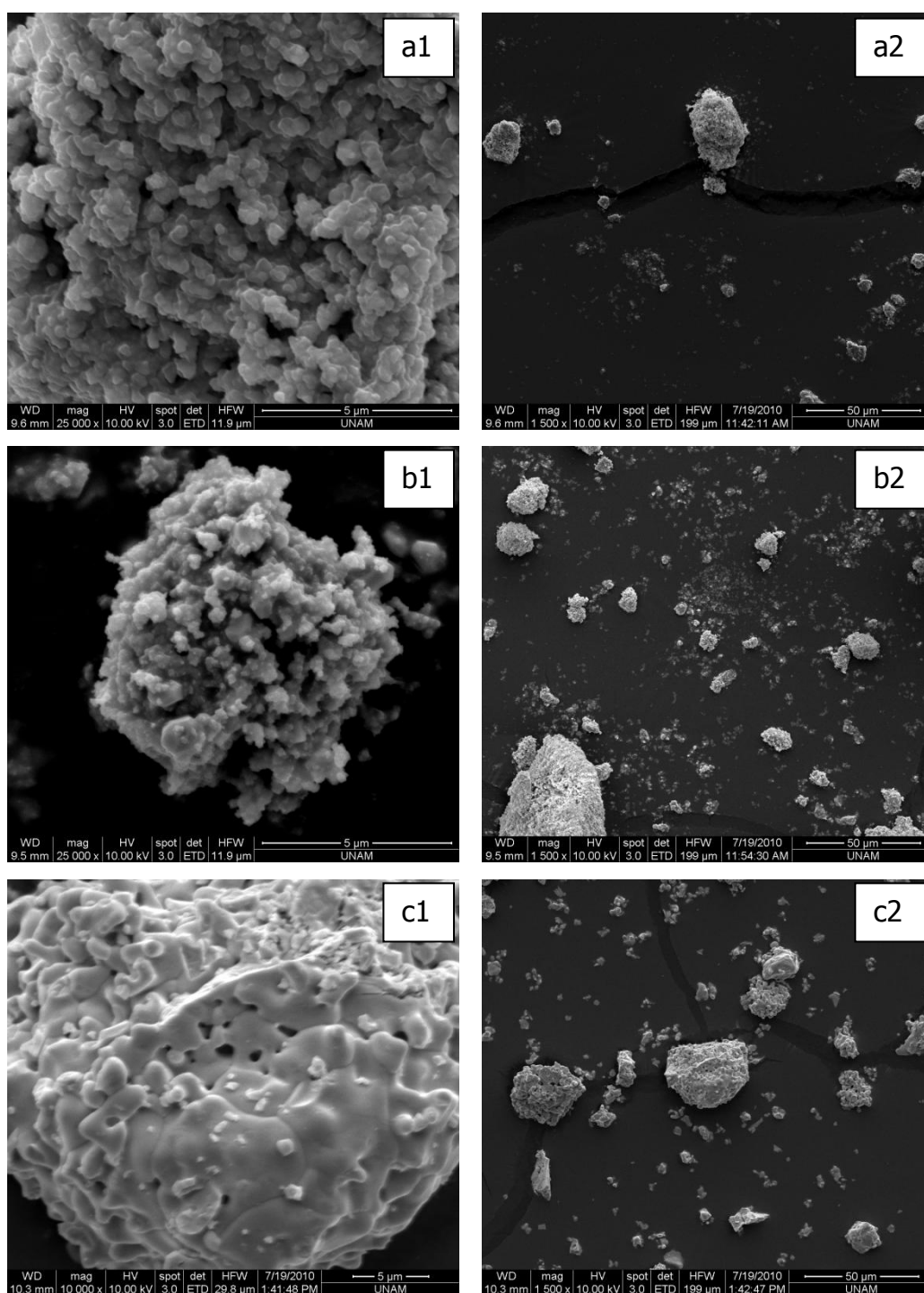
Figure 4.12 SEM micrographs of A6_W_IPA particles (a) before heat treatment and after heat treatment at (b) 600 °C for 10 hours, (c) 1130 °C for 3 minutes, and (d) 1180 °C for 3 minutes. Magnifications in (a1) and (b1) are ×25000, and that in (c1) and (d1) are ×10000, while others are ×1500.

Figure 4.12 SEM micrographs of A6_W_IPA particles (a) before heat treatment and after heat treatment at (b) 600 ^{o}C for 10 hours, (c) 1130 ^{o}C for 3 minutes, and (d) 1180 ^{o}C for 3 minutes. Magnifications in (a1) and (b1) are ×25000, and that in (c1) and (d1) are ×10000, while others are ×1500 (continued).

SEM micrographs of particles produced from A7 after washing with acetone are given in Figure 4.13. Results showed that morphology of the particles was started to change into rod-like structure (like in hydrothermal methods in the literature). Also, weakly agglomerated particles were formed and these could be easily broken by USM. It is implied that acetone was interacting less with the particles during the washing steps.

73
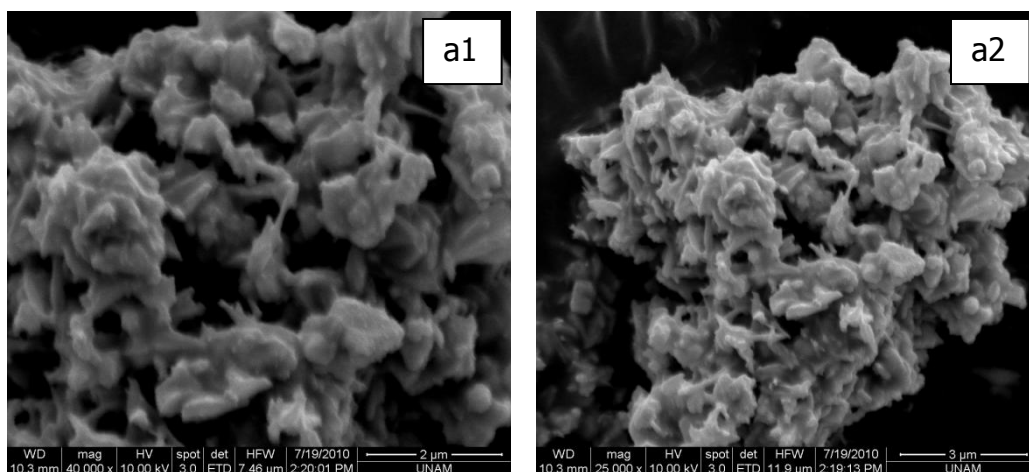
Figure 4.13 SEM micrographs of A7_W_acetone particles after heat treatment at 600 $^{\circ}$C for 10 hours. Magnifications of (a1) and (a2) are ×40000 and ×25000, respectively.

4.2   Effect of ageing time on phase purity

Preliminary experiments showed that HCl concentration plays a crucial role on production of ZrW_2O_8. The required minimum amount of HCl is 3 M in the final solution. Additionally, washing procedure should be taken into account to produce particles that show minimal agglomeration. All preliminary experiments were also done by using smaller volumes of solutions (volume of final solution mixture was 15 ml). In this part, bigger volume of solutions and different ageing times were used to produce ZrW_2O_8. Additionally, produced particles were three or four times washed with acetone and water to prevent the agglomeration. Previously particles washed with acetone gave good solution. There is only one study in which a washing procedure with water was described. In this, washing was continued and repeated until the washing liquor had a pH of 4 to 5 [75].

In this set of experiments, conditions were kept the same as in A6 and A7. In all experiments, 1 day ageing at 80 $^{\circ}$C was applied after combining W and Zr

sources in a third beaker. Then necessary amount of HCl (final [HCl] was 3 M and 5 M for A6 and A7, respectively) was added to the system. After the HCl addition step; 1, 6, 12, 24 and 48 hours of ageing were applied at 90 $^{\circ}$C. This was done mainly to test whether even a shorter ageing time would be possible. In the previous experiments, ZrW_2O_8 was produced by using 24 hours of ageing after HCl addition. However, 48 hours ageing was needed in some of the cases probably due to use of larger volume of solution mixture. The reasons could be inefficient mixing homogeneity and heat transfer in larger volume.

XRD patterns of experiments A6 and A7 (with and without washing steps) after calcination are given in 4.14 (a) and (b), respectively. In Figure 4.14 (a), it is seen that ZrW_2O_8 was produced only by 48 hours ageing after HCl addition, if final HCl concentration was 3M (A6). Particles were 100% crystalline when washing was not applied. However, although phase purity in case that precursor was washed with acetone was not disturbed too much, it was not satisfactory when it was washed with water. On the other hand, Figure 4.14 (b) shows that 24 hours ageing was enough to have 100% single phase ZrW_2O_8 in the unwashed case of experiment A7 (final [HCl] was 5 M). Phase purity was only a little affected by washing the precursor with acetone and water. Additionally, 100% single phase products were obtained in both unwashed and washed cases after 48 hours of ageing.
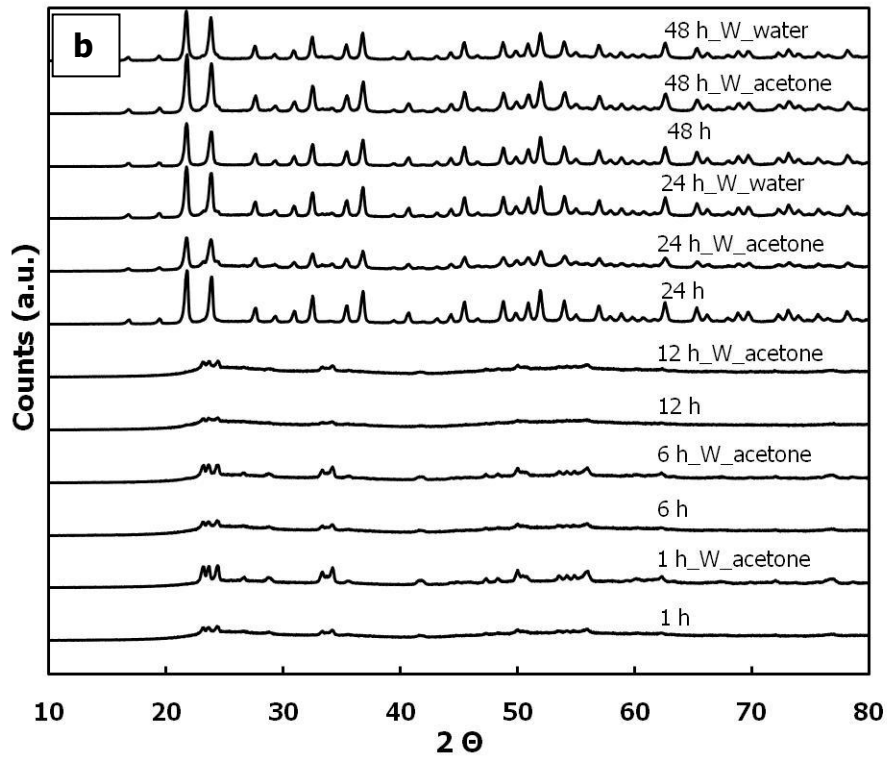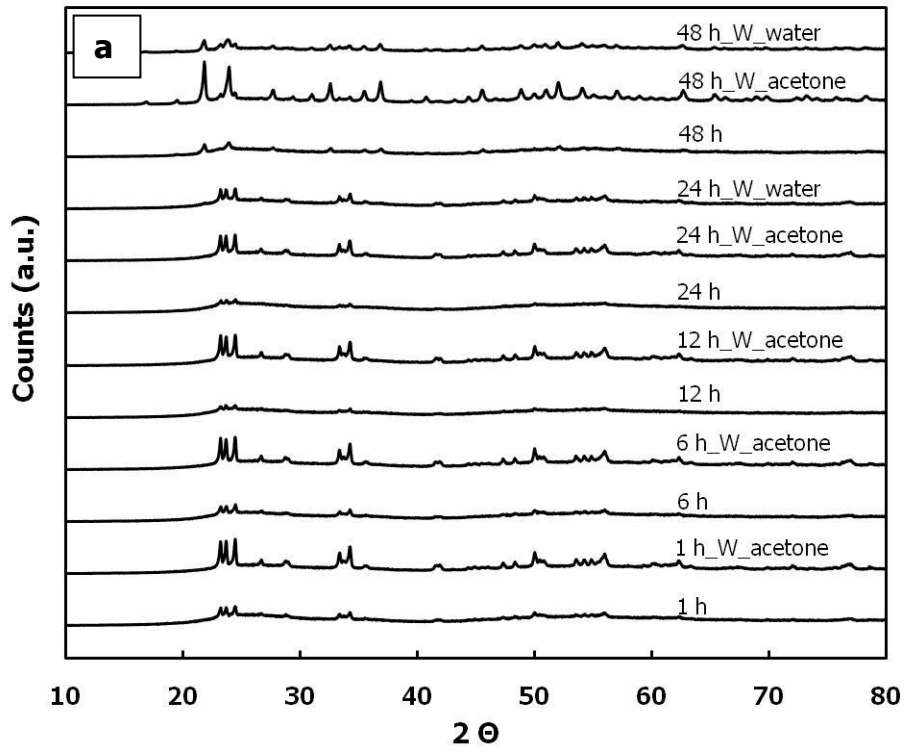
Figure 4.14 XRD patterns of calcined particles (a) A6 and (b) A7 by using different ageing times after HCl addition. W stands for 'washing'.

It was claimed in the literature that precursor particles were crystallized and named as $ZrW_2O_7(OH)_2(H_2O)_2$. However, it was shown in the preliminary experiments that crystalline precursor was not obtained in the repetition of literature. In order to see whether crystal precursor was obtained or not, XRD analysis were done on particles produced from A7 with 24 and 48 hours of ageing after HCl addition and results are given in Figure 4.15. Precursor particles from 24 hours ageing after HCl addition were amorphous while crystalline precursor was started to be seen only after 48 hours ageing. Very little crystallization was seen in case that precursor was not washed and washed with acetone. On the other hand, particles washed with water showed the crystalline peaks that could be perfectly assigned to $ZrW_2O_7(OH)_2(H_2O)_2$ (ICDD-JCPDS-PDF No 28-1500).
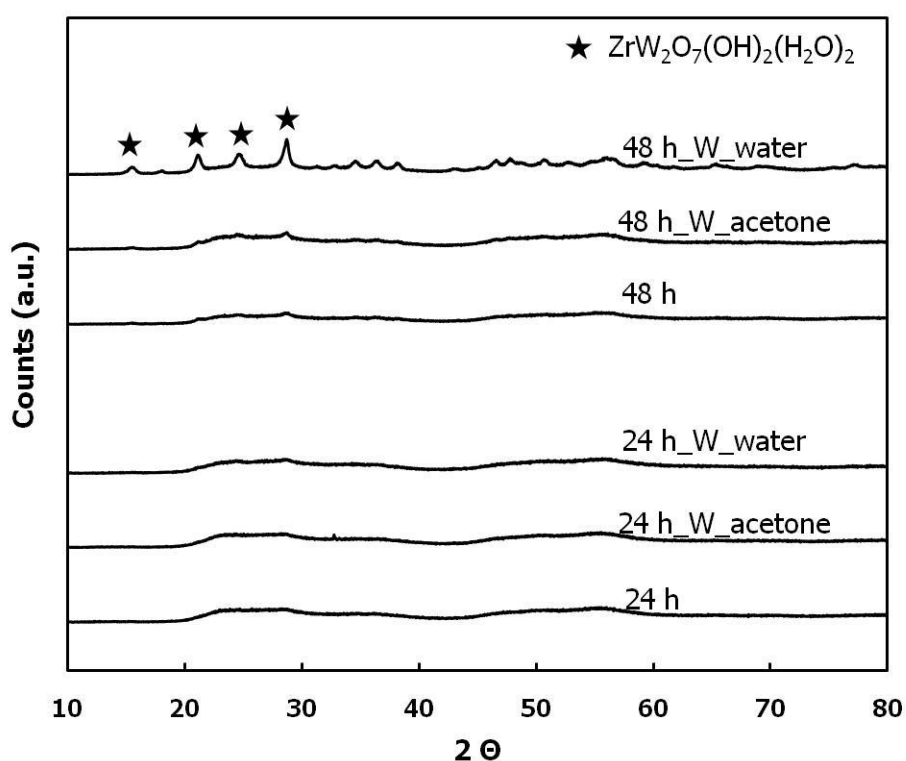
Figure 4.15 XRD patterns of A7 particles before calcination. W stands for 'washing'.

Figure 4.16 shows SEM micrographs of ZrW_2O_8 particles produced from A6 after 48 hours ageing. Larger and agglomerated particles can be spotted in Figure 4.16 (a) in which precursor was not washed. However, washing starts to prevent agglomeration and smaller primary particles were started to be seen in Figure 4.16 (b) and (c). Although there were still some strong agglomerates (therefore larger particles) after washing, the amounts were decreased compared to unwashed case. On the other hand, weak agglomerated particles could be separated easily from each other by USM.
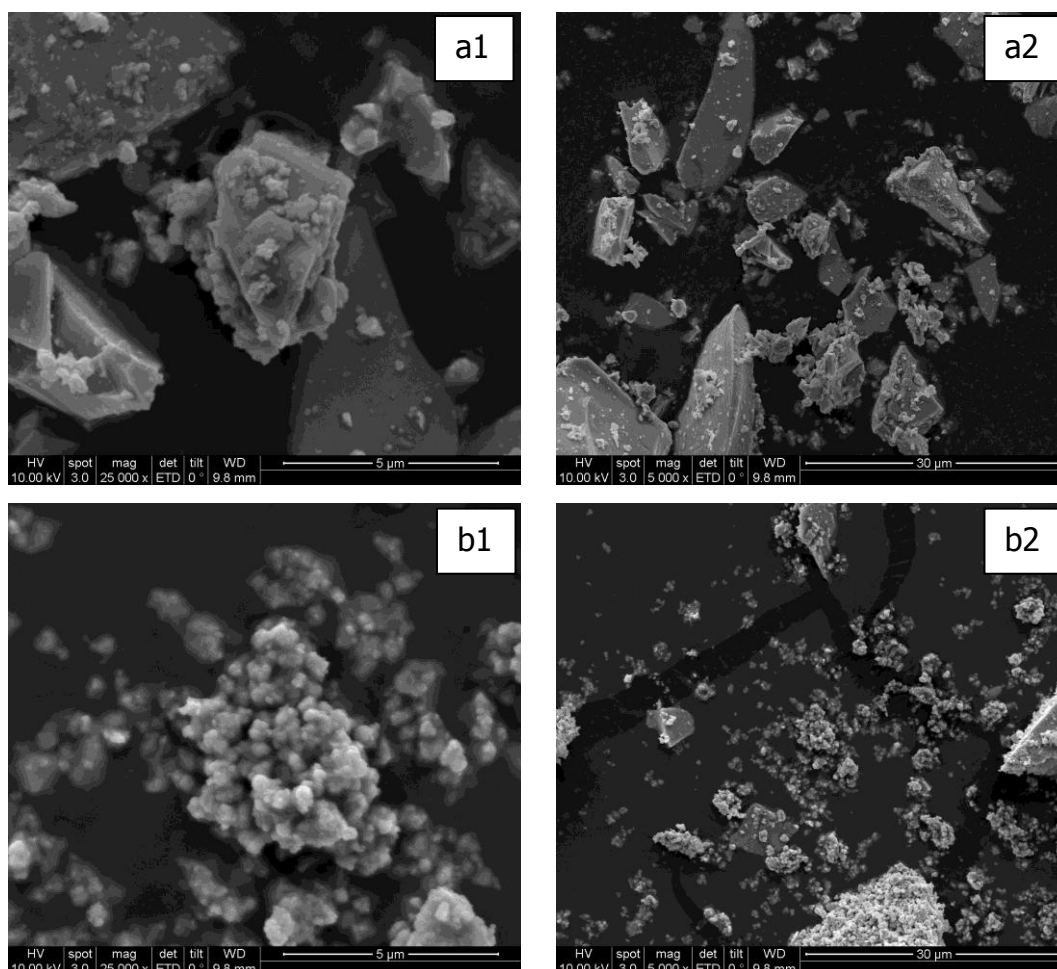
Figure 4.16 SEM micrographs of calcined A6 particles (after 48 hours ageing) (a) unwashed, (b) washed with acetone, and (c) washed with water. Magnifications on the left and right hand side are ×25000 and ×5000, respectively.
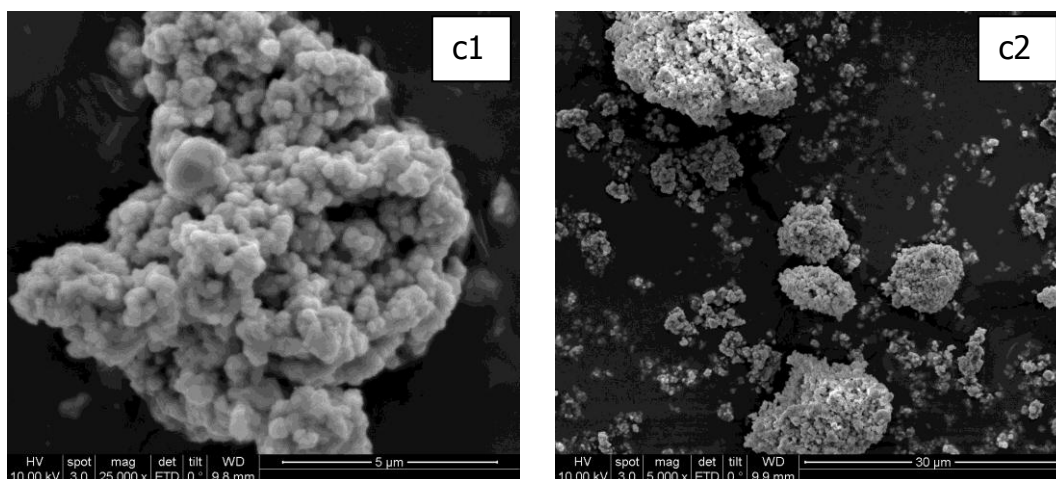
Figure 4.16 SEM micrographs of calcined A6 particles (after 48 hours ageing) (a) unwashed, (b) washed with acetone, and (c) washed with water. Magnifications on the left and right hand side are ×25000 and ×5000, respectively (continued).

SEM micrographs of ZrW_2O_8 particles produced from A7 after 24 and 48 hours of ageing are given in Figure 4.17 and 4.18, respectively. Effects of washing procedures on agglomeration were observed again. Figure 4.17 (a1) shows the surface of the agglomerated particle produced from A7 after 24 hours ageing (washing was not applied). It can be seen that strong agglomerations occurred in the unwashed cases and these particles cannot be broken by USM. Figure 4.18 proves that the low temperature heat treatment at 600 °C did not increase the particle size, which were nearly same before and after calcination for all cases. Additionally, morphology of the particles produced from A7 after 48 hours ageing started to change into rod-like appearance (Figure 4.18). As a consequence, strong agglomerates were formed when the precursor was not washed. However, these strong agglomerates could be minimized in cases where washing was applied to the precursor particles.
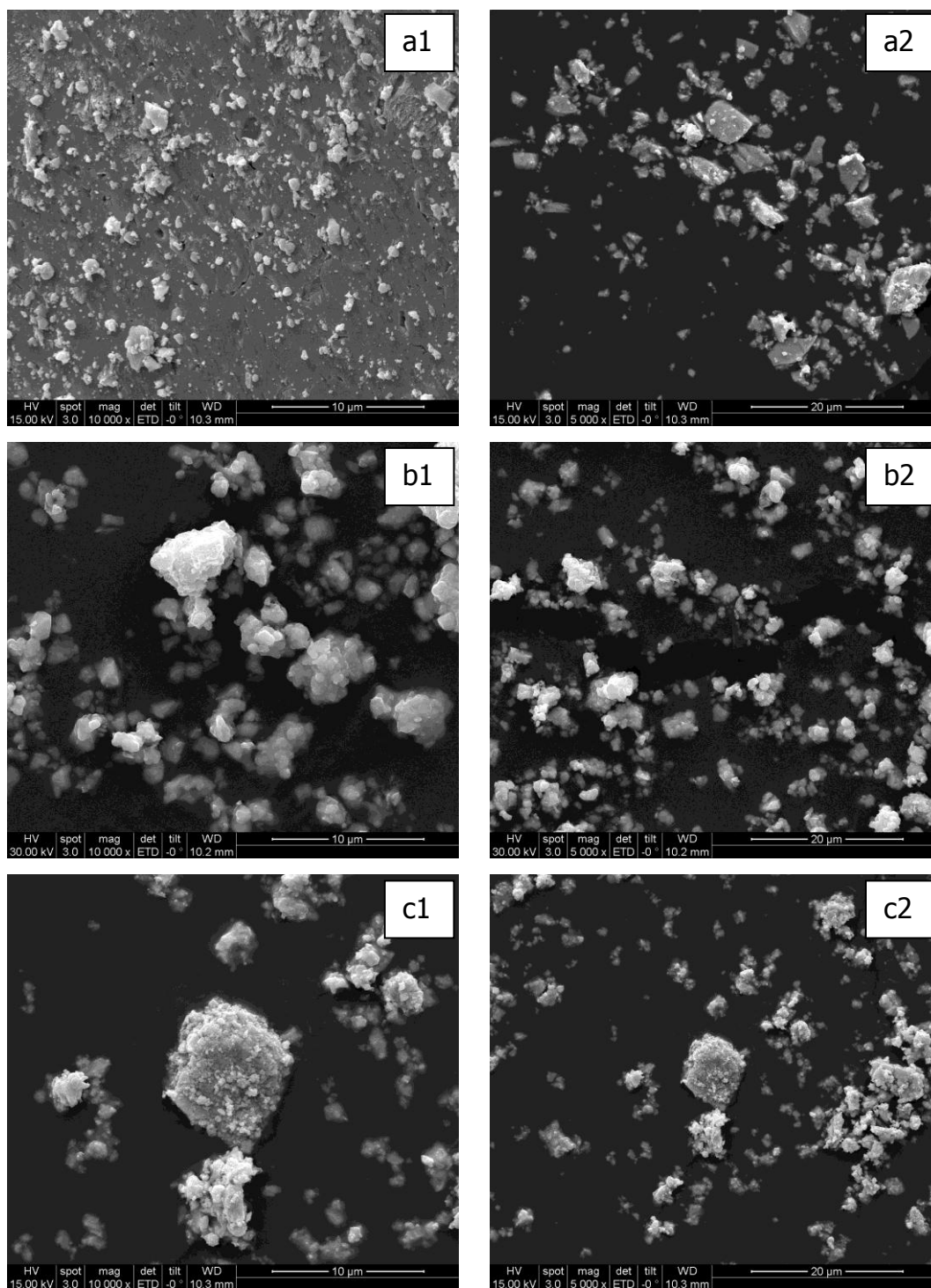
Figure 4.17 SEM micrographs of calcined A7 particles (after 24 hours ageing) (a) unwashed, (b) washed with acetone, and (c) washed with water. Magnifications on the left and right hand side are ×10000 and ×5000, respectively.
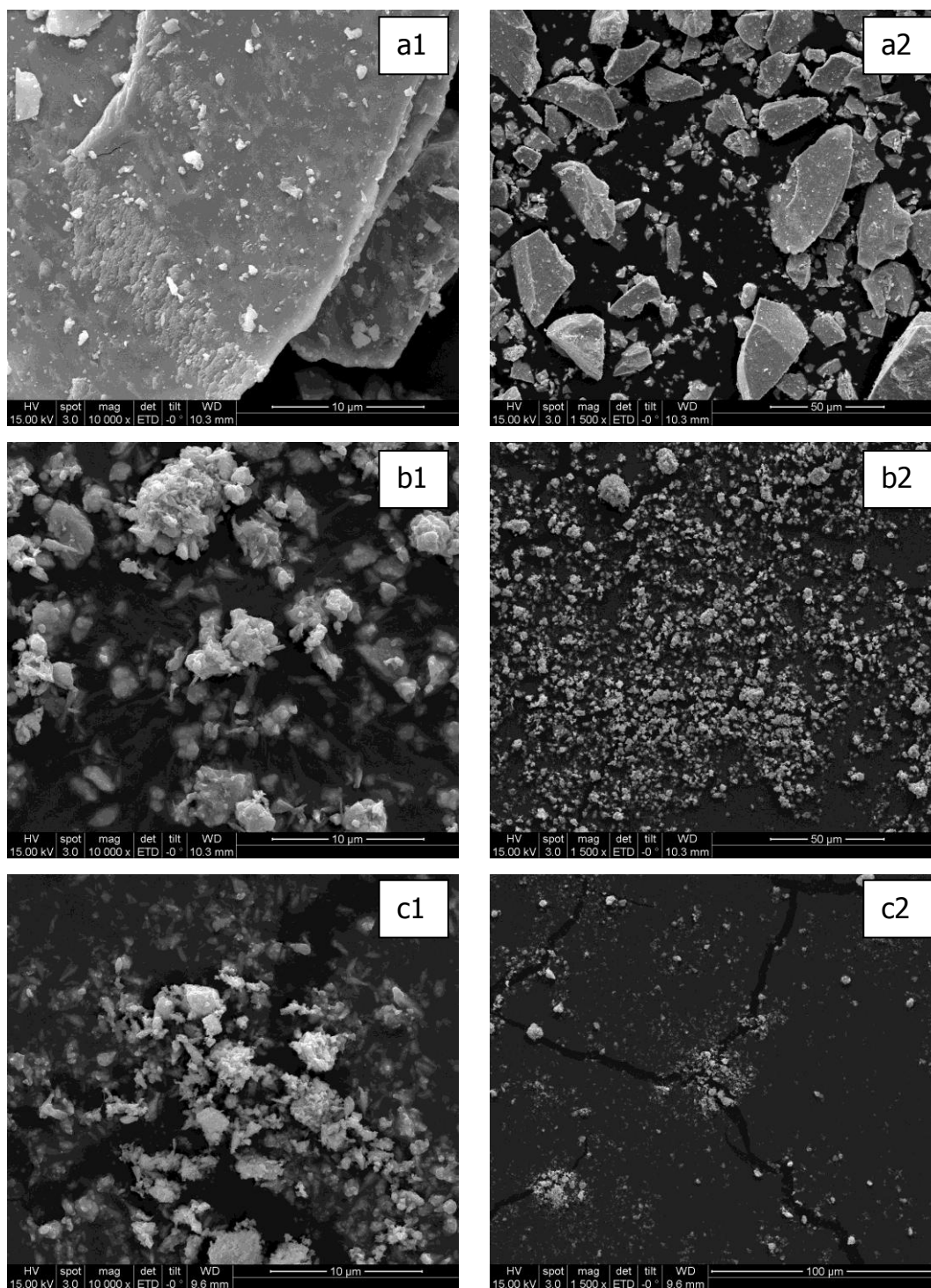
Figure 4.18 SEM micrographs of A7 particles (after 48 hours ageing) before calcination (a) unwashed, (b) washed with acetone, (c) washed with water and after calcination (d) unwashed, (e) washed with acetone, (f) washed with water. Magnifications on the left and right hand side are $\times 10000$ and $\times 1500$, respectively.

81
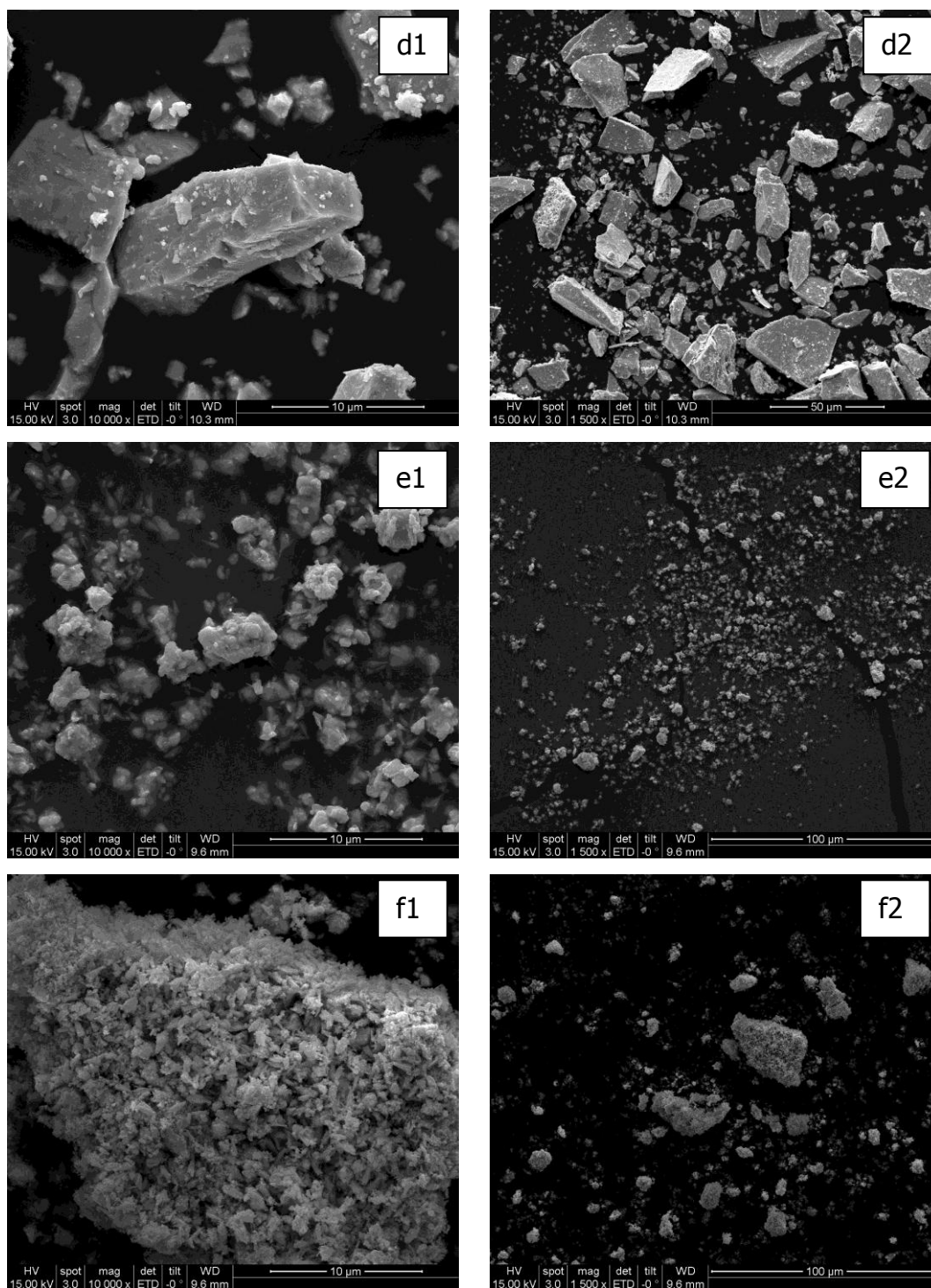
Figure 4.18 SEM micrographs of A7 particles (after 48 hours ageing) before calcination (a) unwashed, (b) washed with acetone, (c) washed with water and after calcination (d) unwashed, (e) washed with acetone, (f) washed with water. Magnifications on the left and right hand side are ×10000 and ×1500, respectively (continued).

Figures 4.19 and 4.20 show the particle size distribution of A6 and A7 particles after 48 hours ageing, respectively. Particle sizes were measured by using both Malvern zeta-sizer, in which nano and submicrometer ranges can be determined, and Malvern master-sizer, in which micrometer size particles can be evaluated. In order to quantify the smaller particles in zeta-sizer, particles were first dispersed in IPA, and only the colloidal particle size distributions between 1 nm and 5 μm were measured. Bigger particles were separated by a simple decantation. On the other hand, both smaller and bigger particles were measured in master-sizer simultaneously. Since zeta-sizer could correctly measure the particle sizes below 1 μm, master-sizer was used to determine the existence of larger particles.

As seen from Figures 4.19(a) and 4.20(a), smaller particles that could be measured in zeta-sizer unit were about 400-600 nm in sizes for both washed and unwashed cases. On the other hand, Figures 4.19(b) and 4.20(b) showed that particles, which were washed after filtering, were smaller in sizes due to minimized agglomeration. Additionally, the amount of particles in submicrometer range was higher in washed cases while the amount of submicrometer particles was very low if precursor was not washed. From the comparison of Figure 4.19(b) with Figure 4.20(b), it is seen that particle sizes were decreased as the HCl concentration increased. The amount of smaller particles was higher in high HCl concentration when it was compared to particle size distributions of the products in which washing was not applied.
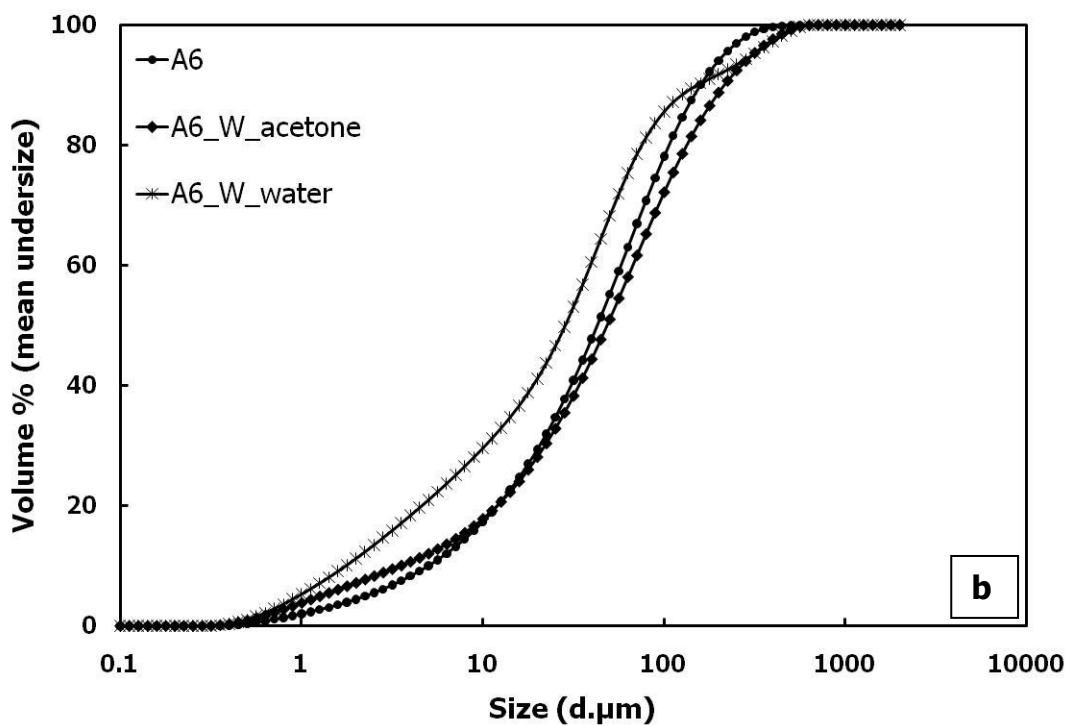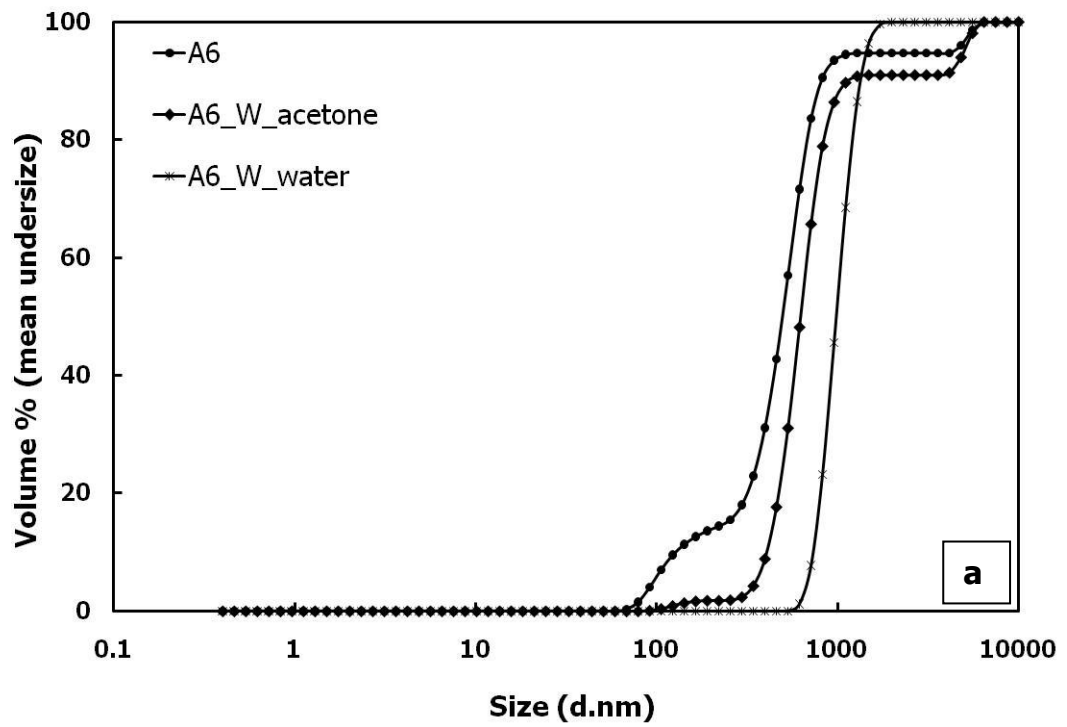
Figure 4.19 Cumulative particle size distributions of experiments A6 particles (after 48 hours ageing) (a) zeta-sizer results and (b) master-sizer results.
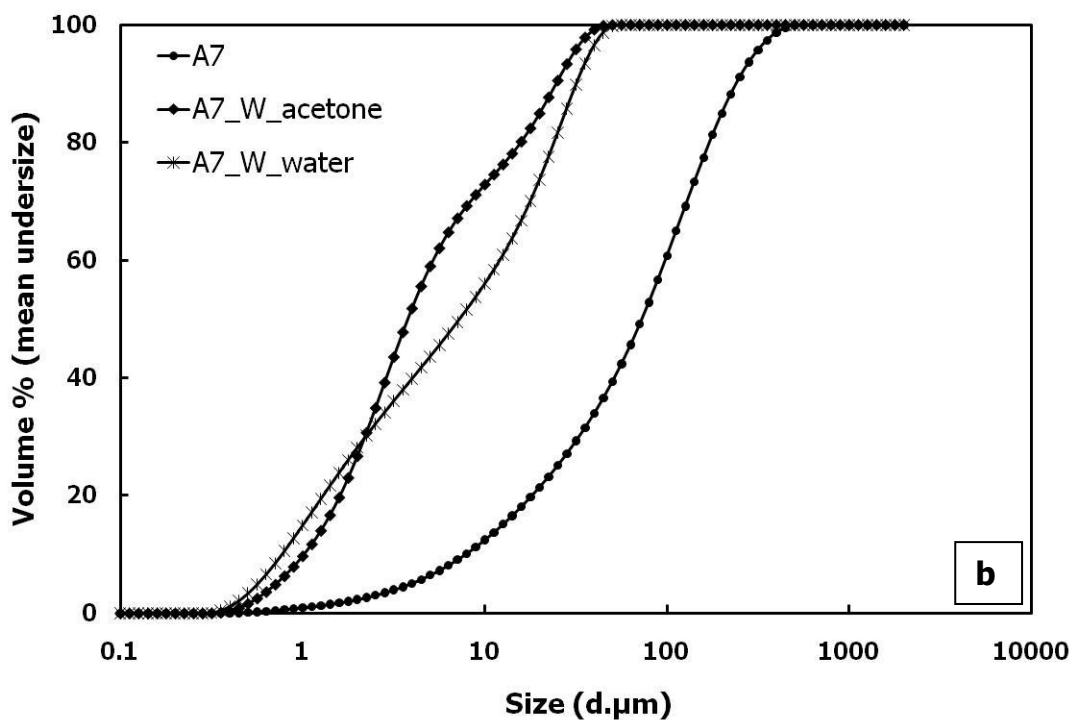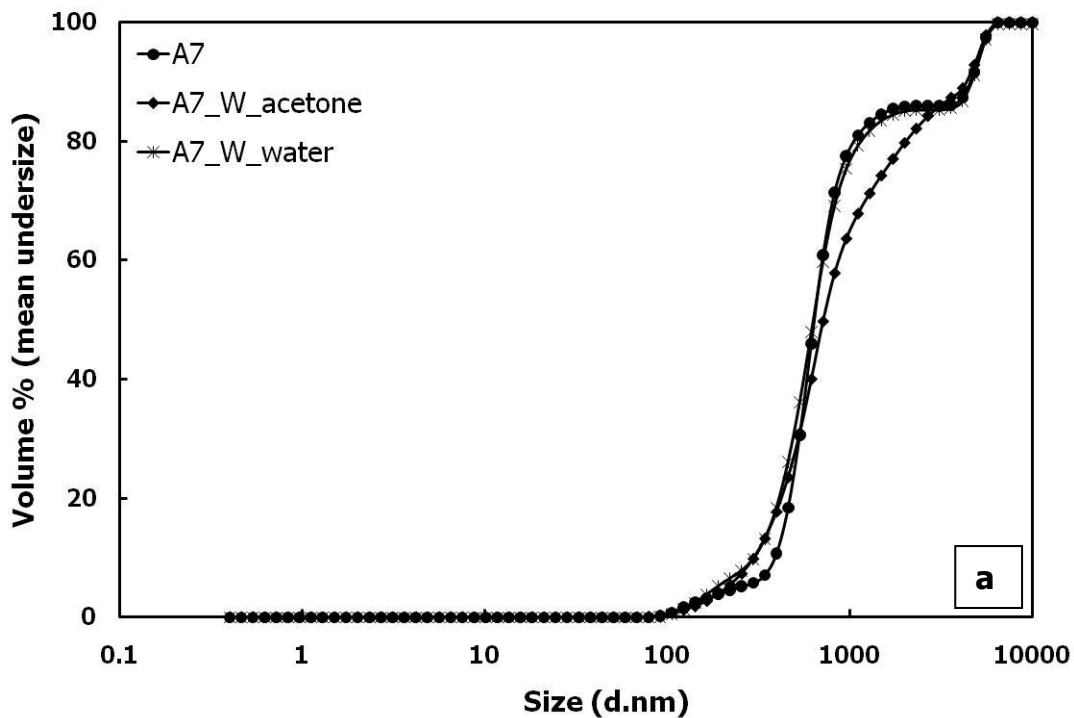
Figure 4.20 Cumulative particle size distributions of experiments A7 particles (after 48 hours ageing) (a) zeta-sizer results and (b) master-sizer results.

85

CHAPTER 5

ZrW$_2$O$_8$-ZrO$_2$ COMPOSITES

Particles produced in experiments A6 and A7 were used for the preparation of composites. Since composite studies were conducted simultaneously with experiments on understanding the effect of washing; in the composite experiments, unwashed ZrW$_2$O$_8$ particles had to be used. However, in the unwashed state, particles were strongly agglomerated, so there were a wide size range of particles after calcination. In order to have good sintering in composites, homogeneous mixing of constituent oxides is important. Therefore, smaller ZrW$_2$O$_8$ particles were separated from strongly agglomerated ones by decantation. To do this, all produced particles were dispersed in a big beaker containing IPA. Then, USM was applied for several minutes. Colloidal particles that could be taken into stable dispersion were separated from the sediments periodically by simple decantation technique. Particle sizes of separated colloidal particles were measured and their distributions are given in Figure 5.1. The average particle sizes were in between 400 and 600 nm.

SEM micrographs of separated ZrW$_2$O$_8$ particles after decantation are given in Figure 5.2. Micrographs show that smaller particles were successfully separated from the larger ones.

Particle size distribution of ZrO_2 particles used in the composite particle blends is given in Figure 5.3. Average sizes were 130 nm. All particle size measurements were done after applying 2 minutes of USM.
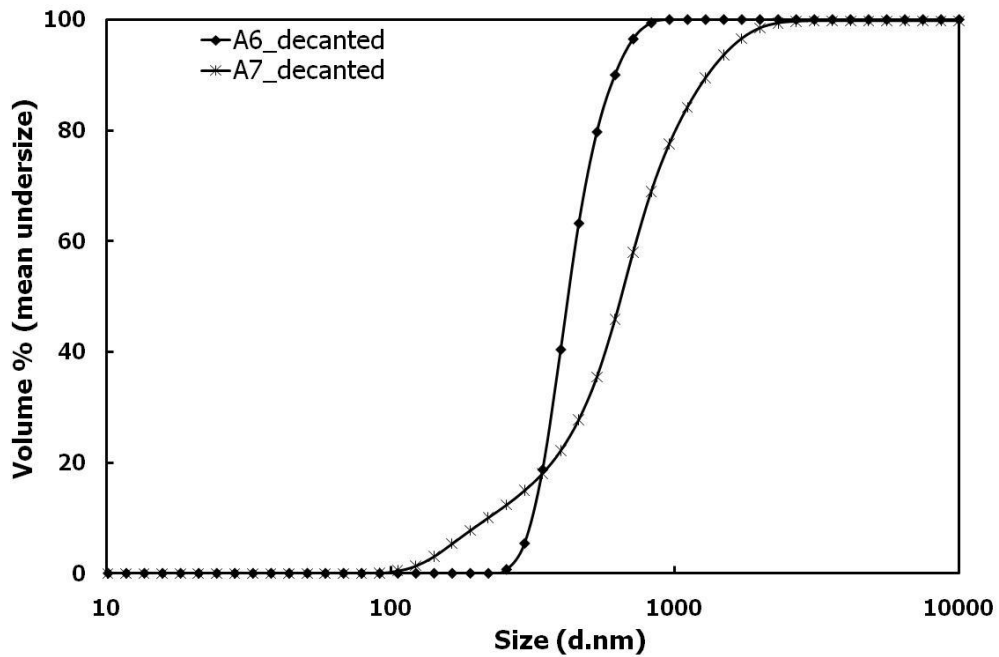
Figure 5.1 Cumulative particle size distributions of decanted A6 and A7.
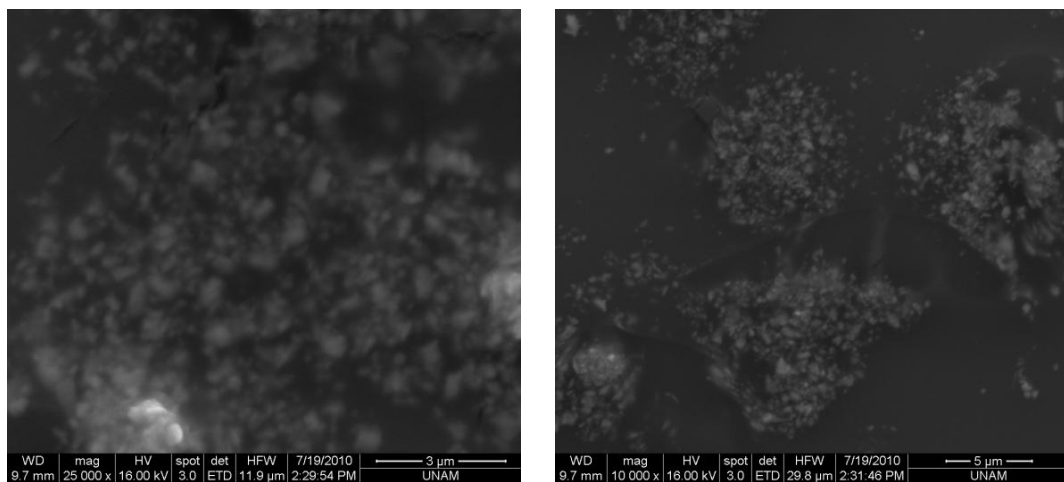
Figure 5.2 SEM micrographs of ZrW_2O_8 particles after decantation.

87
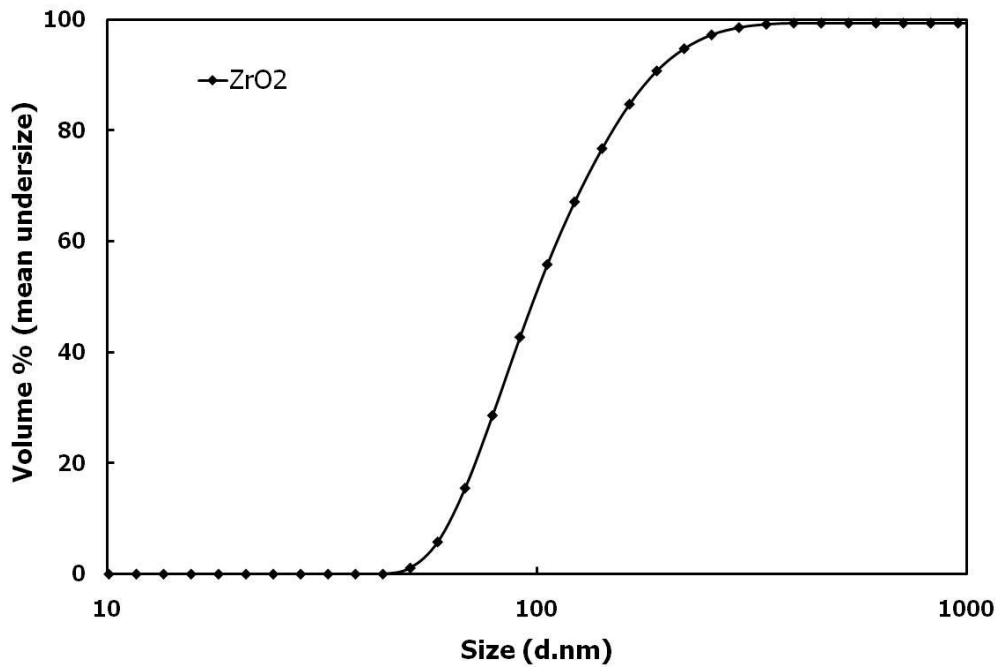
Figure 5.3 Cumulative particle size distribution of commercial ZrO_2 particles.

5.1 Conventional Sintering

Densities and CTE of ZrW_2O_8, ZrO_2, and Al_2O_3 are given in Table 5.1. These values are used in calculating the respective CTE and densities of the composites that would be formed by combining different volume fractions of ZrW_2O_8 and ZrO_2. Values were calculated according to rule of mixtures and necessary amounts of ZrW_2O_8 and ZrO_2 were found by using volume percent to weight percent conversions. In addition, the diameter of the die set used and the thickness of the composite which were 12 mm and 1.5 mm, respectively were considered. Values calculated by using a range of volume fractions are given in Table C.1 (Appendix C) with a sample calculation. Also the necessary amounts of Al_2O_3 in different weight percentages (0.07, 0.15, 0.25, and 0.35) that would be needed as a sintering agent were calculated.

It should be noted that only a selection of the calculated composite compositions were used in actual experiments.

Table 5.1   Densities and CTE values of ZrW_2O_8, ZrO_2, and Al_2O_3.

ZrW_2O_8	
Density (α-phase)	5.08 g/cm^3
CTE (α-phase)	-8.90 x 10^{-6} K^{-1}
CTE (β-phase)	-4.70 x 10^{-6} K^{-1}
CTE (γ-phase)	-1.00 x 10^{-6} K^{-1}
ZrO_2	
Density	5.83 g/cm^3
CTE	9.60 x 10^{-6} K^{-1}
Al_2O_3	
Density	3.97 g/cm^3
CTE	7.60 x 10^{-6} K^{-1}

5.1.1 Effect of the amount of ZrW_2O_8

Data for the first three composites named as C1, C2, and C3 are given in Table 5.2. In these experiments, Al_2O_3 was used as the sintering agent and its amount was kept constant at 0.35 w/o. By keeping all parameters except volume fractions of ZrW_2O_8 and ZrO_2 constant, composite constituents were mixed according to the flow chart given in Figure 3.8. Prepared powders were then pressed uniaxially with 250 MPa and sintered at 1200 $^{\circ}$C for 24 hours in a box furnace.

Table 5.2   Experimental conditions for C1, C2, and C3.

Exp. Name	Volume fractions (%)		Weight (g)		w/o Al_2O_3	Al_2O_3 (mg)
	ZrW_2O_8	ZrO_2	ZrW_2O_8	ZrO_2		
C1	35.00	65.00	0.30	0.64	0.35	3.31
C2	51.90	48.10	0.45	0.48	0.35	3.23
C3	67.15	32.85	0.58	0.32	0.35	3.16

Composite C1 showed neither a geometrical deformation, nor a change in its color and it did not stick to the platinum crucible. However, there were some cracks at the surface of the composite body. On the other hand, C2 sticked from its contact surfaces to the crucible and its color changed to yellow. C3 completely lost its geometrical integrity by melting down, and sodium hydroxide and sulfuric acid treatments had to be used in cleaning the crucible. Therefore XRD, dilatometry, and SEM analysis could not be carried out for sample C3.

XRD patterns of C1 and C2 are given in Figure 5.4 (a). Patterns show that ZrW_2O_8 was decomposed into WO_3 and ZrO_2 in C2 to a large extent. The intensity of the peaks associated with ZrW_2O_8 were very low. This was also reflected on thermal expansion curves given in Figure 5.5. Since WO_3 and ZrO_2 have positive CTE, expansion curve of C2 was also positive. On the other hand, C1 was composed of α-ZrW_2O_8, γ_o-ZrW_2O_8, and γ_t-ZrW_2O_8 after sintering. Applied pressure during pellet preparation was 250 MPa. It was indicated in the literature that α-ZrW_2O_8 can transform into γ_o-ZrW_2O_8 at pressures like 250 MPa [48, 58, 62]. However, there was also expansion and contraction in the system during heat treatment, sintering and quenching steps and these thermal movements have the potential to exert even higher pressures at the contact points of the particles. Therefore α-ZrW_2O_8 in the

composite bodies were also observed to transform into γ_t-ZrW_2O_8 besides γ_o-ZrW_2O_8 indicating that the pressures could have been extented well over 250 MPa. Particle sizes of ZrW_2O_8 remained larger than those of ZrO_2 despite the efforts for reducing them. The size difference between the components could have been an additional reason that had alleviated the pressure buildup among the components that expand and contract in opposite directions during heating up or down. α-ZrW_2O_8 was probably transformed partially into γ_o-ZrW_2O_8 after pressing which can be assumed to turn into γ_t-ZrW_2O_8 to a certain extent because of the higher pressures at the interfaces. A certain amount of amorphization is also possible at intermediate pressures.

Yttrium stabilized ZrO_2 (YSZ) that was commercially supplied was composed of mainly tetragonal phase (ICDD-JCPDS-PDF No 17-0923) with a small amount of monoclinic (ICDD-JCPDS-PDF No 37-1484) inclusions (Appendix B, Figure B7). On the other hand, ZrO_2 in the composite bodies was almost completely in monoclinic phase after sintering, which can be taken as another proof of contact pressures that are predicted to develop. It is known that tetragonal YSZ is known to transform into monoclinic phase at crack tips upon application of pressure to ceramic bodies that have YSZ, a mechanism with which 'tough' ceramics can be produced. Thermal expansion curves of both C1 and C2 are given in Figure 5.4 (b). In C1, near zero thermal expansion with small fluctuations was seen until around 120 ^{o}C (where γ-α phase transition occurs), and then there was a positive expansion because of this phase transition to which a volume expansion accompanied like in literature as exemplified in Figure 2.17. CTE was leveled again to zero after around 200 ^{o}C [48, 58]. C1 should show positive thermal expansion in reference to the calculated values according to rule of mixture (Table C.1 in Appendix C). However, rule of mixture is known to fail for composites, in which thermal stresses and voids exist.
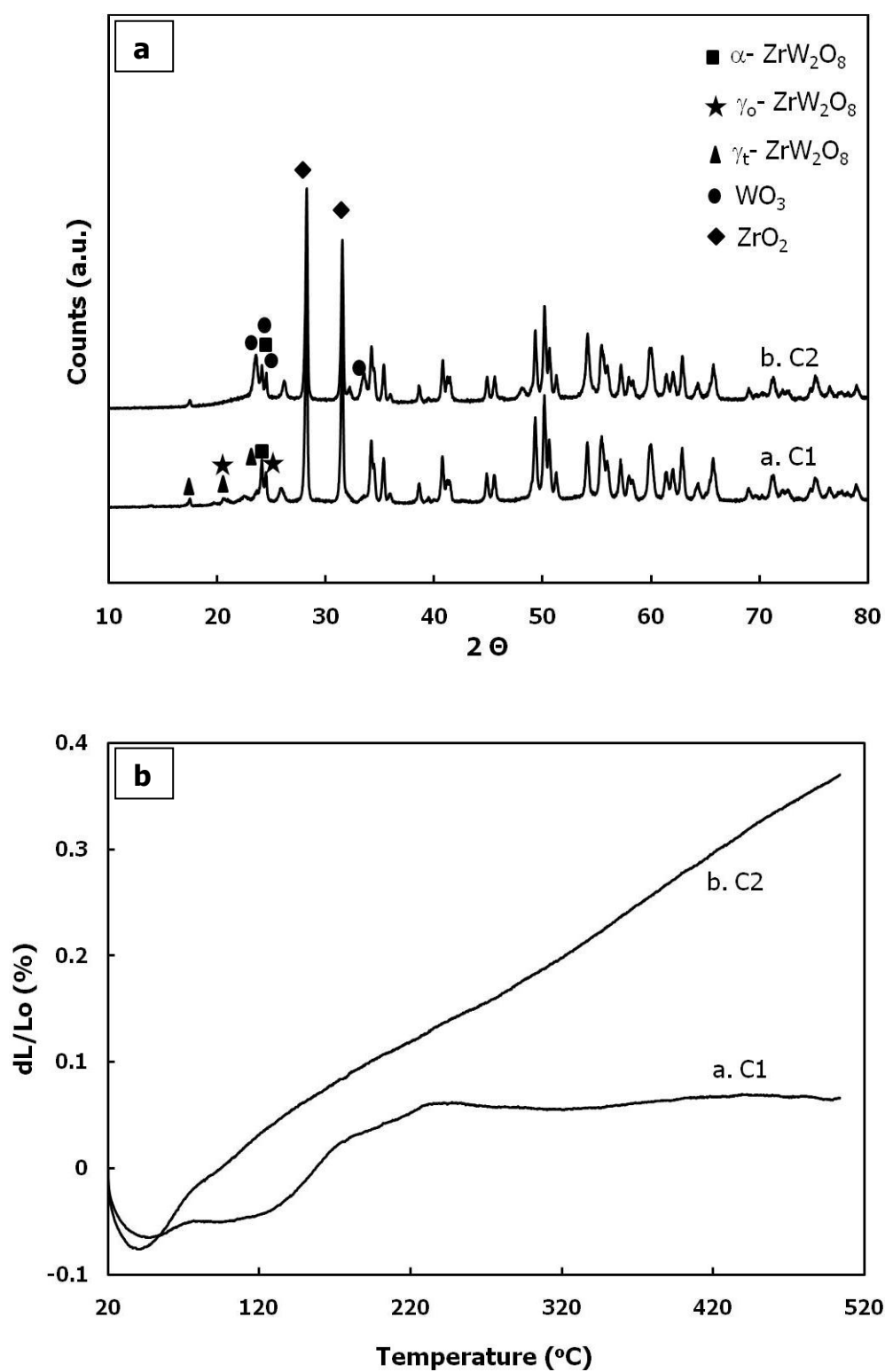
Figure 5.4 (a) XRD patterns and (b) Thermal expansion behaviors of (a) C1 and (b) C2.

SEM micrographs of C1 and C2 are given in Figure 5.5. Expected liquid phase sintering was observed in C1. Although some cracks and not fully dense structures were detected at the fracture surfaces (Figure 5.5 (a)), particle fusion and grain growth was apparent. It should be noted that fracture surfaces are representative of the most heterogeneous and so the most defective parts of sintered bodies. For example a ZrO_2 rich region that possibly forms due to segregation at any stage of powder mixture or pellet preparation cannot have a chance to be sintered in the firing step. Micrographs taken from such surfaces would not be representative of the rest of the structure and it is also necessary to look at the unbroken surfaces of the composites. Figure 5.5 (b) shows the SEM images taken from the surface of C1. It can be inferred from micrographs that sintering was successful; however, some voids were present in the structure. This can explain the deviation from rule of mixtures. Although C2 was decomposed into WO_3 and ZrO_2, liquid phase sintering was also observed as seen in Figure 5.5 (c). This is probably due to the fact that higher ZrW_2O_8 percentages in the bodies have more chance in liquefaction, which on the other hand speeds up the decomposition of ZrW_2O_8 and cause the sticking of pellets on the crucibles or even complete shape loss.
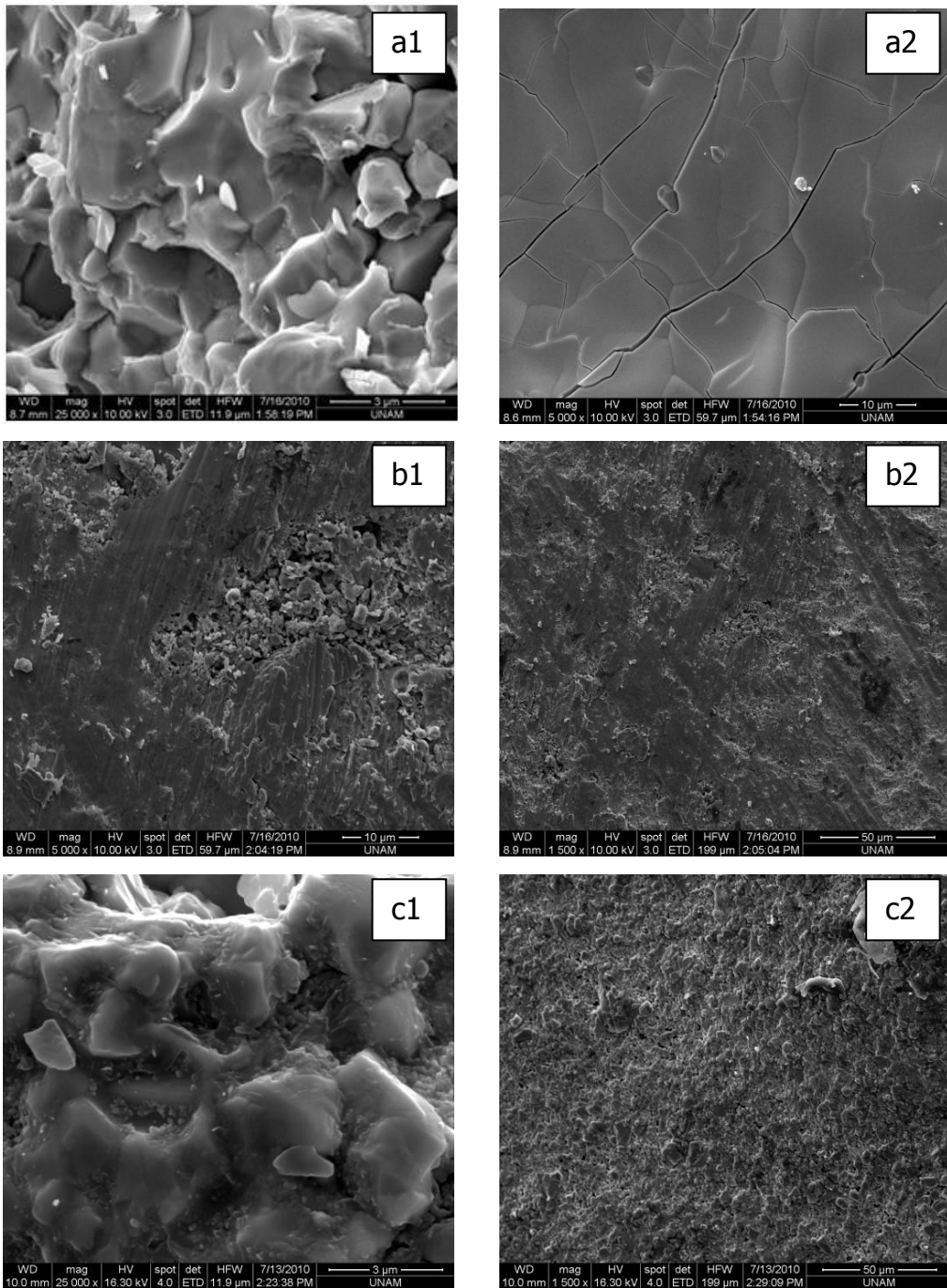
Figure 5.5 SEM micrographs of (a) fracture surface from C1, (b) surface of
C1, and (c) fracture surface from C2. Magnification: in b2 and
c2 ×1500, a2 and b1 ×5000, a1 and c1 ×25000.

94

5.1.2 Effect of the amount of Al_2O_3

In order to see the effect of the amount of sintering agent on sintering behavior, four additional experiments were done with smaller amounts of sintering agent compared to C1 (Table 5.3) while fixing the composition to that of C1 (35% ZrW_2O_8-65% ZrO_2). Since 1200 $^{\circ}$C was close to the melting point of ZrW_2O_8, it was considered that 1190 $^{\circ}$C would be a better choice for sintering. In addition, 6 hours of sintering treatment was preferred, since ZrW_2O_8 particles are blended in already-crystallized forms, unlike in in-situ methods, and probability of excessive liquifaction can be minimized.

Table 5.3   Experimental conditions for C4, C5, C6 and C7.

Exp. Name	Volume fractions (%)		Weight (g)		w/o Al_2O_3	Al_2O_3 (mg)
	ZrW_2O_8	ZrO_2	ZrW_2O_8	ZrO_2		
C4	35	65	0.3	0.64	0.07	0.66
C5	35	65	0.3	0.64	0.15	1.42
C6	35	65	0.6	1.28	0.25	4.72
C7	35	65	0.3	0.64	0.35	3.31

Photographs of composites before and after sintering are given in Figure 5.6. The colors of produced composites did not change after sintering. It was observed that a small amount of concavity forms after quenching, as the amount of Al_2O_3 increases. XRD analysis for C4, C5, C6, and C7 was carried out and patterns are given in Figure 5.7.
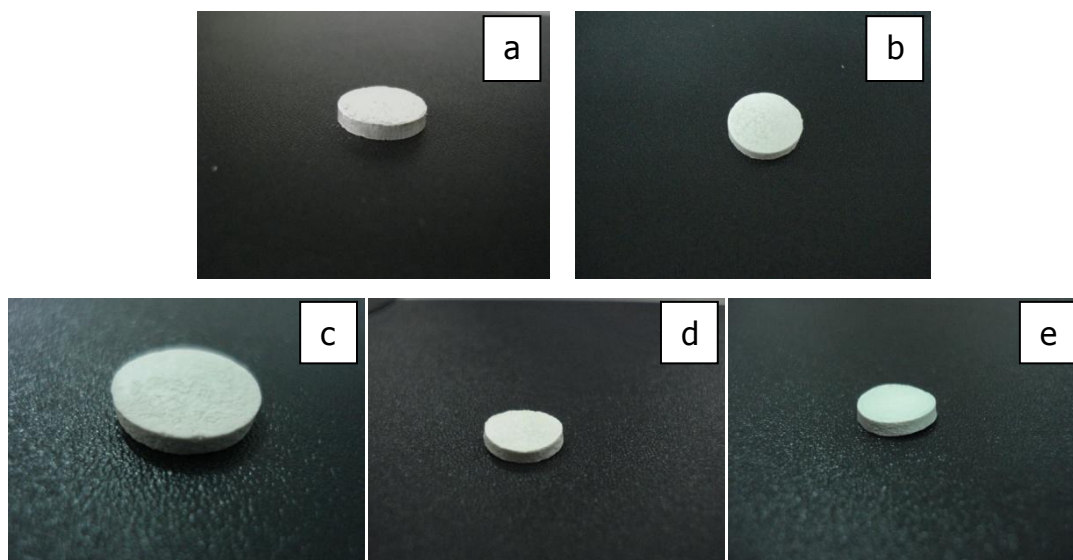
Figure 5.6 Pictures of composites: (a) before sintering C4; after sintering (b) C4, (c) C5, (d) C6, and (e) C7.
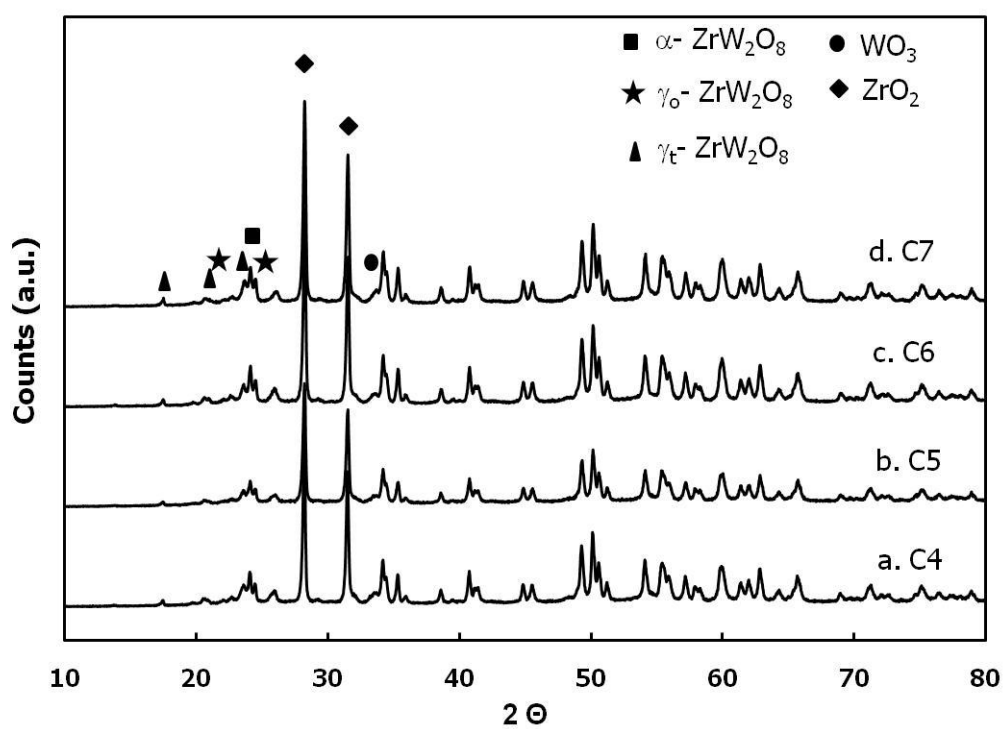
Figure 5.7 XRD patterns of experiments (a) C4, (b) C5, (c) C6, and (d) C7.

It was observed from XRD patterns that all composites contained γ_t-ZrW$_2$O$_8$, γ_o-ZrW$_2$O$_8$, α-ZrW$_2$O$_8$ phases. However, the amount of α-ZrW$_2$O$_8$ was less than that in C1 and there were signs of WO$_3$ peaks which was expected to effect the thermal expansion behavior of composites. Al$_2$(WO$_4$)$_3$ formation was not observed with increasing amount of Al$_2$O$_3$ in any of the composites, but this was not expected since in C1 already the highest amount of sintering agent was used. Minimum amount of WO$_3$ was found in C5 and its thermal expansion curve (Figure 5.8) displayed values close to zero while all other compositions showed PTE. C5 showed nearly zero thermal expansion until the γ-α phase transition region, after which expansion was again close to zero.
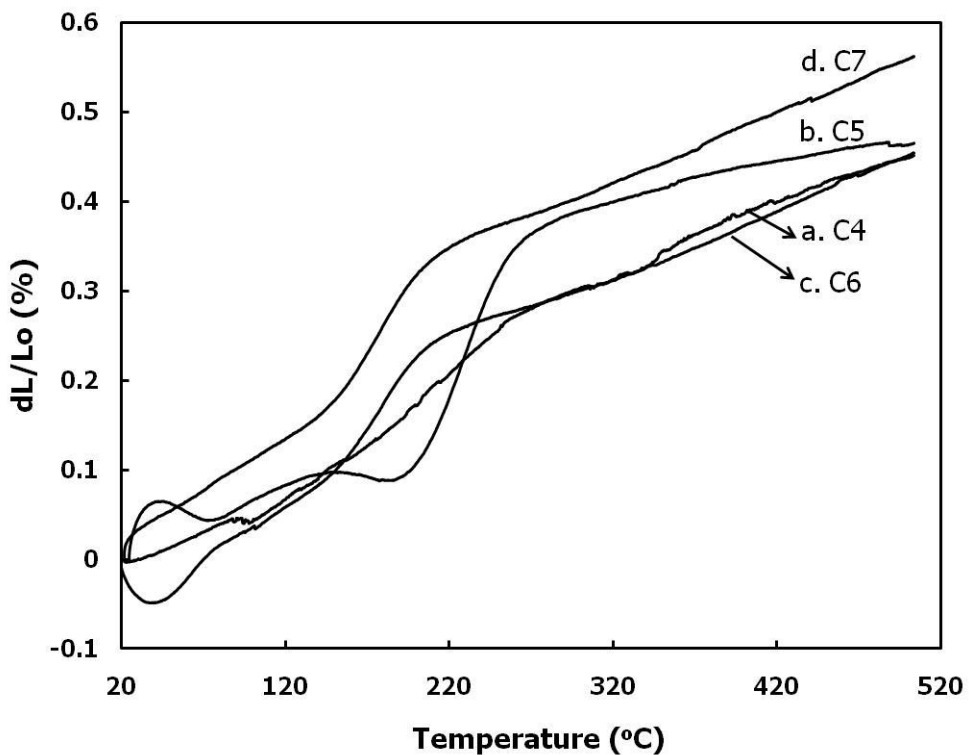
Figure 5.8 Thermal expansion behavior of composites (a) C4, (b) C5, (c) C6 and (d) C7.

97

SEM micrographs of C4, C5, C6, and C7 are given in Figure 5.9. Micrographs showed again that liquid phase sintering initiates in the composites at 1190 ^{o}C even in 6 hours. With this temperature time combination, it was possible to sinter compacts only to certain extent and homogeneous progress of liquid phase in the body was more evident in C6 and C7, which coincidently had higher sintering agent contents. Smaller amounts of sintering agents could be useful in sintering of composites with higher ZrW_2O_8 by keeping the liquid phase forming at minimum. Also the amount of sintering agent could probably be lowered if the desired quantity was precoated over ZrW_2O_8 particles during powder blend preparation. Even though fully dense structures were not observed and due to either remaining voids or WO_3 formation, CTE values were not same as C1, the fact that the extented times at this low temperature might yield in the desired phase assemblies. However, these could be subjects of a future work.
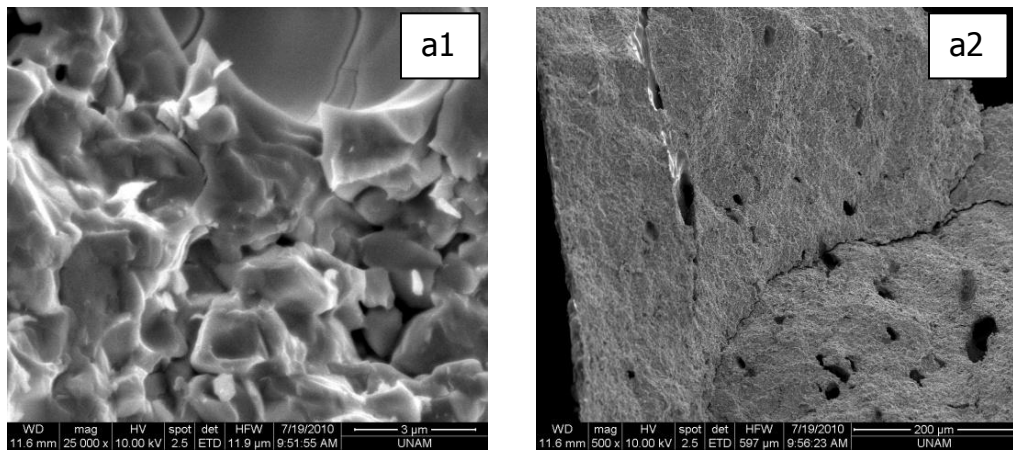
Figure 5.9 SEM micrographs of (a) C4, (b) C5, (c) C6, and (d) C7. Magnifications on the left and right hand side are ×25000 and ×500, respectively.
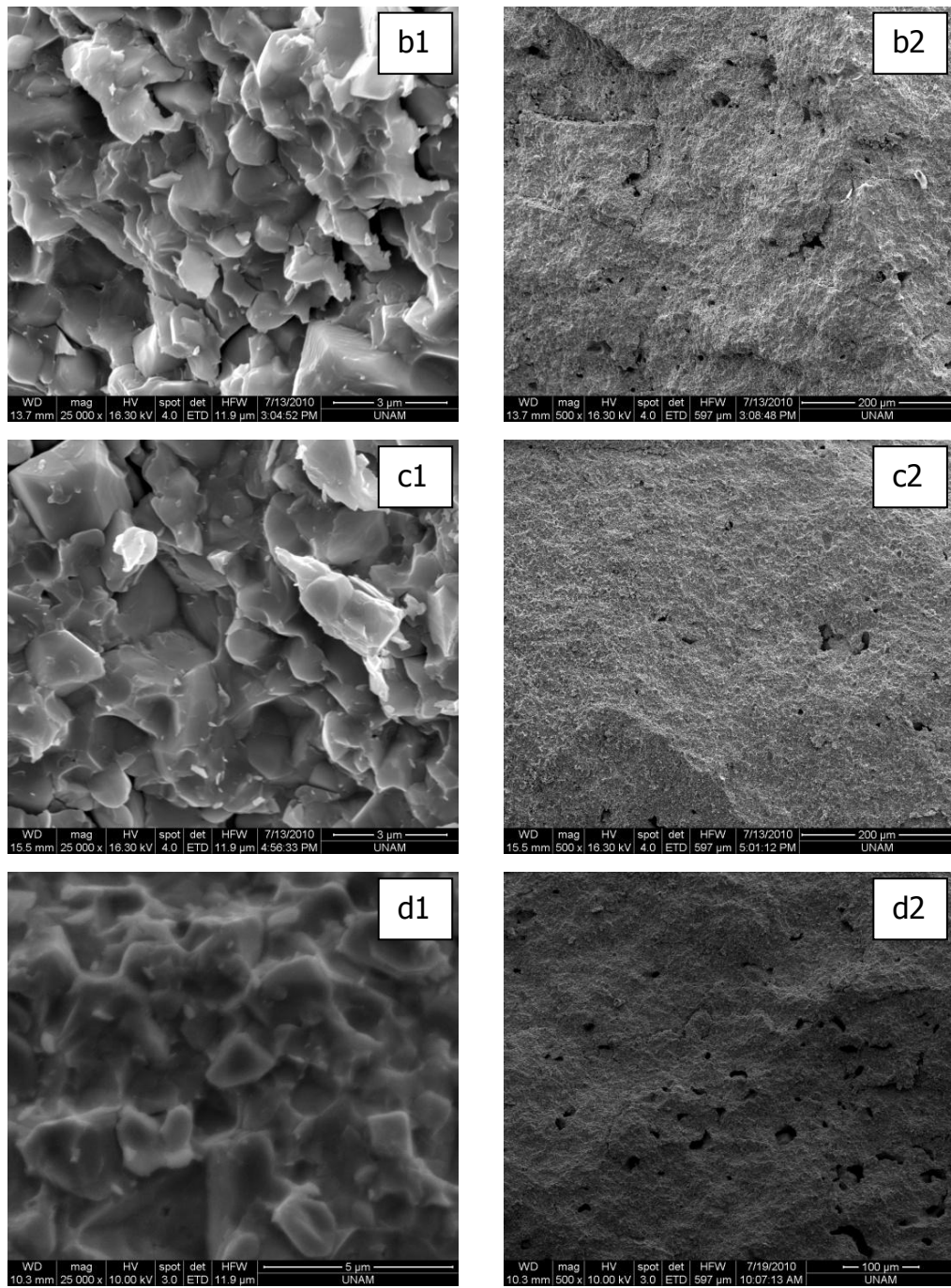
Figure 5.9 SEM micrographs of (a) C4, (b) C5, (c) C6, and (d) C7. Magnifications on the left and right hand side are ×25000 and ×500, respectively (continued).

5.1.3 Effect of sintering time

In order to see the effect of sintering time on the progress of liquid phase formation within the composite structures, C6 was also sintered for 3 hours. C6 was chosen because it seemed to yield the lowest amount of voids in the previous set. XRD patterns and thermal expansion curves are given in Figure 5.10 and Figure 5.11, respectively. XRD patterns were nearly the same for both 3 and 6 hours. On the other hand, thermal expansion curves (Figure 5.11 (b)) showed that although similar expansion behaviors were observed, smaller volume increase occurred after 6 hours of sintering. SEM micrographs of C6 after 3 hours and 6 hours sintering are given in Figure 5.12.
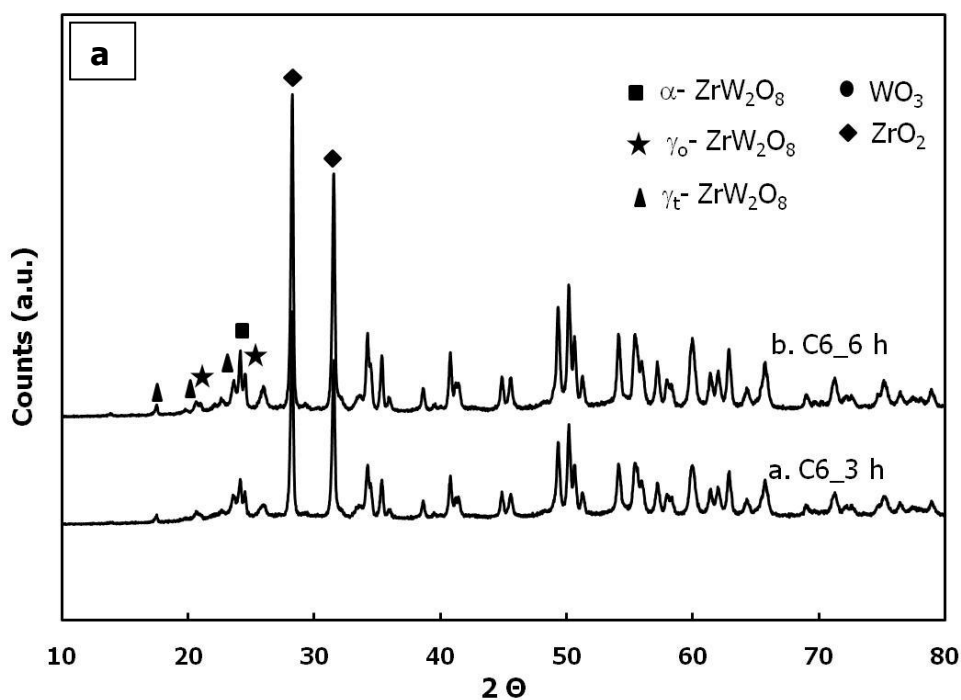
Figure 5.10 XRD patterns of C6 after (a) 3 hours (b) 6 hours sintering.
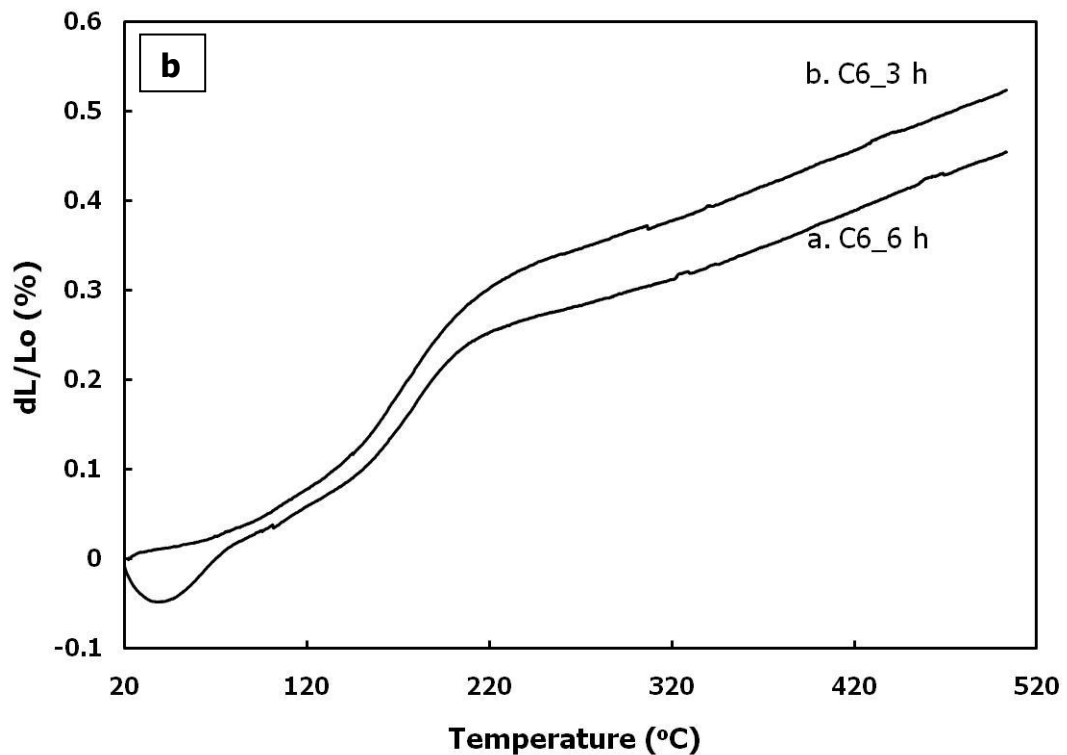
Figure 5.11 Thermal expansion behaviors of C6 after (a) 3 hours (b) 6 hours sintering.

Micrographs showed that 3 hours sintering was not enough for spreading of the liquid phase. Since liquid phase was only formed in some parts of the composite, ZrO_2 rich regions could not be sintered. Therefore, a porous and fragile structure was obtained. It was concluded that liquid phase was diffused into the pores in time and denser structures were formed accordingly. So this also explains that if body is not fully sintered due to some reason like in previous set, it does expand more. When C1 and C5 were compared, it was proven that longer times were needed for conventional sintering methods. It was observed in C1 also that grain sizes increase due to the longer sintering times which lead to denser and stronger structures.
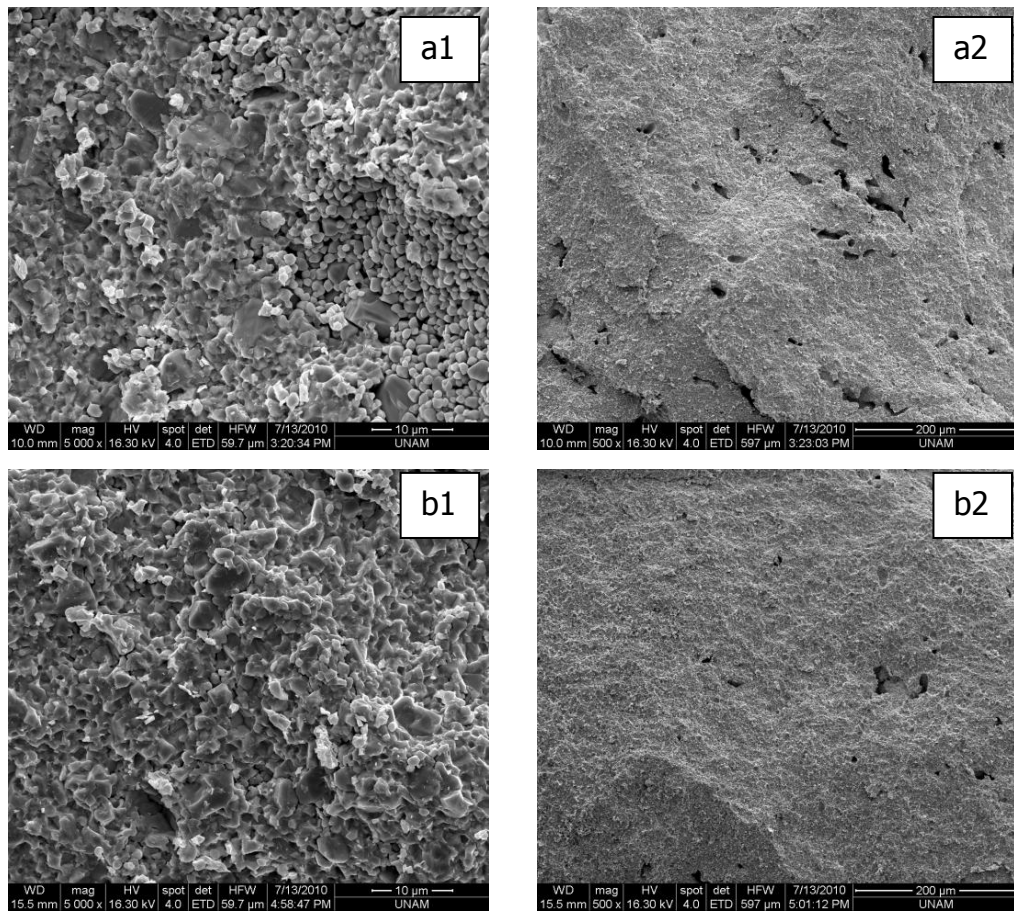
Figure 5.12 SEM micrographs of C6 after (a) 3 hours (b) 6 hours sintering. Magnifications at the left and right hand side are 5000 and 500, respectively.

Denser structures can be obtained if longer sintering times were used, oxides of similar sizes were mixed more homogeneously or smaller size sintering aid particles or precursors could be effectively distributed over the particles for the simultaneous spread of liquid phase upon formation, without forming large voids at the positions it initially forms and leaves. The ratio of total liquid phase forming oxides (alumina and a certain ratio of zirconium tungstate) to zirconia should be a more important factor rather than the amount of alumina alone. However, this could be considered less critical, if one uses a temperature more than 50 °C lower than the melting point of

zirconium tungstate. 24 hours sintering provides a dense structure in C1, although not in accordance with rule of mixture, show near-zero CTE. However, thermal stresses are unavoidable in conventional methods because of the necessity of a quenching step. Furthermore, there are always thermal stresses and voids in the structures due to the non-harmonic expansion and contraction behavior of ZrW_2O_8 and ZrO_2 particles during cooling down or even the real use. Therefore, it is not surprising to have deviation in measured CTE with respect to what is calculated from rule of mixture.

5.2   Spark Plasma Sintering (SPS)

The values for density and CTE for different volume fractions of ZrW_2O_8 and ZrO_2 were calculated from rule of mixture using Table 5.1 and tabulated in Table C2 (in Appendix C). In this case, diameter of the die is 20 mm and thickness of the composites is taken to be 4 mm for S1-S4 and 2 mm for others. In all experiments, applied pressure and pulse time were kept constant at 50MPa and 12ms/2ms, respectively.

Initial experiments (S1 and S2) were performed using lower sintering temperatures like 600-650 ^{o}C similar to literature [1, 53]. The experimental conditions are given in Table 5.4. As a first step in sintering process, temperature was increased at a rate of 100 ^{o}C/min until 450 ^{o}C, and then decreased to 50 ^{o}C/min to the desired sintering temperature (650 ^{o}C and 600 ^{o}C for S1 and S2, respectively). Additionally, 50MPa pressure was applied uniaxially to composites during sintering. Required amounts of ZrW_2O_8 and ZrO_2 were calculated by assuming thickness of the composites as 4mm. Thus, thicker pellets were obtained.

Table 5.4   Experimental conditions for S1 and S2.

Exp. Name	Volume fractions (%)		Weight (g)[a]		Until 450°C		After 450°C		Sintering	
	ZrW_2O_8	ZrO_2	ZrW_2O_8	ZrO_2	°C/min	time (min)	°C/min	time (min)	T (°C)	time (min)
S1	35.00	65.00	2.23	4.76	100	4.5	50	4	650	10
S2	100.00	0.00	7.00	0.00	100	4.5	50	3	600	10

[a]ZrW_2O_8 and ZrO_2 amounts were calculated by assuming diameter and thickness as 20 mm and 4 mm, respectively.

XRD patterns and SPS process diagrams are given in Figures 5.13 and 5.14, respectively. Applied temperature, pressure, and punch motion can be followed from Figure 5.14. Red line shows applied temperature while blue line represents the punch motions. A sintering event is always associated with a volume decrease. Therefore, if sintering starts at any temperature this can practically be followed from changes in punch motion, which shows up as a peak in the punch motion diagram.

Figure 5.13 XRD patterns of composites (a) S1 and (b) S2.

Figure 5.14 SPS process diagrams of experiments (a) S1 and (b) S2.

Figure 5.14 SPS process diagrams of experiments (a) S1 and (b) S2 (continued).

As seen in Figure 5.14 and 5.15, sintering cannot be achieved in either case because of the insufficient temperature applied. There was no peak formation in the blue lines. Based on obtained results in conventional sintering, S1 was prepared with 35% ZrW_2O_8 and 65% ZrO_2. From XRD patterns, it was observed that also no phase transitions occurred in ZrW_2O_8 at the applied temperature and pressure. Additionally, ZrO_2 was mostly tetragonal and almost no monoclinic phases existed. S2 was prepared by only α-ZrW_2O_8 particles similar to literature [53]. In literature almost fully dense structure was obtained after 600 $^{\circ}$C sintering; however sintering was not achieved in S2. The reason is thought to be the particle size of used ZrW_2O_8. Particles used in the only SPS work reported in the literature have the smallest particle sizes (50-300 nm) ever [53], whereas 400-600 nm particles were used in C2. Size of the particles affects the temperature and pressure that can be attained at the grain boundaries in SPS. Thus, smaller particles can be sintered at lower temperatures in SPS technique. Phase transitions did not occur at 50 MPa according to XRD patterns (Figure 5.13 (b)) when sintering was not accomplished. The specific advantage of being

106

able to sinter at 600-650 $^{\circ}$C would have been the possibility of preventing the quenching step. However, this does not seem feasible with the particles produced in the first part of this work.
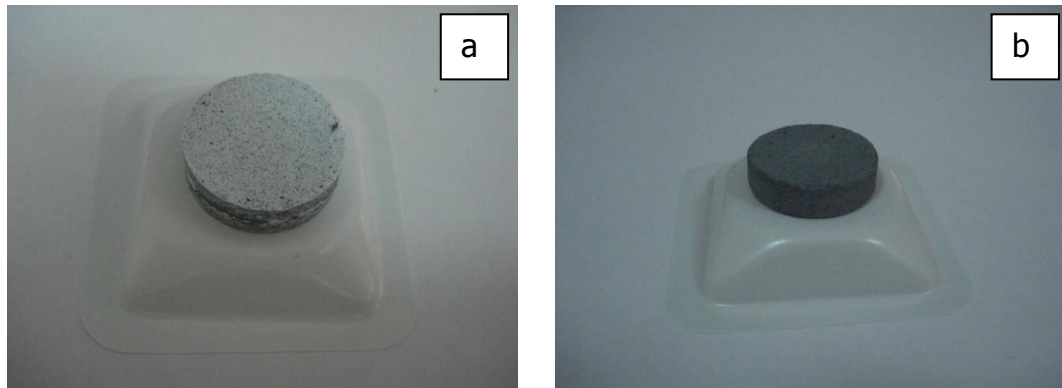
Figure 5.15 Pictures of composites after treatment at 600 and 650 $^{\circ}$C for (a) S1 and (b) S2, respectively.

Since sintering was not achieved in S1 and S2, it was planned to sinter particles at higher temperatures and new experiments (S3 and S4) were carried out accordingly (experimental conditions can be seen in Table 5.5). In conventional methods, quenching should be applied after sintering to prevent phase transition. Since quenching cannot be applied in SPS, composite bodies were cooled by SPS cooling system. Cooling was achieved by water circulation system around the die rather than quenching.

Table 5.5   Experimental conditions for S3 and S4.

Exp. Name	Volume fractions (%)		Weight (g)[a]		Until 450°C		After 450°C		Sintering	
	ZrW_2O_8	ZrO_2	ZrW_2O_8	ZrO_2	°C/ min	time (min)	°C/ min	time (min)	T (°C)	time (min)
S3	51.90	48.10	3.31	3.52	100	4.5	200	3.3	1150	10
S4	51.90	48.10	3.31	3.52	100	4.5	200	2.45	1000	5

[a]ZrW_2O_8 and ZrO_2 amounts were calculated by assuming diameter and thickness as 20 mm and 4 mm, respectively.

XRD patterns and SPS process diagrams of S3 and S4 are given in Figures 5.16 and 5.17, respectively. It was reported that thermal expansion values of produced composites by SPS method are very close to that of calculated ones according to rule of mixture [1]. By considering this, S3 and S4 were prepared at a point where thermal expansion value of α-ZrW_2O_8 is zero. Therefore, volume fractions of ZrW_2O_8 and ZrO_2 were 51.9% and 48.1%, respectively. It was decided to sinter S3 at 1150 °C in the initial trial. However, SPS die exploded during sintering. From SPS process diagram in Figure 5.17 (a), it can be seen that there is a sharp peak representing this explosion. XRD patterns in Figure 5.16 (a) showed that a great majority of ZrW_2O_8 turned into WO_3 and ZrO_2 in S3. Since phase transition from ZrW_2O_8 to its oxides occurred during sintering, vaporized WO_3 probably caused pressure development inside the die. Nevertheless three peaks were observed in blue line (Figure 5.17 (a)), and it was thought that sintering might have been started in the first two peaks just before the explosion. Since these two peaks were at around 1000 °C, it was decided to sinter S4 at that temperature. Additionally, 5 minutes sintering (instead of 10 minutes as in the case of S3) was applied to prevent any possible phase transition. As it is understood from Figure 5.17 (b), sintering was performed successfully.

XRD patterns in Figure 5.16 (b) showed that α-ZrW_2O_8 is the main product and a certain amount of γ_t-ZrW_2O_8 present. Applied pressure was 50MPa in SPS techniques while 250 MPa in conventional methods. It was proved from XRD patterns of S1 and S2 that 50 MPa did not cause any phase transition in composites. Although 50MPa was not enough to have phase transition in different phases of ZrW_2O_8, γ_t-ZrW_2O_8 was formed after sintering and its amount is higher than in composites produced by conventional sintering. The reason is interprated as: SPS is claimed to provide higher temperatures and pressures at the grain boundaries even if applied temperature and pressure are low. Therefore, particles can be sintered at low temperatures in very short time. In S4, the real pressure and temperature at the gain boundaries were certainly higher than applied 50 MPa and 1000 ^{o}C. This situation resulted to have phase transition from α-ZrW_2O_8 to γ_t-ZrW_2O_8 depending on the pressure. Since higher temperatures and pressures are formed at the grain boundaries, γ_t-ZrW_2O_8 formation is more evident in SPS when compared to conventional sintering. Also ZrO_2 being transformed from tetragonal to mostly monoclinic is the other evidence of pressure that is exerted on particle contacts due to constituents' expansion and contraction with temperature changes.
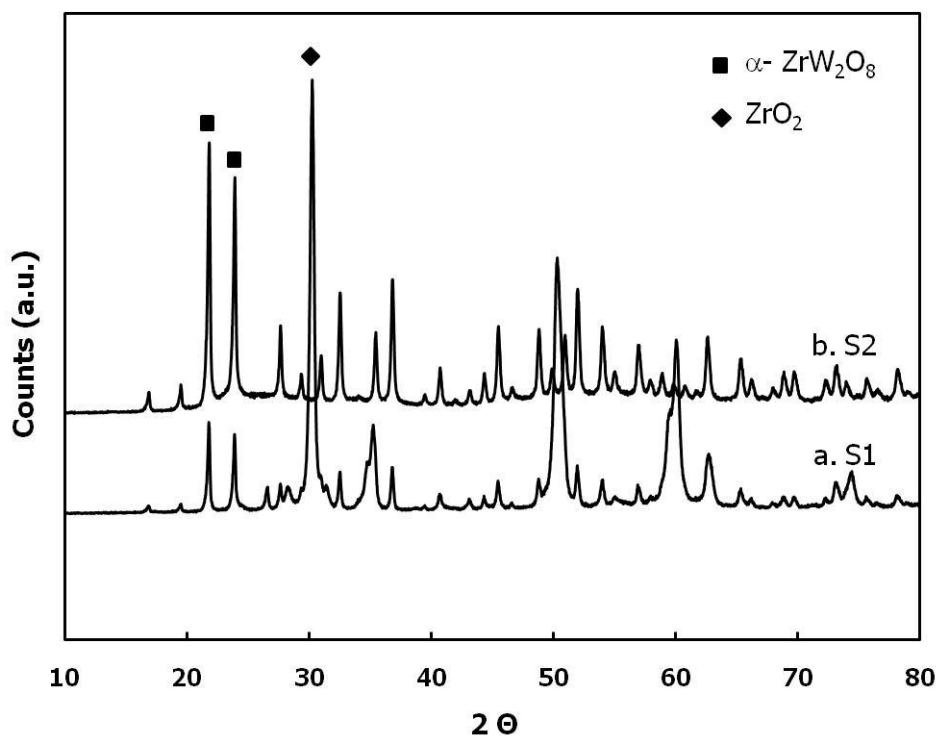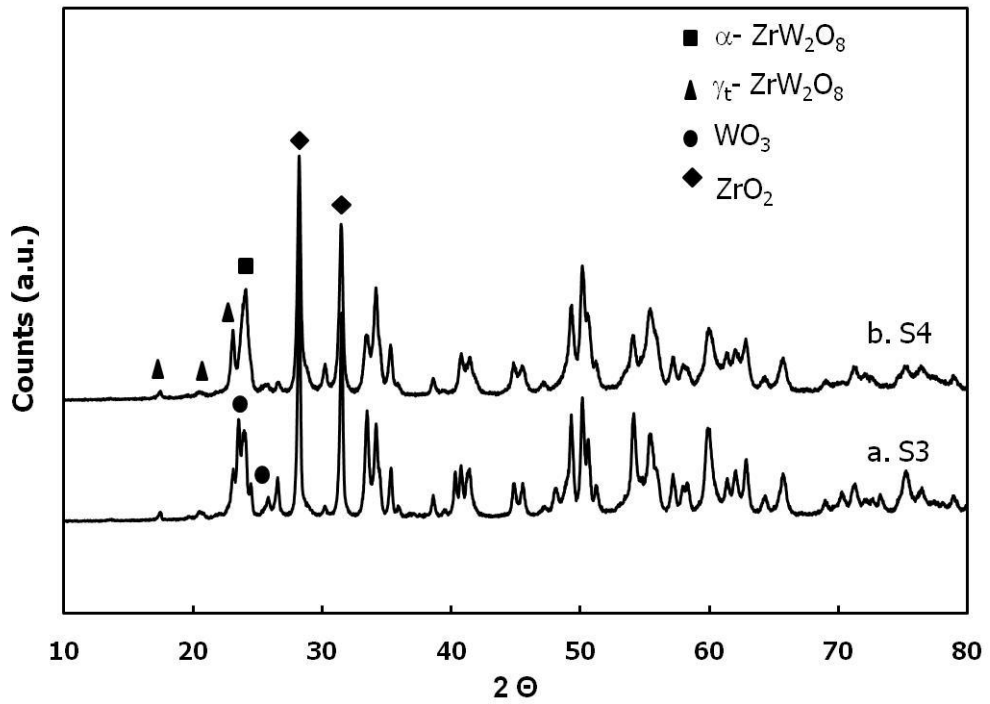
Figure 5.16 XRD patterns of composites (a) S3 and (b) S4.
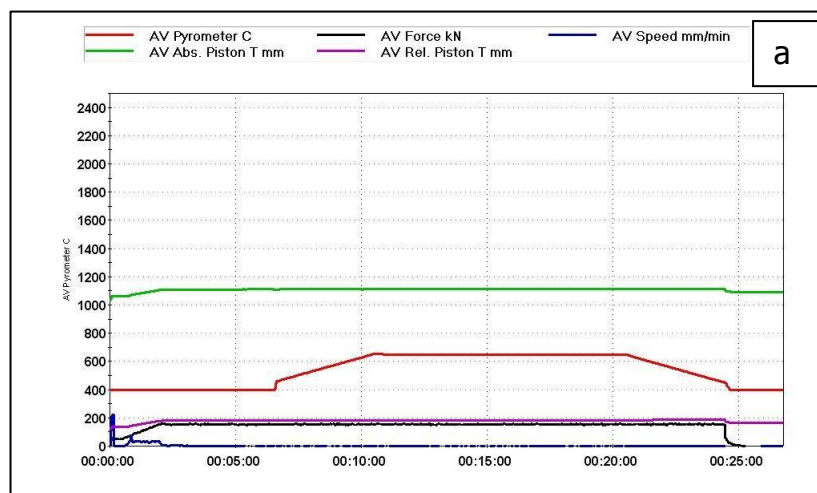

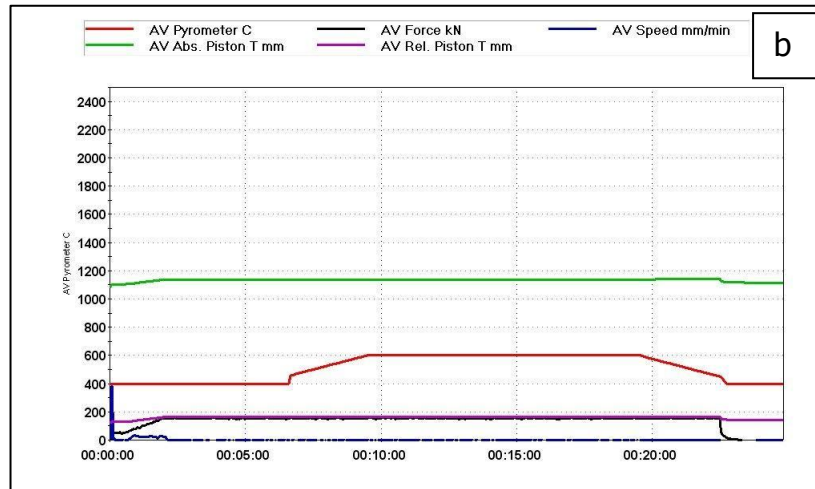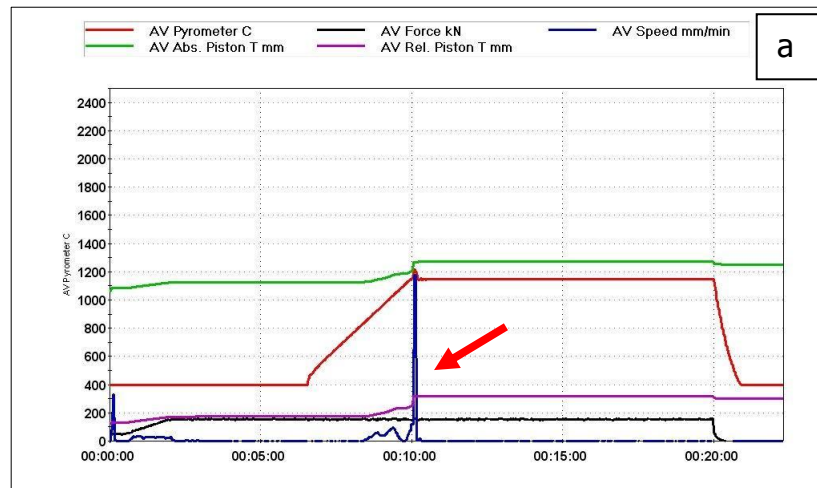**Figure 5.17** SPS process diagrams of experiments (a) S3 and (b) S4.
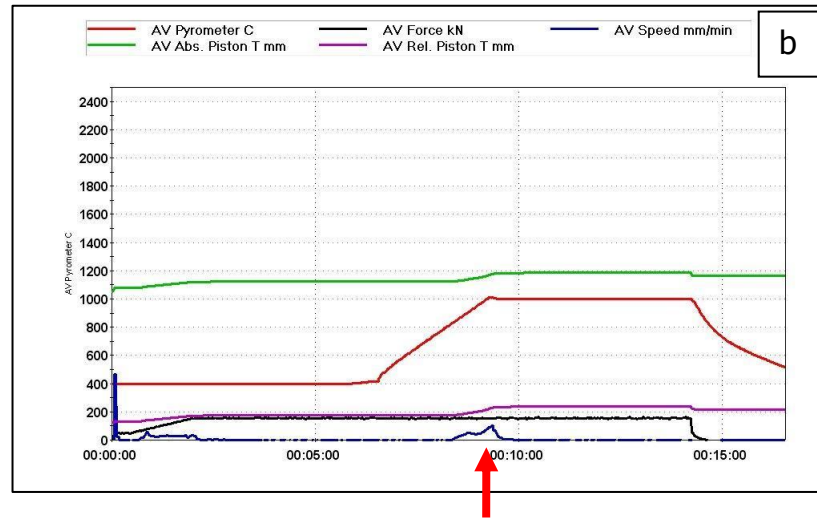
Figure 5.17 SPS process diagrams of experiments (a) S3 and (b) S4 (continued).

Appearance of S3 and S4 can be seen in Figure 5.18. Since S3 exploded during sintering, it lost the pellet form. On the other hand, S4 was successfully sintered. Additionally, the fracture strength was high in S4. Besides, a thin grey layer was formed on the surface of the composites after sintering. Factors that cause this formation are listed as;

- Possible reduction of W due to vacuum atmosphere employed during sintering.
- Formation of tungsten carbide (WC) due to the reduced W, where C comes from the die.
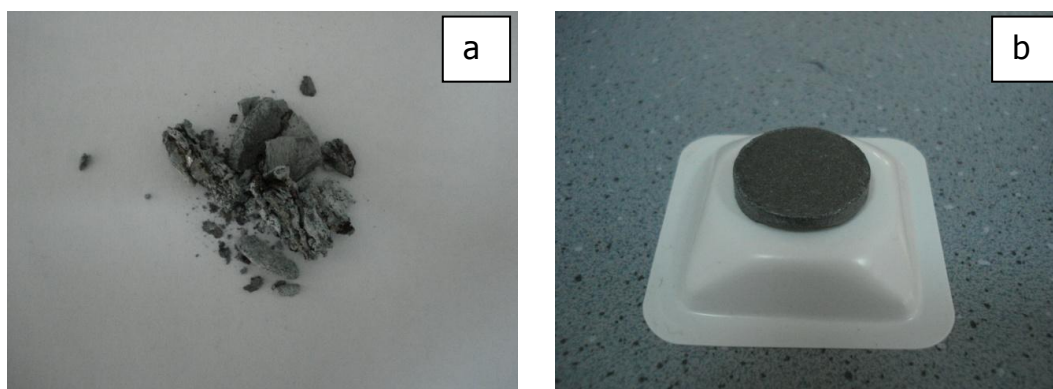
Figure 5.18 Pictures of composites after sintering for (a) S3 and (b) S4.

Following successful sintering in S4, two more experiments (S5 and S6) were also performed to examine the effect of ZrW_2O_8 amount and their experimental conditions are given in Table 5.6. All composites were sintered at 1000 °C for 5 minutes.

Table 5.6 Experimental conditions for S4, S5, and S6.

Exp. Name	Volume fractions (%)		Weight (g)[a]		Until 450°C		After 450°C		Sintering	
	ZrW_2O_8	ZrO_2	ZrW_2O_8	ZrO_2	°C/ min	time (min)	°C/ min	time (min)	T (°C)	time (min)
S5	35.00	65.00	1.12	2.38	100	4.5	200	2.45	1000	5
S4	51.90	48.10	3.31	3.52	100	4.5	200	2.45	1000	5
S6	55.00	45.00	1.62	1.52	100	4.5	200	2.45	1000	5

[a]ZrW_2O_8 and ZrO_2 amounts were calculated by assuming diameter and thickness as 20 mm and 2 mm, respectively for S5 and S6.

All parameters were kept constant except volume fractions of powders. Since a thick composite was obtained in S4, required amounts for S5 and S6 were calculated by assuming diameter and thickness as 20 mm and 2 mm, respectively. Therefore, thinner composites were obtained.

XRD patterns of S4, S5 and, S6 are seen in Figure 5.19. Patterns showed that while monoclinic ZrO_2 was mostly found in S4, tetragonal ZrO_2 was transformed only to a certain extent in S5 and S6. Additionally, α-ZrW_2O_8 and γ_t-ZrW_2O_8 were observed in all composites. However, S4 was composed mostly of α-ZrW_2O_8 whereas S5 and S6 were transformed mostly to γ_t-ZrW_2O_8. Since thinner composites were obtained from S5 and S6, higher pressure and temperature could have been exerted at the grain boundaries. Therefore, extent of phase transition from α-ZrW_2O_8 to γ_t-ZrW_2O_8 was higher in S5 and S6. It could also be claimed that the thinner the composites the larger the portion of pressure taken over by ZrW_2O_8. This might imply indirectly that ZrW_2O_8 is more sensitive to pressure and starts to transform earlier than ZrO_2. However, these need to be further investigated. Apart from these, peak intensity of ZrO_2 was higher (as expected) in S5, which contains higher amount of ZrO_2 in it.
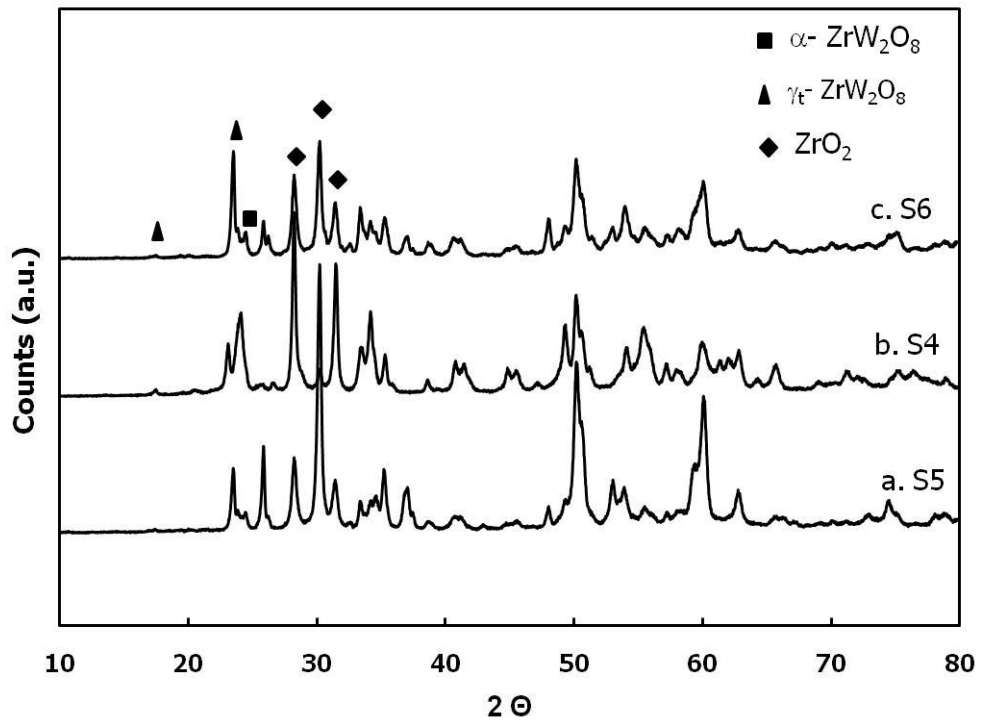
Figure 5.19 XRD patterns of composites (a) S5, (b) S4, and (c) S6.

SPS process diagrams of S5 and S6 in Figure 5.20 showed that sintering was carried out successfully. As seen in Figure 5.21, grey color was again formed at the surface of the composite as a very thin layer. Also, thickness differences can easily be seen by comparing Figure 5.21 with Figure 5.18 (b).
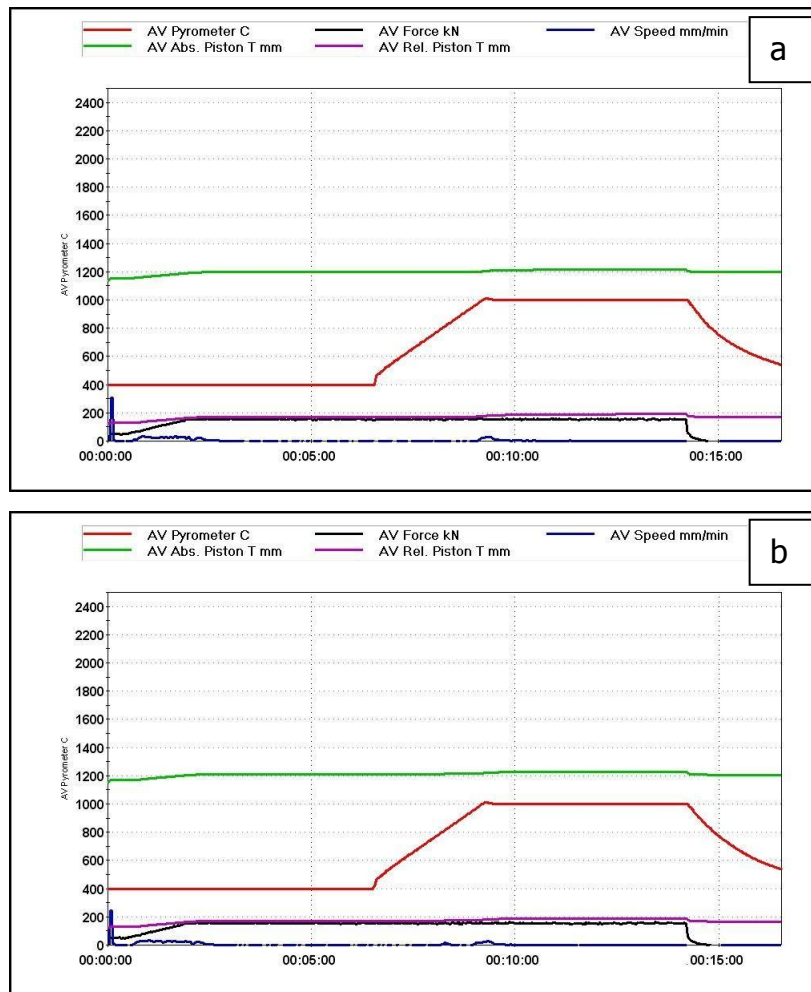
Figure 5.20 SPS process diagrams of (a) S5, and (c) S6.
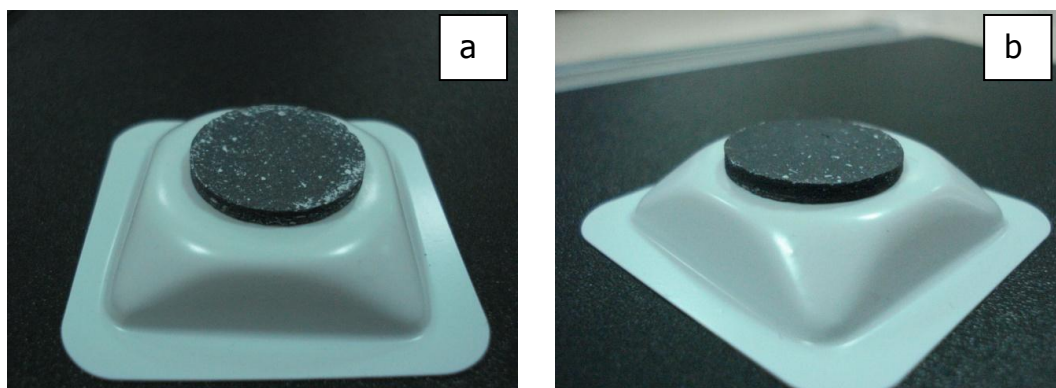
Figure 5.21 Pictures of composites after sintering (a) S5, and (b) S6.

115

Thermal expansion curves for S4, S5, and S6 are given in Figure 5.22. Since S5 contains less amount of ZrW_2O_8, positive thermal expansion was observed. This situation was compatible with calculated value from rule of mixture given in Appendix C. As in the case of conventional sintering, nearly zero thermal expansion was seen until around 120 ^{o}C (where γ-α phase transition occurs) in S4 and S6, and then there was positive expansion because of γ-α phase transition in which volume expansion occurred. Finally thermal expansion was again zero after around 200 ^{o}C. Best result was obtained from S6. When CTE values in SPS are compared with those of composites from conventional sintering, measured values are close to the calculated values from rule of mixture in SPS technique. Therefore, rule of mixture is much more applicable in SPS than conventional sintering. It could be claimed that this is due to the better sintered densities and smaller amounts of residual stresses due to less severe quenching conditions. In addition sintering was achieved without the use of sintering aids, which seem to leave voids in sintered bodies upon liquefaction in conventional sintering. This might be an additional factor of deviation from rule of mixture in conventionally sintered bodies.
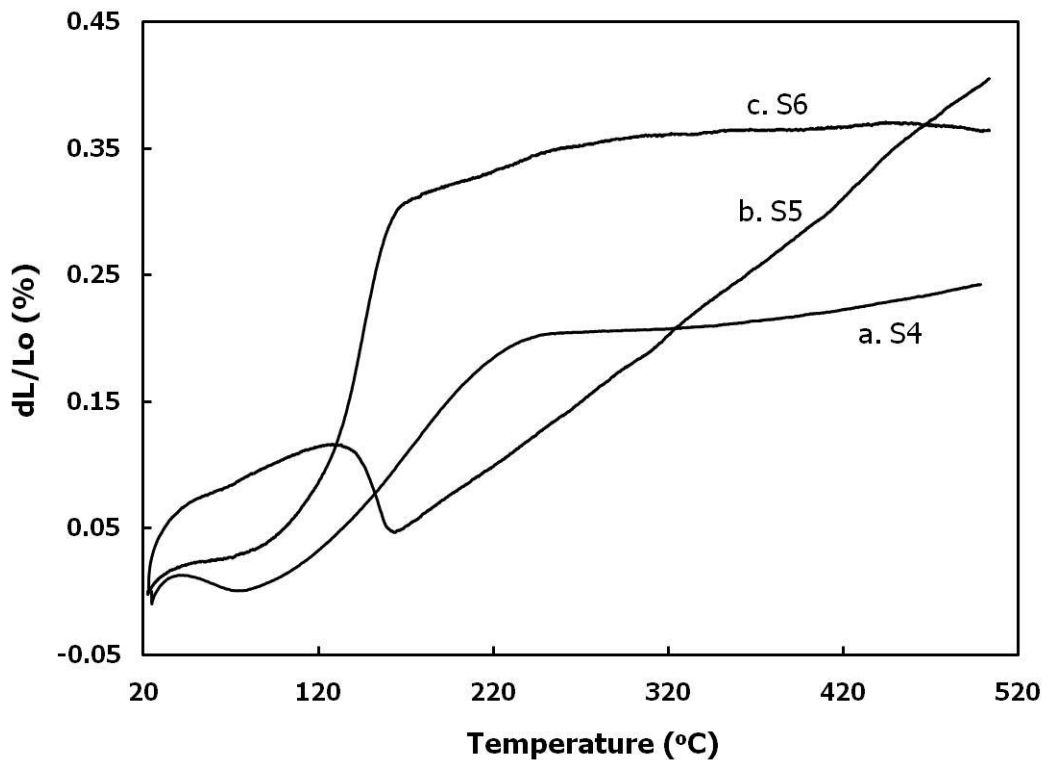
Figure 5.22 Thermal expansion behaviors of composites (a) S4, (b) S5, and (c) S6.

SEM micrographs of S4, S5, and S6 are seen in Figure 5.23. Sintering took place and more importantly grain sizes did not increase. One of the advantages of SPS is that sintering can be achieved without an increase in grain size observed in the micrographs. By considering that the composite can break at the weakest points (ZrO_2 rich regions), it would be more representative to look at the surfaces of the composites. When the images in Figure 5.23 (c) and (d) were compared, sintering can be easily observed from the surface of S6, as expected. Furthermore, ZrO_2 particles were clearly seen on the fracture surfaces of all composites (Figure 5.23 (a), (b), and (c)). 5 minutes sintering was probably not enough to have fully dense structures. In order to have a 100% dense composite, it would be better to extent the applied sintering times in S4, S5, and S6. Even though the

117

composites were prepared in alcohol to have better homogeneity, a non-harmonic expansion and contraction can be expected in the structure due to difference in particle sizes of ZrW_2O_8 and ZrO_2.
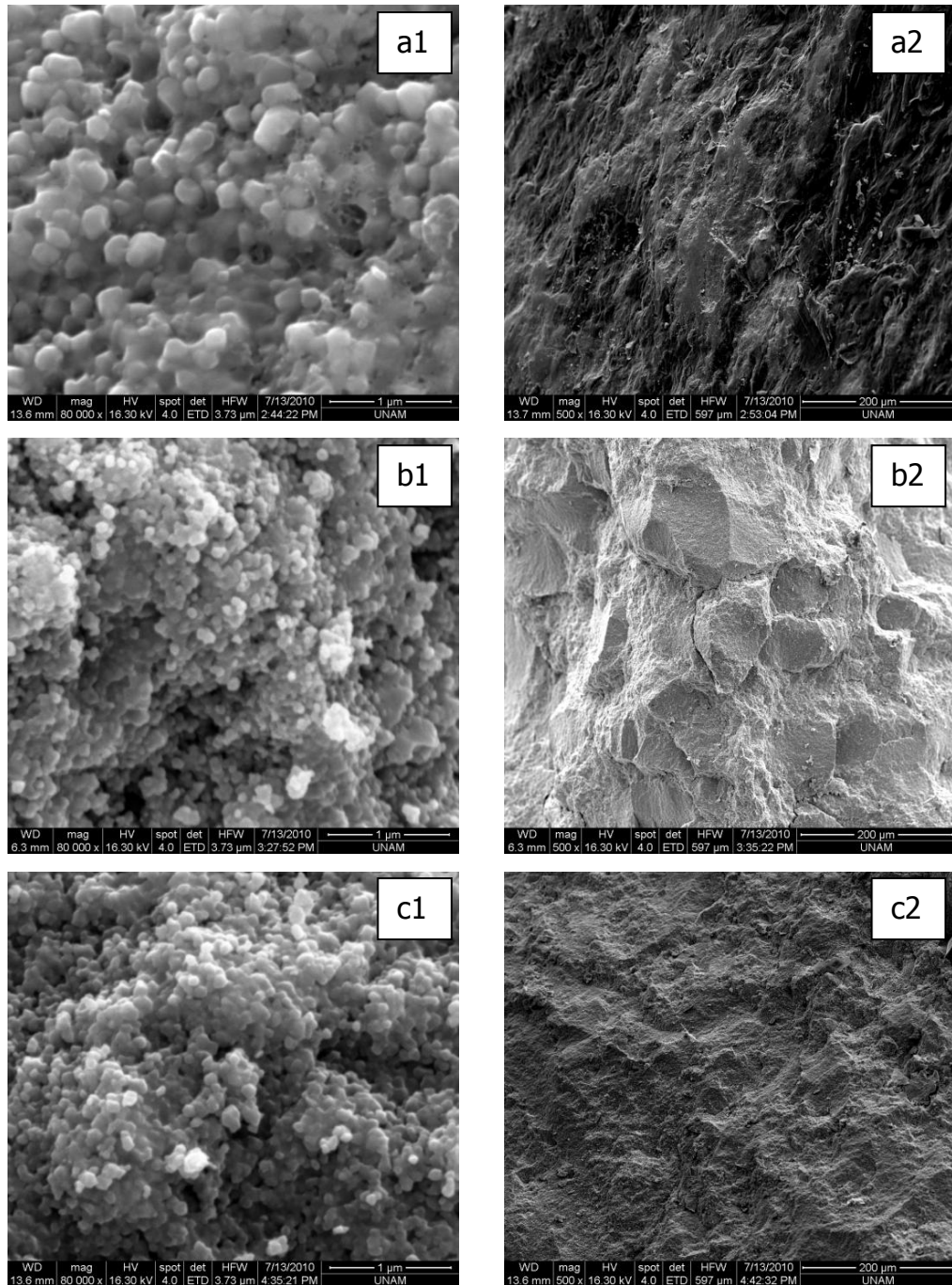
Figure 5.23 SEM micrographs of (a) S4, (b) S5, (c) S6 from fracture surfaces, and (d) S6 from composite surface.
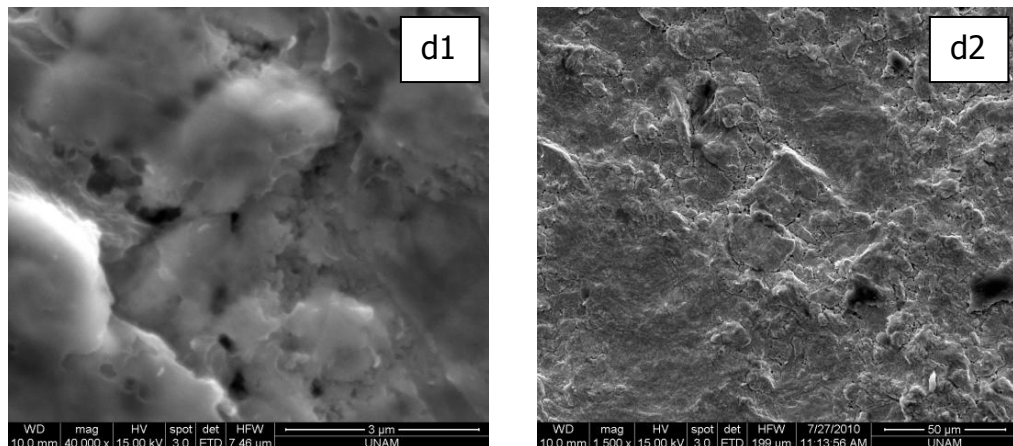
Figure 5.23 SEM micrographs of (a) S4, (b) S5, (c) S6 from fracture surfaces, and (d) S6 from composite surface (continued).

In order to examine the effect of Al_2O_3 on the structure of composites, some additional experiments were carried out by using 0.25 w/o sintering agent and experimental conditions are given in Table 5.7. Since required amounts were calculated by assuming diameter and thickness as 20 mm and 2 mm, thin composites were obtained.

First conducted experiment is named as S7 and sintering was performed in three steps to find the required temperature. Since melting point of expected $Al_2(WO_4)_3$ phase is 950 $^{\circ}$C, S7 (S7_1st run) was first taken to 650 $^{\circ}$C in order not to have any explosion as in the case of S3. Figure 5.24 (a) shows that sintering cannot be achieved in S7_1st run (there was no peak formation in blue line). Without taking out the composite from die, it (S7_2nd run) was taken to 750°C; however, there was still no sintering observed (Figure 5.24 (b)). Finally, same composite was taken to 850 $^{\circ}$C (S7_3rd run) and sintering was not observed at that temperature either (Figure 5.24 (c)). Then, it was decided to apply the same procedure in previous experiments, and S8 was conducted at 1000 $^{\circ}$C for 5 minutes. It can be understood from SPS process diagram in Figure 5.24 (d) that sintering was achieved in S8. Afterwards,

another experiment named as S9 was carried out at 850 ^{o}C by increasing the volume fraction of ZrW_2O_8. Blue lines in Figure 5.24 (e) indicate that sintering can be achieved at lower sintering temperatures when ZrW_2O_8 amount was higher in the composite body.

Table 5.7 Experimental conditions for S7, S8, and S9.

Exp. Name	Volume fractions (%)		Weight (g)[a]		Al_2O_3 (mg)	After 450°C		Sintering	
	ZrW_2O_8	ZrO_2	ZrW_2O_8	ZrO_2		^{o}C/min	time (min)	T (^{o}C)	time (min)
S7-1st run	35.00	65.00	1.12	2.38	8.75	10	4	650	10
S7-2nd run	35.00	65.00	1.12	2.38	8.75	50	6	750	10
S7-3rd run	35.00	65.00	1.12	2.38	8.75	50	8	850	10
S8	35.00	65.00	1.12	2.38	8.75	200	2.45	1000	5
S9	51.90	48.10	1.66	1.76	8.55	200	2	850	5

[a]ZrW_2O_8 and ZrO_2 amounts were calculated by assuming diameter and thickness as 20 mm and 2 mm, respectively.

Figure 5.24 SPS process diagrams of (a) S7-1st run, (b) S7-2nd run, (c) S7-3rd run, (d) S8, and (e) S9.

121
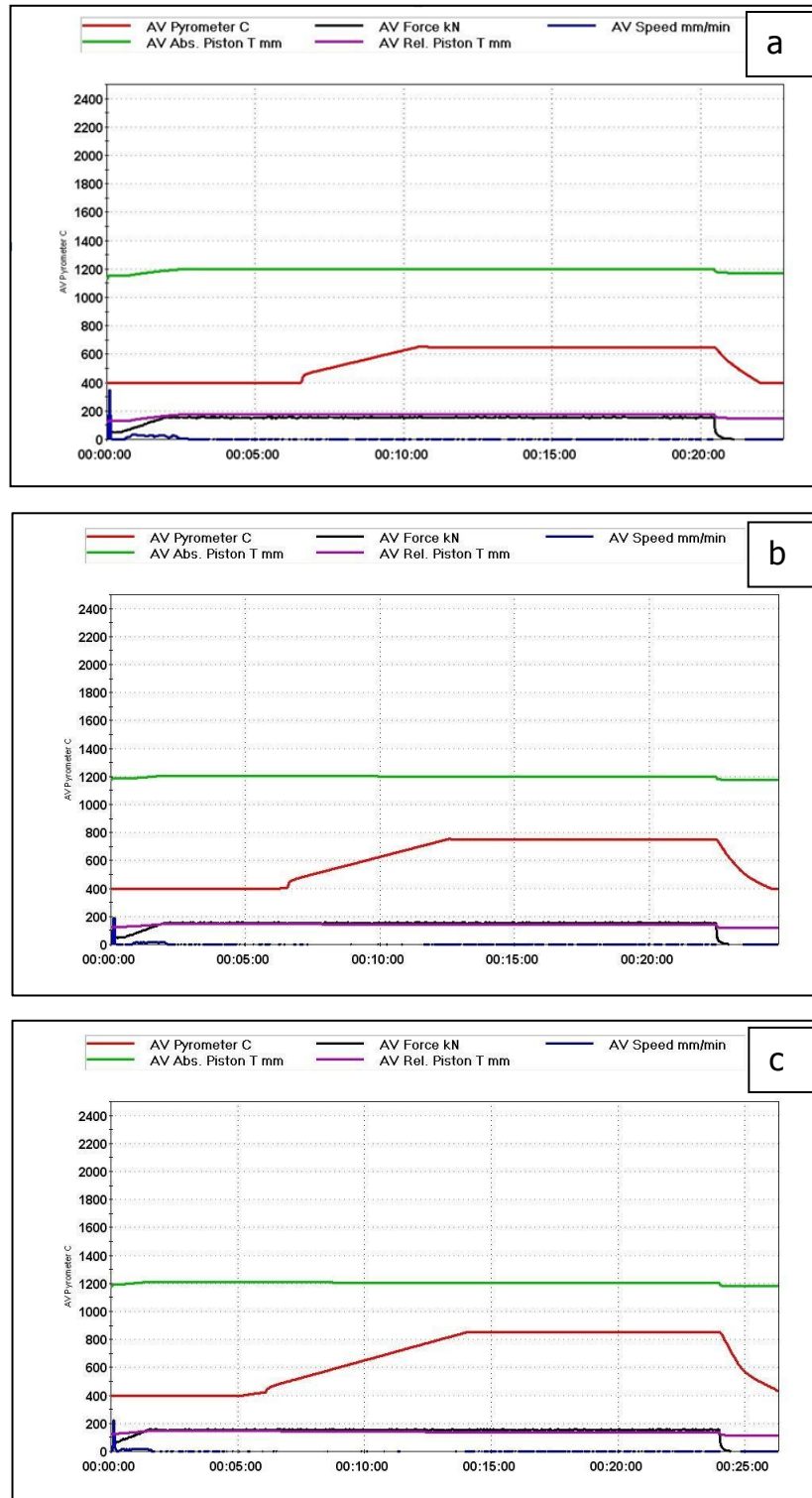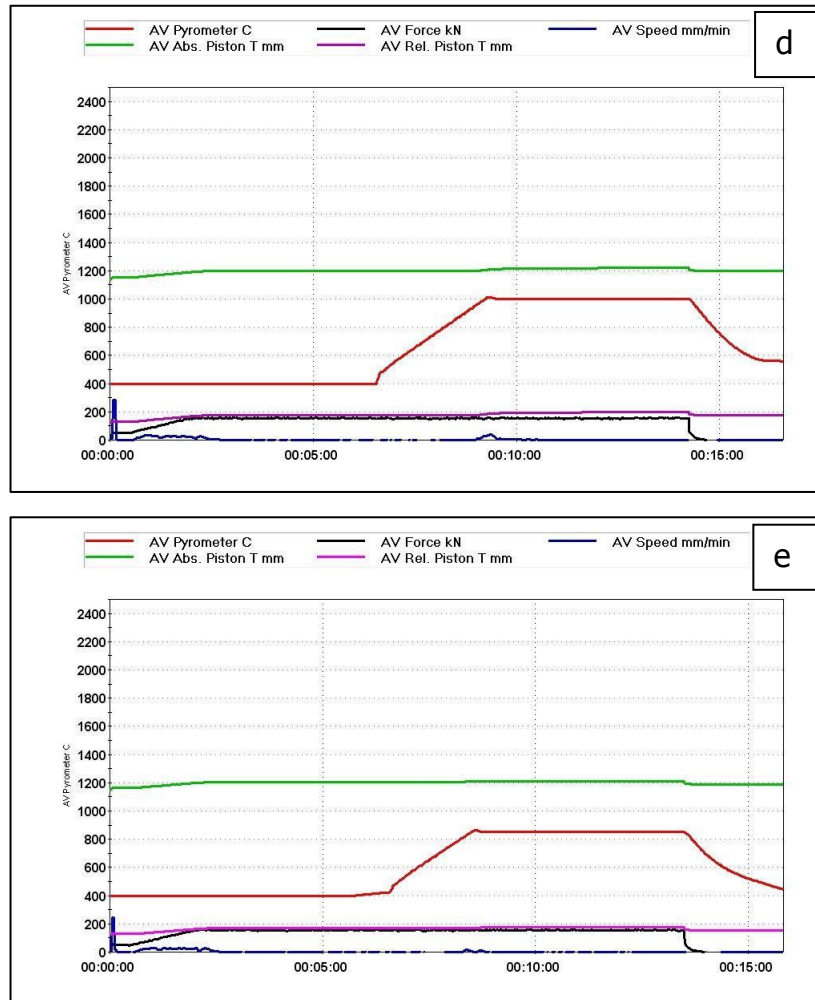
Figure 5.24 SPS process diagrams of (a) S7-1st run, (b) S7-2nd run, (c) S7-3rd run, (d) S8, and (e) S9 (continued).

Composites in which sintering agent was used were very fragile after sintering. Moreover, the color of the composites became dark blue as seen in Figure 5.25. Blue color indicates W reduction, which affects not only the color change but also fracture strength of the produced composites. Even though grey thin layer was observed on the surface of S8 and S9, the color of the inside were again blue. The structure of the composites was destroyed due to the use of Al_2O_3 as well as W reduction. XRD patterns in Figure 5.26 showed that ZrW_2O_8 transformed into WO_3 and ZrO_2 and formed WO_3 was

122

reacted with Al_2O_3 to form $Al_2(WO_4)_3$. Therefore, it was concluded that SPS triggers the formation of $Al_2(WO_4)_3$ in short durations.

In SEM micrographs (Figure 5.27), liquid phase sintering was observed; however, this situation disturbs the structure. Thermal expansion behaviors in Figure 5.28 also support the formation of $Al_2(WO_4)_3$.
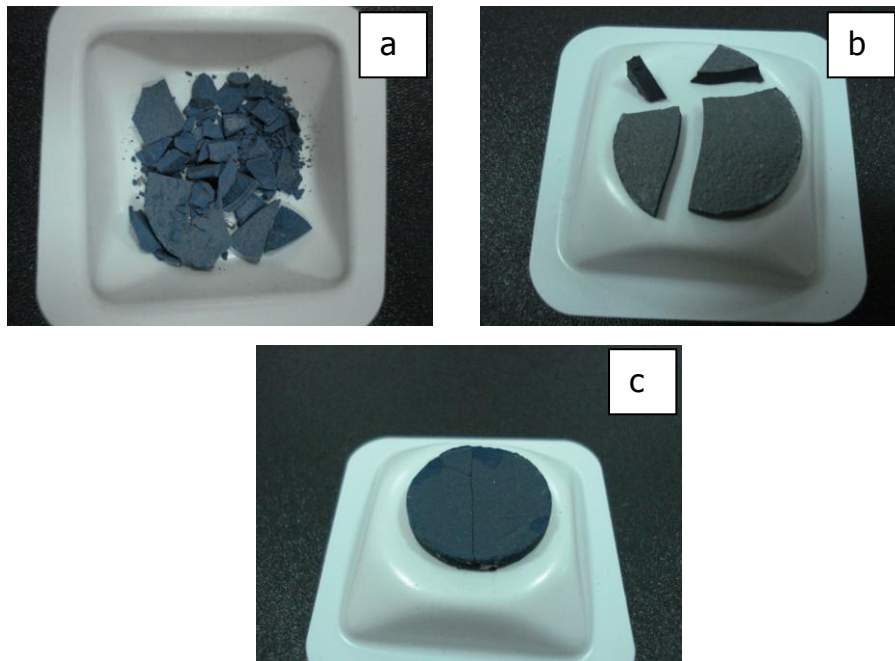
Figure 5.25 Pictures of composites after sintering for (a) S7, (b) S8, and (b) S9.
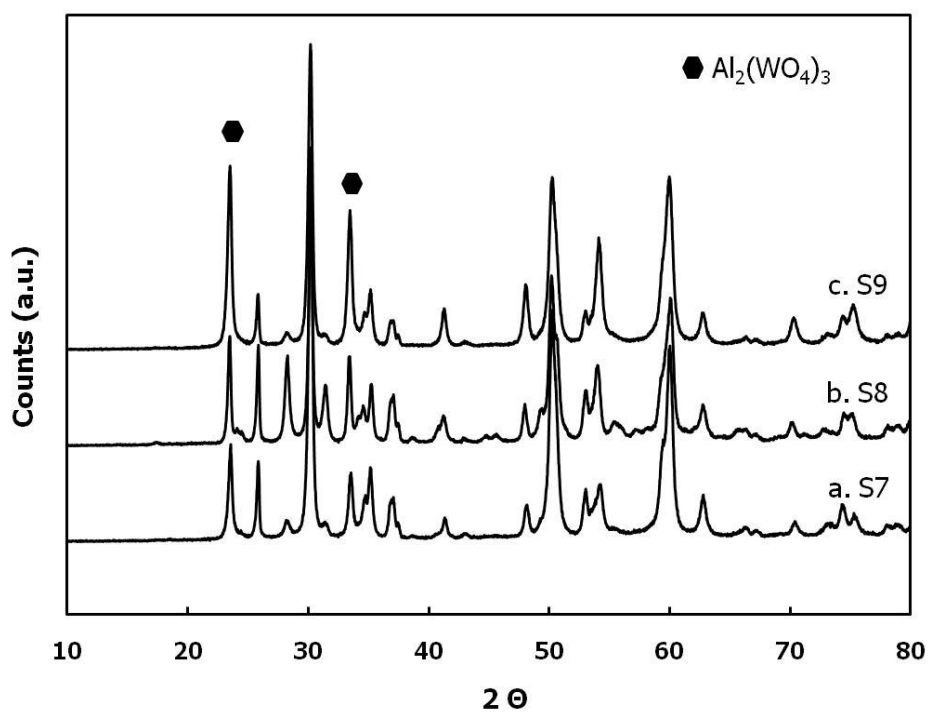
Figure 5.26 XRD patterns of experiments (a) S7, (b) S8, and (c) S9.
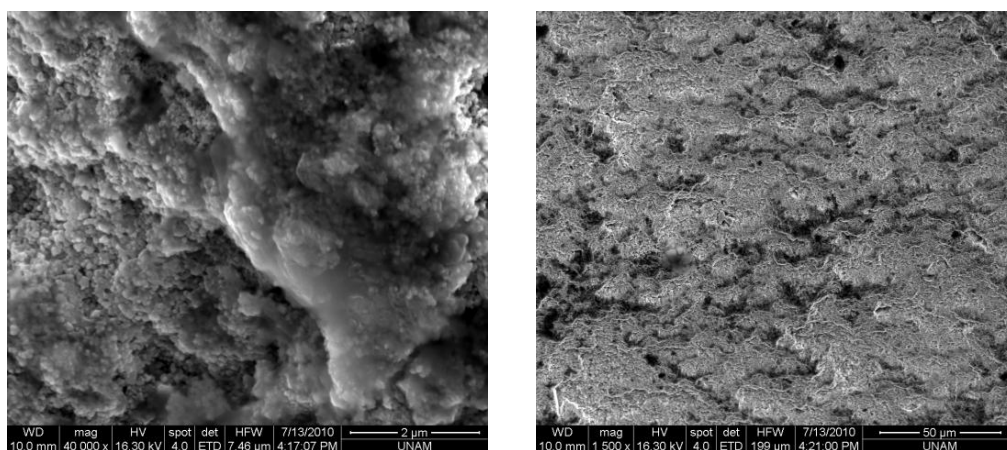
Figure 5.27 SEM micrographs of S8.
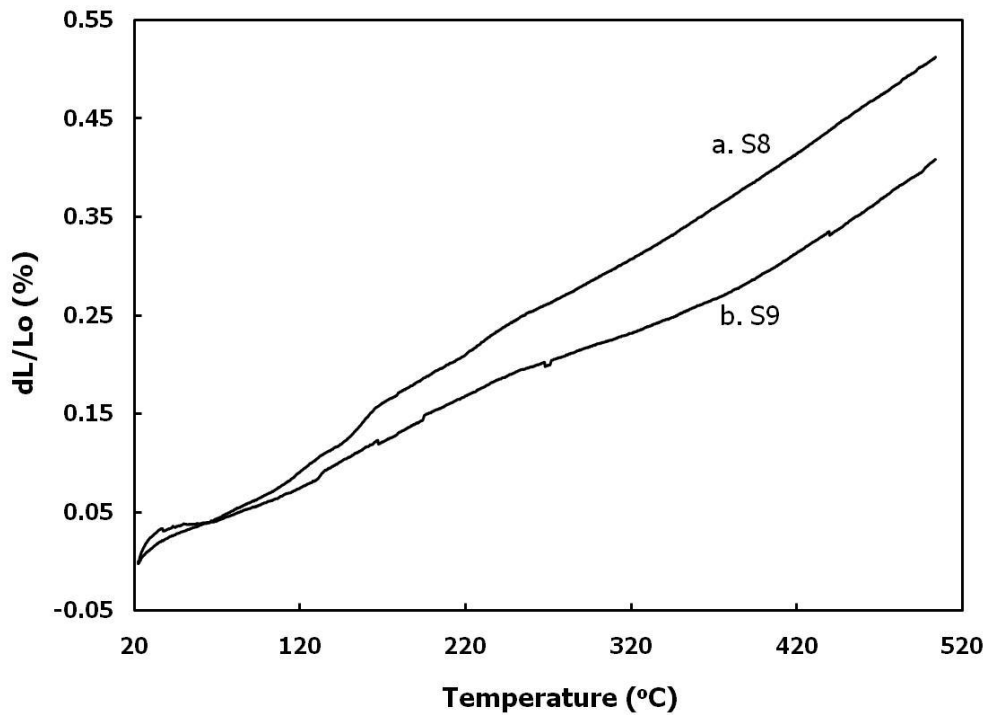
Figure 5.28 Thermal expansion behaviors of experiments (a) S8 and (b) S9.

As a consequence, best results were obtained from C1 in conventional, and S4 and S6 in SPS technique. CTE of C1 containing 0.35% ZrW_2O_8, 65%ZrO_2, and 35 w/o Al_2O_3 was 0.20 x 10^{-6}/K (this value is very close to obtained results in literature). Additionally, the density of C1 was about 90%, but it probably had residual thermal stresses due to quenching step. On the other hand, CTE of S4 (0.52-0.48 ZrW_2O_8-ZrO_2) and S6 (0.55-0.45 ZrW_2O_8-ZrO_2) were 2.83 x 10^{-6}/K and 0.94 x 10^{-6}/K, respectively. Their densities were about 96%.

It is also important to note that although the phase diagram dictated decomposition of ZrW_2O_8 to ZrO_2 and WO_3 at 1000 ^{o}C, this decomposition does not take place under the SPS conditions. But rather an α to γ transition

125

takes place. This is possible according to studies in literature; however, seeing it in a sintering process in this study was significant.

In either conventional or SPS methods, the formation of high pressure phases of ZrW_2O_8 or ZrO_2, should be taken as the response of the system to severe thermal mismatches at the constituent contact points. These could be highly critical adapting process steps like quenching. On the other hand, they could also be negated through some post heat treatment steps.

CHAPTER 6

CONCLUSIONS

This study was based on the synthesis of zirconium tungstate particles and production of ZrW_2O_8-ZrO_2 ceramic-ceramic composites with tunable CTE.

A novel precipitation method for the synthesis of ZrW_2O_8 precursor was developed using relatively low cost tungsten source, namely tungstic acid (TA). Solubility of TA constitutes an important problem against its use in such precursors; a problem which was solved by dissolving TA under the presence of hydrogen peroxide. Since the solubility of zirconium ions is higher than that of tungsten ions at low pH values, use of 15% excess Zr source was critical in obtaining phase purity. It was found that HCl concentration plays a crucial role in the crystallization of precursor at 600 ^{o}C. The reasons of high HCl usage were investigated and its effects on phase purity and particle sizes were analyzed. The minimum [HCl] was determined to be 3 M at the final solution mixture for the production of single phase ZrW_2O_8. Although the crystallite sizes were under 100 nm, size of the secondary particles was larger due to agglomeration. However, agglomeration can be lowered by washing the precursor after filtering. Washing with acetone and water yielded the single phase product, whereas ethanol and isopropyl alcohol cause less pure products. The required ageing time was reduced to 2 days at 90°C for small scale production while it is 3 days for large scale production. Both of these are comparable to the lowered ageing times in the hydrothermal processes described in literature.

127

For the composite studies ZrW_2O_8-ZrO_2 system was chosen. Since some of the particles were in micrometer sizes in the case of unwashed ZrW_2O_8, decantation was applied to attain submicrometer particles (400-600 nm), which were then used in the composite applications. Conventional and spark plasma sintering (SPS) methods were used in composite preparation. Required ZrW_2O_8 and ZrO_2 fractions were determined to have zero thermal expansion composites in each method and systematic experiments were carried out with different time and temperatures. Sintering at 1200 ^{o}C for 24 hours yielded a zero thermal expansion composite in conventional method, while temperature and time can be lowered to 1000 ^{o}C and 5 minutes in SPS. The results showed that the CTE's of the composites were very close to what was calculated according to rule of mixture for SPS, whereas there was a deviation from rule of mixture in conventional sintering method. The densities of the zero thermal expansion composites were 90 and 96% for conventional and SPS method, respectively.

CHAPTER 7

RECOMMENDATIONS

Recommendations for future possibilities can be given as follows:

Precursor

1. Since agglomerations produce larger particles, dispersing agents can be used at the precursor level to minimize agglomerations.

2. In order to produce particles lower than 100 nm, different techniques like micro-emulsion (reverse micelle system), in which three phases can be used; water phase inside the micelles, surfactants and solvent phase outside the micelles. Therefore, the chemical reaction can occur inside the micelles. By arranging water to solvent ratio, particle sizes can be better controlled.

Composites

1. After sintering, composites have different phases of ZrW_2O_8 due to residual stresses. Therefore, they show positive thermal expansion at 120-220 ^{o}C. By applying short-time post treatment, all phase transformed particles can be turned into α-ZrW_2O_8. It was indicated in the literature that γ phase cannot be permanently turned into α phase at low temperatures; however, 600 ^{o}C was adequate for permanent γ-α phase transition [27]. Another study showed that heat treatment temperatures can be raised up to 750-900 ^{o}C [63].

2. Micro-cracks were formed after quenching the produced composites in conventional methods. It was reported in the literature that these micro-cracks can be eliminated by heating the quenched composites at 300 ^{o}C for 1 hour [50].

3. In order to prevent the reduction of tungsten during sintering in SPS, sintering can be performed under air or nitrogen atmosphere

REFERENCES

1.   Kanamori, K., Kineri, T., Fukuda, R., Kawano, T., and Nishio, K., *Low-temperature sintering of ZrW_2O_8–SiO_2 by spark plasma sintering*, Journal of Materials Science, 44(3), p. 855-860, 2009.

2.   De Buysser, K., *Negative Thermal Expansion in Substituted ZrW_2O_8 and its Ceramic Composites*, PhD thesis, *Inorganic and Physical Chemistry*, Universiteit Gent, 2007.

3.   Roy, R., Agrawal, D.K., and Mckinstry, H.A., *Very Low Thermal-Expansion Coefficient Materials*, Annual Review of Materials Science, 19, p. 59-81, 1989.

4.   Sleight, A.W., *Compounds That Contract on Heating†*, Inorganic Chemistry, 37(12), p. 2854-2860, 1998.

5.   Calllister, W.D., *Materials Science and Engineering an Introduction*, *7th ed. ed*. 2007, USA: John Wiley & Sons, Inc.

6.   Mary, T.A., Evans, J.S.O., Vogt, T., and Sleight, A.W., *Negative Thermal Expansion from 0.3 to 1050 Kelvin in ZrW_2O_8*, Science, 272(5258), p. 90-92, 1996.

7.   Mittal, R., Chaplot, S.L., Schober, H., Kolesnikov, A.I., Loong, C.K., Lind, C., and Wilkinson, A.P., *Negative thermal expansion in cubic $ZrMo_2O_8$: Inelastic neutron scattering and lattice dynamical studies*, Physical Review B, 70(21), p. 214303, 2004.

8.   Sleight, A.W., *Negative thermal expansion materials*, Current Opinion in Solid State and Materials Science, 3(2), p. 128-131, 1998.

9.   Sleight, A.W.P., OR), Thundathil, Mary A. (Corvallis, OR), Evans, John S. O. (Corvallis, OR), *Negative thermal expansion materials*, The State of Oregon, acting by and through the Oregon State Board of (Corvallis, OR): United States, 1996.

10.   Chen, J.C., Huang, G.C., Hu, C., and Weng, J.P., *Synthesis of negative-thermal-expansion ZrW_2O_8 substrates*, Scripta Materialia, 49(3), p. 261-266, 2003.

11.   Graham, J., Wadsley, A.D., Weymouth, J.H., and Williams, L.S., *A new ternary oxide, ZrW_2O_8*, J. Am. Ceram. Soc., 42, p. 570, 1959.

12. Kameswari, U., Sleight, A.W., and Evans, J.S.O., *Rapid synthesis of ZrW$_2$O$_8$ and related phases, and structure refinement of ZrWMoO$_8$*, International Journal of Inorganic Materials, 2(4), p. 333-337, 2000.

13. Kowach, G.R., *Growth of single crystals of ZrW$_2$O$_8$*, Journal of Crystal Growth, 212(1/2), p. 167-172, 2000.

14. Luke, L.Y., Chang, M.G., and Phillips, S.B., *Condensed Phase Relations in the Systems ZrO$_2$-WO$_2$-WO$_3$ and HfO$_2$-WO$_2$-WO$_3$*, Journal of the American Ceramic Society, 50(4), p. 211-215, 1967.

15. Nishiyama, S., Hayashi, T., and Hattori, T., *Synthesis of ZrW$_2$O$_8$ by quick cooling and measurement of negative thermal expansion of the sintered bodies*, Journal of Alloys and Compounds, 417(1-2), p. 187-189, 2006.

16. Closmann, C., Sleight, A.W., and Haygarth, J.C., *Low-Temperature Synthesis of ZrW$_2$O$_8$ and Mo-Substituted ZrW$_2$O$_8$*, Journal of Solid State Chemistry, 139(2), p. 424-426, 1998.

17. Colin, J.A., Camper, D.V., Gates, S.D., Simon, M.D., Witker, K.L., and Lind, C., *Zirconium tungstate hydroxide hydrate revisited: Crystallization dependence on halide and hydronium ions*, Journal of Solid State Chemistry, 180(12), p. 3504-3509, 2007.

18. De Buysser, K., Smet, P., Schoofs, B., Bruneel, E., Poelman, D., Hoste, S., and Van Driessche, I., *Aqueous sol–gel processing of precursor oxides for ZrW$_2$O$_8$ synthesis*, Journal of Sol-Gel Science and Technology, 43(3), p. 347-353, 2007.

19. De Buysser, K., Van Driessche, I., Schaubroeck, J., and Hoste, S., *EDTA assisted sol–gel synthesis of ZrW$_2$O$_8$*, Journal of Sol-Gel Science and Technology, 46(2), p. 133-136, 2008.

20. Georgi, C. and Kern, H., *Preparation of zirconium tungstate (ZrW$_2$O$_8$) by the amorphous citrate process*, Ceramics International, 35(2), p. 755-762, 2009.

21. Kanamori, K., Kineri, T., Fukuda, R., Nishio, K., and Yasumori, A., *Preparation and Formation Mechanism of ZrW$_2$O$_8$ by SolGel Process*, Journal of the American Ceramic Society, 91, p. 3542-3545, 2008.

22. Khazeni, N., Özerciyes, B., Maviş, B., Gündüz, G., and Üner, Ç., *A Precursor for Synthesis of Zirconium Tungstate*, Proceedings of the 11th International Conference of the European Ceramic Society, Krakow, Poland, p. 116-118, 2009.

23. Kozy, L.C., Tahir, M.N., Lind, C., and Tremel, W., *Particle size and morphology control of the negative thermal expansion material cubic zirconium tungstate*, Journal of Materials Chemistry, 19(18), p. 2760-2765, 2009.

24. Lind, C. and Wilkinson, A.P., *Seeding and the Non-Hydrolytic Sol-Gel Synthesis of ZrW_2O_8 and $ZrMo_2O_8$*, Journal of Sol-Gel Science and Technology, 25(1), p. 51-56, 2002.

25. Vural, İ., Khazeni, N., Mavis, B., Gündüz, G., and Çolak, Ü., *Microemulsion Synthesis Strategies for ZrW_2O_8 Precursors*, Advances in Science and Technology, 62, p. 61-69, 2010.

26. Vural, İ., Mavis, B., Gündüz, G., Çolak, Ü., and Khazeni, N., *Zirkonyum Tungstat (ZrW_2O_8) Öncüllerinin Çöz-Pel Yöntemi İle Düşük Sıcaklık ve Yaşlandırma Sürelerinde Elde Edilmesi*, UKMK 2010 - 9. Ulusal Kimya Mühendisliği Kongresi, Gazi Üniversitesi Kimya Mühendisliği Bölümü, Ankara-Türkiye, p. 279-280, 2010.

27. Wilkinson, A.P., Lind, C., and Pattanaik, S., *A New Polymorph of ZrW_2O_8 Prepared Using Nonhydrolytic Sol−Gel Chemistry*, Chemistry of Materials, 11(1), p. 101-108, 1998.

28. Xing, Q., Xing, X., Yu, R., Du, L., Meng, J., Luo, J., Wang, D., and Liu, G., *Single crystal growth of ZrW_2O_8 by hydrothermal route*, Journal of Crystal Growth, 283(1-2), p. 208-214, 2005.

29. Xing, X., Xing, Q., Yu, R., Meng, J., Chen, J., and Liu, G., *Hydrothermal synthesis of ZrW_2O_8 nanorods*, Physica B: Condensed Matter, 371(1), p. 81-84, 2006.

30. Yang, X., Cheng, X., Yan, X., Yang, J., Fu, T., and Qiu, J., *Synthesis of ZrO_2/ZrW_2O_8 composites with low thermal expansion*, Composites Science and Technology, 67(6), p. 1167-1171, 2007.

31. Sun, X., Yang, J., Liu, Q., and Cheng, X., *Influence of sodium dodecyl benzene sulfonate (SDBS) on the morphology and negative thermal expansion property of ZrW_2O_8 powders synthesized by hydrothermal method*, Journal of Alloys and Compounds, 481(1-2), p. 668-672, 2009.

32. Sutton, M.S. and Talghader, J., *Zirconium tungstate (ZrW_2O_8) based micromachined negative thermal-expansion thin films*, Journal of Microelectromechanical Systems, 13(4), p. 688-695, 2004.

33. Evans, J.S.O., Mary, T.A., and Sleight, A.W., *Negative thermal expansion materials*, Physica B: Condensed Matter, 241-243, p. 311-316, 1997.

34. Barrera, G.D., Bruno, J.A.O., Barron, T.H.K., and Allan, N.L., *TOPICAL REVIEW: Negative thermal expansion*, Journal of Physics: Condensed Matter, 17(4), p. R217-R252, 2005.

35. Heine, V., Patrick, R.L., Martin, W., and Dove, T., *Geometrical Origin and Theory of Negative Thermal Expansion in Framework Structures*, Journal of the American Ceramic Society, 82(7), p. 1793-1802, 1999.

36. Evans, J.S.O., Mary, T.A., Vogt, T., Subramanian, M.A., and Sleight, A.W., *Negative Thermal Expansion in ZrW_2O_8 and HfW_2O_8*, Chem. Mater., 8(12), p. 2809-2823, 1996.

37. Evans, J.S.O., David, W.I.F., and Sleight, A.W., *Structural investigation of the negative thermal expansion material ZrW_2O_8*, Acta Crystallographica Section B, 55, p. 333-340, 1999.

38. Tsuji, T., Yamamura, Y., and Nakajima, N., *Thermodynamic properties of negative thermal expansion materials ZrW_2O_8 substituted for Zr site*, Thermochimica Acta, 416(1-2), p. 93-98, 2004.

39. Yan, X., Yang, X., Cheng, X., Fu, T., Qiu, J., and Liu, H., *High pure negative thermal expansion material ZrW_2O_8 powders synthesized by combustion method*, Journal of the Chinese ceramic society, 34(9), p. 1066, 2006.

40. Kofteros, M., Rodriguez, S., Tandon, V., and Murr, L.E., *A preliminary study of thermal expansion compensation in cement by ZrW_2O_8 additions*, Scripta Materialia, 45(4), p. 369-374, 2001.

41. Verdon, C. and Dunand, D.C., *High-temperature reactivity in the ZrW_2O_8-Cu system*, 36(9), p. 1075-1080, 1997.

42. Yilmaz, S., *Thermal mismatch stress development in Cu-ZrW_2O_8 composite investigated by synchrotron X-ray diffraction*, Composites Science and Technology, 62(14), p. 1835-1839, 2002.

43. Yilmaz, S., *Phase transformations in thermally cycled Cu/ZrW_2O_8 composites investigated by synchrotron x-ray diffraction*, Journal of Physics: Condensed Matter, 14(3), p. 365, 2002.

44. Watanabe, H., Tani, J., Kido, H., and Mizuuchi, K., *Thermal expansion and mechanical properties of pure magnesium containing zirconium tungsten phosphate particles with negative thermal expansion*, Materials Science and Engineering: A, 494(1-2), p. 291-298, 2008.

45. Sullivan, L.M. and Lukehart, C.M., *Zirconium Tungstate (ZrW₂O₈)/Polyimide Nanocomposites Exhibiting Reduced Coefficient of Thermal Expansion*, Chemistry of Materials, 17(8), p. 2136-2141, 2005.

46. Tani, J.-i., Kimura, H., Hirota, K., and Kido, H., *Thermal expansion and mechanical properties of phenolic resin/ZrW₂O₈ composites*, Journal of Applied Polymer Science, 106(5), p. 3343-3347, 2007.

47. De Buysser, K., Lommens, P., de Meyer, C., Bruneel, E., Hoste, S., and Van Driessche, I., *ZrO₂-ZrW₂O₈ composites with tailor-made thermal expansion*, Ceramics-Silikaty, 48(4), p. 139-144, 2004.

48. Lommens, P., De Meyer, C., Bruneel, E., De Buysser, K., Van Driessche, I., and Hoste, S., *Synthesis and thermal expansion of ZrO₂/ZrW₂O₈ composites*, Journal of the European Ceramic Society, 25(16), p. 3605-3610, 2005.

49. Niwa, E., Wakamiko, S., Ichikawa, T., Wang, S., Hashimoto, T., Takahashi, K., and Morito, Y., *Preparation of Dense ZrO₂/ZrW₂O₈ Cosintered Ceramics with Controlled Thermal Expansion Coefficients*, Journal of the Ceramic Society of Japan, 112(1305), p. 271-275, 2004.

50. Sun, L. and Kwon, P., *ZrW₂O₈/ZrO₂ composites by in situ synthesis of ZrO₂+WO₃: Processing, coefficient of thermal expansion, and theoretical model prediction*, Materials Science and Engineering: A, 527(1-2), p. 93-97, 2009.

51. Yang, X., Xu, J., Li, H., Cheng, X., and Yan, X., *In Situ Synthesis of ZrO₂/ZrW₂O₈ Composites With Near-Zero Thermal Expansion*, Journal of the American Ceramic Society, 90(6), p. 1953-1955, 2007.

52. Tani, J.-i., Takahashi, M., and Kido, H., *Fabrication and thermal expansion properties of ZrW₂O₈/Zr₂WP₂O₁₂ composites*, Journal of the European Ceramic Society, 30(6), p. 1483-1488, 2010.

53. Kanamori, K., Kineri, T., Fukuda, R., Nishio, K., Hashimoto, M., and Mae, H., *Spark Plasma Sintering of SolGel Derived Amorphous ZrW₂O₈ Nanopowder*, Journal of the American Ceramic Society, 92, p. 32-35, 2009.

54. Levin, E.M., Robins, C.R., and McMurdie, H.F., *Phase Diagrams for Ceramist*, ed. Reser, M.K. 1969: The American Ceramic Society.

55. Achary, S.N., Mukherjee, G.D., Tyagi, A.K., and Vaidya, S.N., *Preparation, thermal expansion, high pressure and high temperature behavior of $Al_2(WO_4)_3$*, Journal of Materials Science, 37(12), p. 2501-2509, 2002.

56. Biest, O.V.D., *Modelling of the Field Assisted Sintering Technology (FAST) or Spark Plasma Sintering (SPS)*, Department of Metallurgy and Metarials Engineering, Katholieke Universiteit Leuven, 1999.

57. Aalund, R., *Spark Plasma Sintering*, Ceramic Industry, Powell, Ohio, BNP Media, 2008.

58. Evans, J.S.O., Hu, Z., Jorgensen, J.D., Argyriou, D.N., Short, S., and Sleight, A.W., *Compressibility, Phase Transitions, and Oxygen Migration in Zirconium Tungstate, ZrW2O8*, Science, 275(5296), p. 61-65, 1997.

59. Hu, Z., Jorgensen, J.D., Teslic, S., Short, S., Argyriou, D.N., Evans, J.S.O., and Sleight, A.W., *Pressure-induced phase transformation in ZrW_2O_8 -- Compressibility and thermal expansion of the orthorhombic phase*, Physica B: Condensed Matter, 241-243, p. 370-372, 1997.

60. Jorgensen, J.D., Hu, Z., Teslic, S., Argyriou, D.N., Short, S., Evans, J.S.O., and Sleight, A.W., *Pressure-induced cubic-to-orthorhombic phase transition in ZrW_2O_8*, Physical Review B, 59(1), p. 215, 1999.

61. Sleight, A.W., *Isotropic Negative Thermal Expansion*, Annual Review of Materials Science, 28(1), p. 29-43, 1998.

62. Grzechnik, A., Crichton, W.A., Syassen, K., Adler, P., and Mezouar, M., *A New Polymorph of ZrW_2O_8 Synthesized at High Pressures and High Temperatures*, Chemistry of Materials, 13(11), p. 4255-4259, 2001.

63. Noailles, L.D., Peng, H.h., Starkovich, J., and Dunn, B., *Thermal Expansion and Phase Formation of ZrW_2O_8 Aerogels*, Chemistry of Materials, 16(7), p. 1252-1259, 2004.

64. Gaur, R., *Modern hydrometallurgical production methods for tungsten*, JOM Journal of the Minerals, Metals and Materials Society, 58(9), p. 45-49, 2006.

65. Chemical Structures, retrieved from http://www.chemicalbook.com, last visited on 20/02/2011.

66.   Baker, A.P., Hodgson, S.N.B., and Edirisinghe, M.J., *Production of tungsten oxide coatings, via sol-gel processing of tungsten anion solutions*, Surface and Coatings Technology, 153, p. 184-193, 2002.

67.   Agnihotry, S.A., Sharma, N., and Deepa, M., *Ion Exchange Derived Precursor Materials for Deposition of WO_3 Electrochromic Films: Spectroscopic Investigations*, Journal of Sol-Gel Science and Technology, 24, p. 265-270, 2001.

68.   Balaji, S., Djaoued, Y., Albert, A.-S.b., Ferguson, R.Z., and Brüning, R., *Hexagonal Tungsten Oxide Based Electrochromic Devices: Spectroscopic Evidence for the Li Ion Occupancy of Four-Coordinated Square Windows*, Chemistry of Materials, 21(7), p. 1381-1389, 2009.

69.   Santato, C., Odziemkowski, M., Ulmann, M., and Augustynski, J., *Crystallographically Oriented Mesoporous WO_3 Films: Synthesis, Characterization, and Applications*, Journal of the American Chemical Society, 123(43), p. 10639-10649, 2001.

70.   Balaji, S., Albert, A.-S., Djaoued, Y., and Brüning, R., *Micro-Raman spectroscopic characterization of a tunable electrochromic device for application in smart windows*, Journal of Raman Spectroscopy, 40(1), p. 92-100, 2009.

71.   Balaji, S., Djaoued, Y., Albert, A.-S., Ferguson, R., Brüning, R., and Su, B.-L., *Construction and characterization of tunable meso-/macroporous tungsten oxide-based transmissive electrochromic devices*, Journal of Materials Science, 44(24), p. 6608-6616, 2009.

72.   Zhang, L., Howe, J.Y., Zhang, Y., and Fong, H., *Synthesis and Characterization of Zirconium Tungstate Ultra-Thin Fibers*, Crystal Growth & Design, 9(2), p. 667-670, 2009.

73.   Özerciyes, B., *A Novel Precursor for Synthesis of Zirconium Tungstate and Preliminary Studies for Nanofiber Production*, thesis, *Chemical Engineering*, Middle East Technical University, Ankara, 2009.

74.   Kepert, D.L., *The Early Transition Metals*. Vol. 499. 1972, New York: Academic Press Inc. (London) Ltd.

75.   De Meyer, C., *Perspectives in the chemistry of negative thermal expansion*, thesis, *Chemistry*, Universiteit Gent, 2004.

APPENDIX A

CRYSTALLOGRAPHIC DATA

The crystallographic data for the unit cell parameters and space groups of all three phases of ZrW_2O_8 are given in Table A.1, A.2, and A.3. The fractional atomic coordinates are only given for the α and β phases [75].

Table A.1 Crystallographic data for α-ZrW_2O_8.

α-ZrW_2O_8 P2$_1$3	Atom	x/a	y/b	z/c
Cell parameters at 20°C		a (Å) 9.1569(3)		
	Zr1	0.0004(3)	0.0004(3)	0.0004(3)
	W1	0.3409(3)	0.3409(3)	0.3409(3)
	W2	0.6009(3)	0.6009(3)	0.6009(3)
	O1	0.0529(3)	-0.2069(3)	-0.0619(4)
	O2	0.0697(4)	-0.0575(3)	0.2132(3)
	O3	0.4914(4)	0.4914(4)	0.4914(4)
	O4	0.2322(3)	0.2322(3)	0.2322(3)

Table A.2   Crystallographic data for β-ZrW$_2$O$_8$.

β-ZrW$_2$O$_8$ Pa-3	Atom	x/a	y/b	z/c
Cell parameters at 210°C		a (Å) 9.1371(5)		
	Zr1	0.0000(0)	0.0000(0)	0.0000(0)
	W1	0.3394(5)	0.3394(5)	0.3394(5)
	W2	0.6035(5)	0.6035(5)	0.6035(5)
	O1	0.0549(3)	-0.2089(2)	-0.0671(3)
	O3	0.5055(0)	0.5055(0)	0.5055(0)
	O4	0.2322(4)	0.2322(4)	0.2322(4)

Table A.3   Crystallographic data for γ-ZrW$_2$O$_8$.

γ-ZrW$_2$O$_8$ P2$_1$2$_1$2$_1$	Atom	x/a	y/b	z/c
Cell parameters at 20°C		a (Å) 9.0608(2)	b (Å) 27.0141(6)	c (Å) 8.9191(2)

APPENDIX B

POSITION AND INTENSITY OF STANDARD PEAKS OF ALL POSSIBLE PHASES

ICDS card numbers and cards of $ZrW_2O_7(OH)_2(H_2O)_2$, ZrW_2O_8, WO_3, and different phases of ZrO_2 are tabulated in Table B.1 and Table B.2, respectively. Intensity values smaller than 10% are not given in the table. Figures B.1 through B.6 give presentation of ICDS cards given in Table B.2 as a visual aid.

Table B.1   ICDS card numbers of different structures.

Phases	ICDD-JCPDS-PDF No
$ZrW_2O_7(OH)_2(H_2O)_2$	28-1500
α-ZrW_2O_8	50-1868
WO_3	72-0677
m-ZrO_2	37-1484
t-ZrO_2	17-0923
c-ZrO_2	27-0997

Table B.2 ICDS cards of different structures.

ZrW₂O₇(OH)₂(H₂O)₂		α-ZrW₂O₈		WO₃	
2Θ	Intensity	2Θ	Intensity	2Θ	Intensity
20.984	100	21.569	100	24.35	100
24.571	95	23.662	90	23.11	97
15.451	85	36.68	35	23.58	94
28.493	85	32.318	30	34.15	51
34.439	25	27.443	25	33.25	44
36.236	25	35.193	25	16.88	40
47.621	25	51.922	25	33.55	27
38.016	17	45.391	20	34.08	24
46.358	13	48.748	20	26	21
17.905	12	30.724	18	41.86	17
31.226	10	53.933	18	49.89	17
50.493	10	50.838	16	41.42	16
52.649	10	19.295	14	37.82	14
56.515	10	56.908	14	35.38	14
		16.695	12	48.24	11
		29.183	10	47.23	11
		40.639	10		

Table B.2 (Continued).

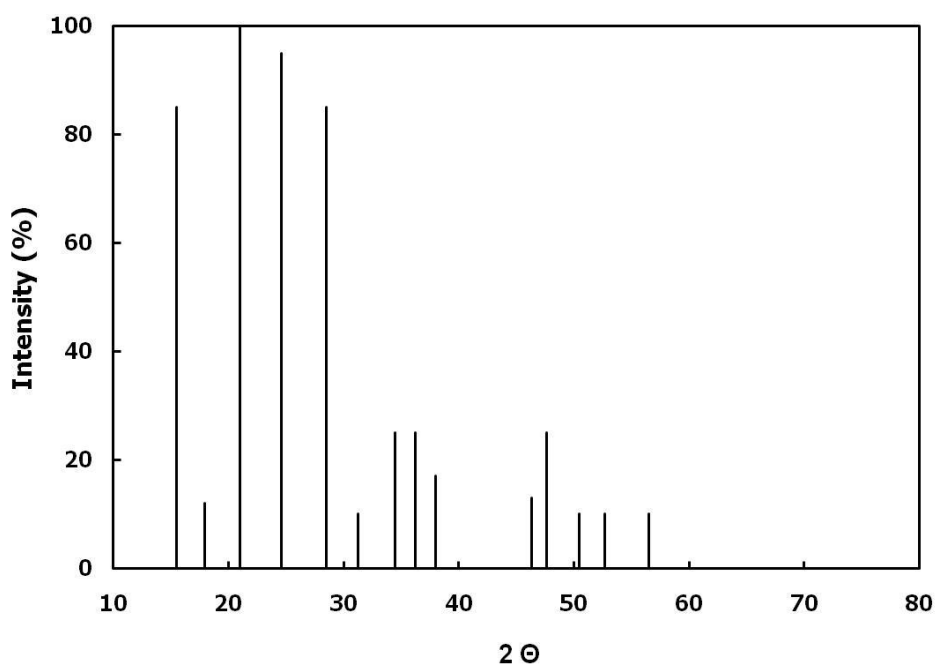| m-ZrO₂		t-ZrO₂		c-ZrO₂	
2Θ	Intensity	2Θ	Intensity	2Θ	Intensity
28.175	100	30.166	100	30.509	100
31.468	68	49.783	65	50.686	50
50.116	22	59.722	45	35.193	25
34.160	21	50.371	35	60.337	20
49.266	18	35.306	25		
24.048	14	58.556	25		
35.309	13	34.465	18		
50.559	13	62.116	12		
40.725	12	80.672	12		
34.383	11				
54.104	11				
55.270	11				
55.400	11				
24.441	10				

Figure B.1 Standard peaks of $ZrW_2O_7(OH)_2(H_2O)_2$.
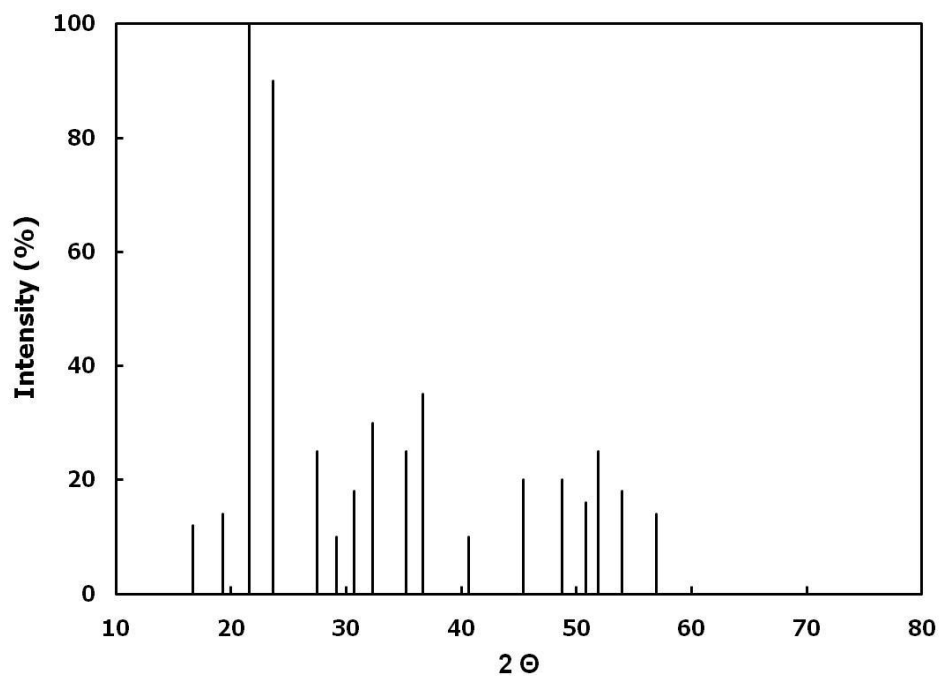
Figure B.2 Standard peaks of ZrW_2O_8.

142
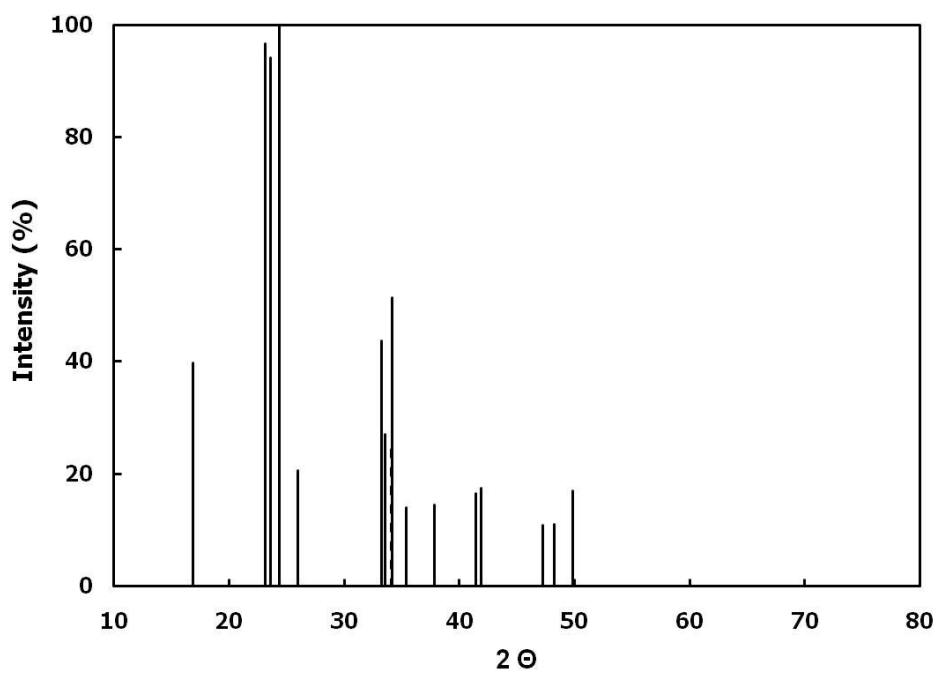
Figure B.3 Standard peaks of WO$_3$.
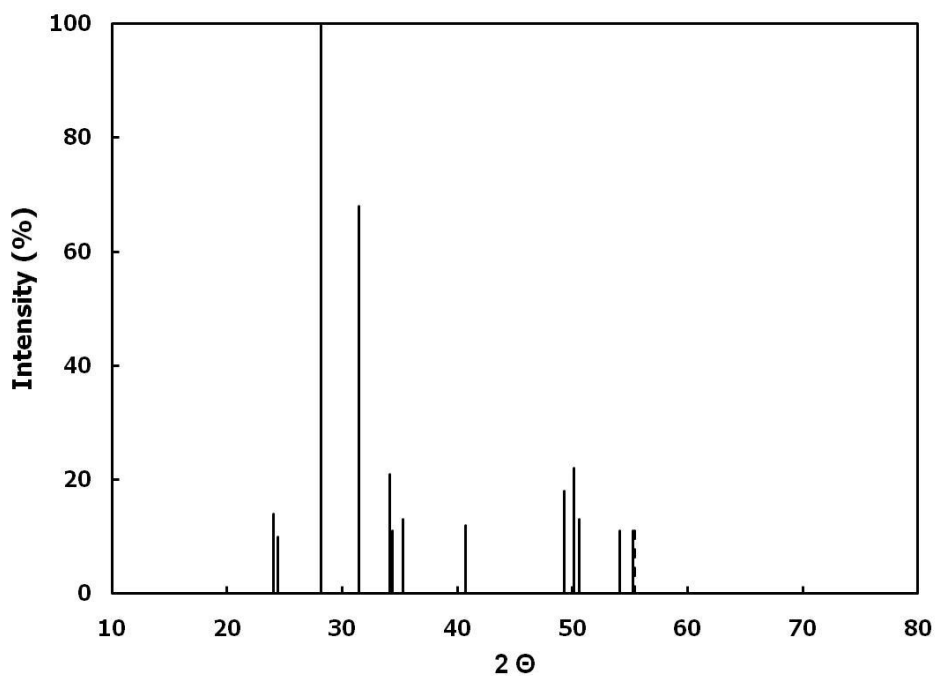

Figure B.4 Standard peaks of m-ZrO$_2$.
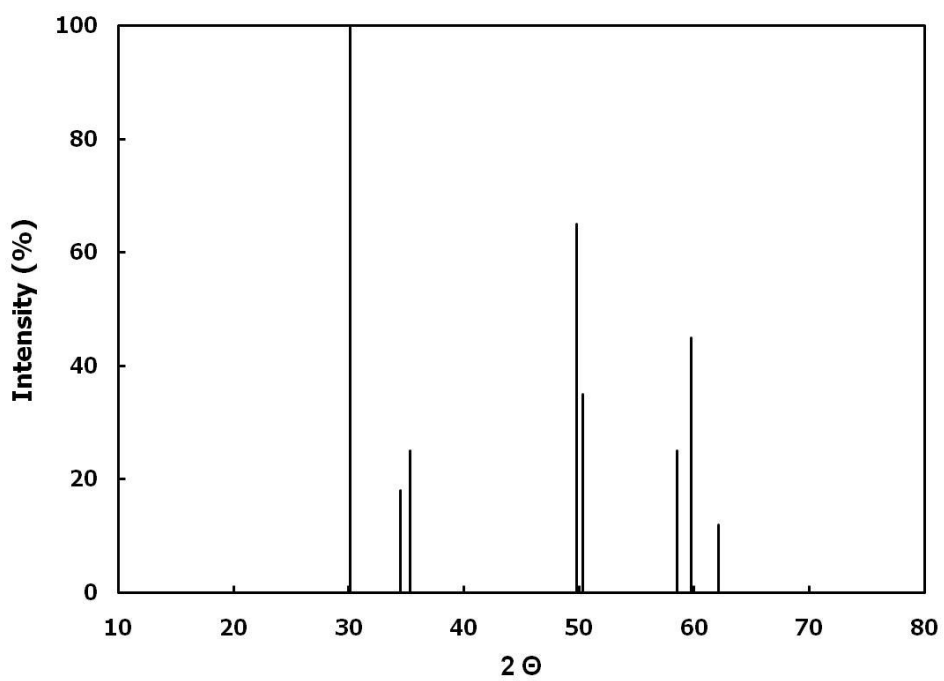
Figure B.5 Standard peaks of t-ZrO_2.
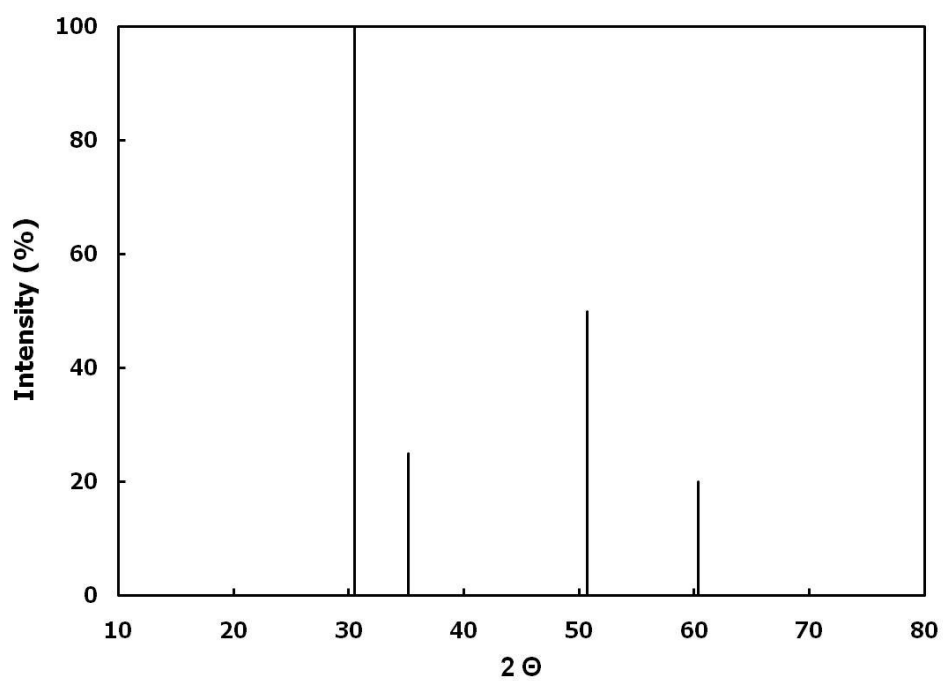
Figure B.6 Standard peaks of c-ZrO_2.

144
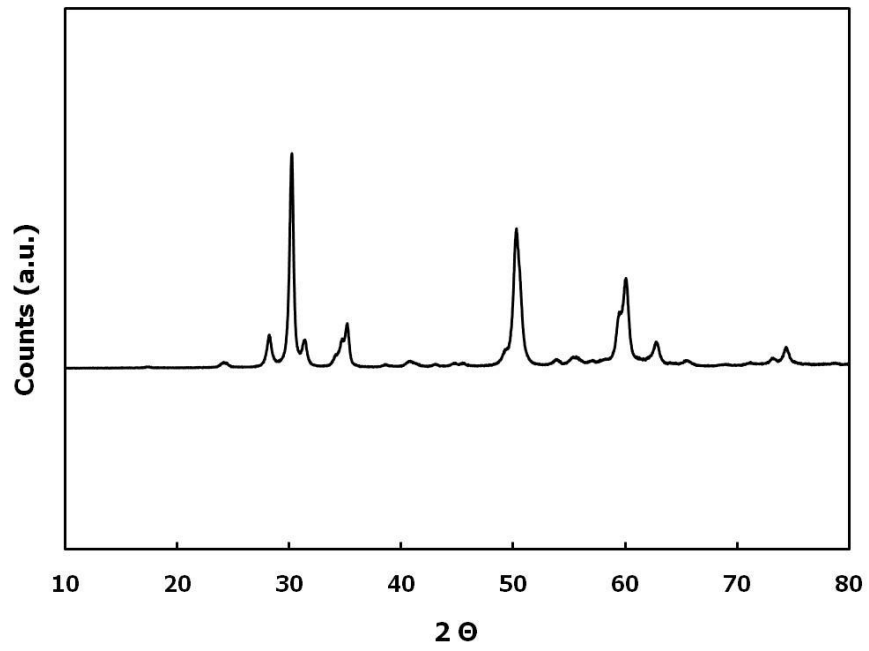
Figure B.7 XRD patterns of commercial ZrO$_2$ used in composites.

APPENDIX C

CALCULATIONS FOR COMPOSITES

Density and thermal expansion values of ZrW_2O_8, ZrO_2, and Al_2O_3 in Table 5.1 were used to calculate the expected CTE, and density of the composites for different volume fractions of ZrW_2O_8 and ZrO_2. Calculations were done according to rule of mixtures as explained in Chapter 3. Necessary amounts of ZrW_2O_8 and ZrO_2 to obtain negative, positive or zero coefficients were tabulated using an additional volume percent to weight percent conversion and considering the diameter of the die and thickness of the composite. Calculated values for conventional and SPS experiments are given in Table C.1 and C.2, respectively. It should be noted that not all of the calculated compositions were actually used in calculations. Only a selection of those with desired values were chosen in actual experiments. A sample calculation for a composite with 35 vol% ZrW_2O_8 and 65 vol% ZrO_2 that is to be sintered with conventional method is given below:

Calculations

Volume fraction of ZrW_2O_8:   v.f. ZrW_2O_8 = 0.35

Volume fraction of ZrO_2:   v.f. ZrO_2 = 0.65

Diameter of die: D   = 20 mm

Thickness of composite: t   = 1.5 mm

                    w/o Al_2O_3 = 0.25

$$\text{CTE} (\alpha) = \left(\text{v.f.} \, ZrW_2O_8 \times \text{CTE} \, (\alpha ZrW_2O_8)\right) + \left(\text{v.f.} \, ZrO_2 \times \text{CTE}(ZrO_2)\right)$$

$$\text{CTE} (\alpha) = \left(0.35 \times (-8.90 \times 10^{-6})\right) + \left(0.65 \times (9.60 \times 10^{-6})\right) = 3.13 \times 10^{-6}$$

$$\text{CTE} (\beta) = \left(\text{v.f.} \, ZrW_2O_8 \times \text{CTE} \, (\beta ZrW_2O_8)\right) + \left(\text{v.f.} \, ZrO_2 \times \text{CTE}(ZrO_2)\right)$$

$$\text{CTE} (\beta) = \left(0.35 \times (-4.70 \times 10^{-6})\right) + \left(0.65 \times (9.60 \times 10^{-6})\right) = 4.60 \times 10^{-6}$$

$$\text{CTE} (\gamma) = \left(\text{v.f.} \, ZrW_2O_8 \times \text{CTE} \, (\gamma ZrW_2O_8)\right) + \left(\text{v.f.} \, ZrO_2 \times \text{CTE}(ZrO_2)\right)$$

$$\text{CTE} (\gamma) = \left(0.35 \times (-1.00 \times 10^{-6})\right) + \left(0.65 \times (9.60 \times 10^{-6})\right) = 5.89 \times 10^{-6}$$

$$\text{w.f.} \, ZrW_2O_8 = \frac{\text{v.f.} \, ZrW_2O_8 \times \rho \, ZrW_2O_8}{(\text{v.f.} \, ZrW_2O_8 \times \rho \, ZrW_2O_8) + (\text{v.f.} \, ZrO_2 \times \rho \, ZrO_2)}$$

$$\text{w.f.} \, ZrW_2O_8 = \frac{0.35 \times 5.08}{(0.35 \times 5.08) + (0.65 \times 5.83)} = 0.32$$

$$\text{w.f.} \, ZrO_2 = 1 - \text{w.f.} \, ZrW_2O_8 = 1 - 0.32 = 0.68$$

$$\rho \, \text{comp.} = (\text{v.f.} \, ZrW_2O_8 \times \rho \, ZrW_2O_8) + (\text{v.f.} \, ZrO_2 \times \rho \, ZrO_2)$$

$$\rho \, \text{comp.} = (0.35 \times 5.08) + (0.65 \times 5.83) = 5.57 \, g/cm^3$$

$$\text{V comp.} = \pi \times \left(\frac{D}{2}\right)^2 \times t$$

$$\text{V comp.} = \pi \times \left(\frac{12 \times 10^{-3}}{2}\right)^2 \times (1.5 \times 10^{-3}) = 0.17 \, cm^3$$

$$\text{M comp.} = \rho \, \text{comp} \times \text{V comp} = 5.57 \times 0.17 = 0.94 \, g$$

$$ZrW_2O_8 \, \text{needed} = \text{w.f.} \, ZrW_2O_8 \times \text{M comp} = 0.32 \times 0.94 = 0.30 \, g$$

$$ZrO_2 \, \text{needed} = \text{w.f.} \, ZrO_2 \times \text{M comp} = 0.68 \times 0.94 = 0.64 \, g$$

$$Al_2O_3 \, \text{needed} = (ZrW_2O_8 \, \text{needed} + ZrO_2 \, \text{needed}) \times (\text{w/o} \, Al_2O_3)$$

$$Al_2O_3 \, \text{needed} = (0.30 + 0.64) \times (0.25 \times 10) = 2.36 \, mg$$

Table C.1 Calculated values for conventional sintering at different volume fractions.

Volume fraction		Rule of mixture (x10^{-6})			Weight (g)		Weight fraction		Density of comp.	Mass of comp	g needed		0.07 w/o	0.15 w/o	0.25 w/o	0.35 w/o
ZrW_2O_8	ZrO_2	CTE (α)	CTE (β)	CTE (γ)	ZrW_2O_8	ZrO_2	ZrW_2O_8	ZrO_2			ZrW_2O_8	ZrO_2	mg Al_2O_3	mg Al_2O_3	mg Al_2O_3	mg Al_2O_3
0.30	0.70	4.05	5.31	6.42	1.52	4.08	0.27	0.73	5.61	0.95	0.26	0.69	0.67	1.43	2.38	3.33
0.35	0.65	3.13	4.60	5.89	1.78	3.79	0.32	0.68	5.57	0.94	0.30	0.64	0.66	1.42	2.36	3.31
0.40	0.60	2.20	3.88	5.36	2.03	3.50	0.37	0.63	5.53	0.94	0.34	0.59	0.66	1.41	2.35	3.28
0.45	0.55	1.28	3.17	4.83	2.29	3.21	0.42	0.58	5.49	0.93	0.39	0.54	0.65	1.40	2.33	3.26
0.50	0.50	0.35	2.45	4.30	2.54	2.92	0.47	0.53	5.46	0.93	0.43	0.49	0.65	1.39	2.31	3.24
0.519	0.481	0.00	2.18	4.10	2.64	2.80	0.48	0.52	5.44	0.92	0.45	0.48	0.65	1.38	2.31	3.23
0.53	0.47	-0.21	2.02	3.98	2.69	2.74	0.50	0.50	5.43	0.92	0.46	0.46	0.65	1.38	2.30	3.23
0.55	0.45	-0.58	1.74	3.77	2.79	2.62	0.52	0.48	5.42	0.92	0.47	0.45	0.64	1.38	2.30	3.22
0.60	0.40	-1.50	1.02	3.24	3.05	2.33	0.57	0.43	5.38	0.91	0.52	0.40	0.64	1.37	2.28	3.19
0.65	0.35	-2.43	0.31	2.71	3.30	2.04	0.62	0.38	5.34	0.91	0.56	0.35	0.63	1.36	2.27	3.17
0.6715	0.3285	-2.82	0.00	2.48	3.41	1.92	0.64	0.36	5.33	0.90	0.58	0.32	0.63	1.36	2.26	3.16
0.70	0.30	-3.35	-0.41	2.18	3.56	1.75	0.67	0.33	5.31	0.90	0.60	0.30	0.63	1.35	2.25	3.15

Table C.2   Calculated values for SPS at different volume fractions.

Volume fraction		Rule of mixture (x10^{-6})			Weight (g)		Weight fraction		Density of comp.	Mass of comp	g needed		0.07 w/o	0.15 w/o	0.25 w/o	0.35 w/o
ZrW$_2$O$_8$	ZrO$_2$	CTE (α)	CTE (β)	CTE (γ)	ZrW$_2$O$_8$	ZrO$_2$	ZrW$_2$O$_8$	ZrO$_2$	comp.	comp	ZrW$_2$O$_8$	ZrO$_2$	mg Al$_2$O$_3$	mg Al$_2$O$_3$	mg Al$_2$O$_3$	mg Al$_2$O$_3$
0.3	0.7	4.05	5.31	6.42	1.52	4.08	0.27	0.73	5.61	3.52	0.96	2.56	8.80	0.3	0.7	4.05
0.35	0.65	3.13	4.60	5.89	1.78	3.79	0.32	0.68	5.57	3.50	1.12	2.38	8.75	0.35	0.65	3.13
0.4	0.6	2.20	3.88	5.36	2.03	3.50	0.37	0.63	5.53	3.47	1.28	2.20	8.69	0.4	0.6	2.20
0.45	0.55	1.28	3.17	4.83	2.29	3.21	0.42	0.58	5.49	3.45	1.44	2.01	8.63	0.45	0.55	1.28
0.5	0.5	0.35	2.45	4.30	2.54	2.92	0.47	0.53	5.46	3.43	1.60	1.83	8.57	0.5	0.5	0.35
0.519	0.481	0.00	2.18	4.10	2.64	2.80	0.48	0.52	5.44	3.42	1.66	1.76	8.55	0.519	0.481	0.00
0.53	0.47	-0.21	2.02	3.98	2.69	2.74	0.50	0.50	5.43	3.41	1.69	1.72	8.53	0.53	0.47	-0.21
0.55	0.45	-0.58	1.74	3.77	2.79	2.62	0.52	0.48	5.42	3.40	1.76	1.65	8.51	0.55	0.45	-0.58
0.6	0.4	-1.50	1.02	3.24	3.05	2.33	0.57	0.43	5.38	3.38	1.92	1.47	8.45	0.6	0.4	-1.50
0.65	0.35	-2.43	0.31	2.71	3.30	2.04	0.62	0.38	5.34	3.36	2.07	1.28	8.39	0.65	0.35	-2.43
1	0	-8.90	-4.70	-1.00	5.08	0.00	1.00	0.00	5.08	3.19	3.19	0.00	7.98	1	0	-8.90